UNIVERSITÀ DEGLI STUDI DI TORINO

DEPARTMENT OF VETERINARY SCIENCES

PhD in VETERINARY SCIENCES FOR ANIMAL HEALTH
AND FOOD SAFETY

XXXIV cycle

TITLE:

NEXT GENERATION SEQUENCING TO IDENTIFY POTENTIAL MOLECULAR TARGETS IN KINASE DOMAIN OF CANINE OSTEOSARCOMA

PhD CANDIDATE:
Dr CECILIA GOLA

SUPERVISOR:
Prof RAFFAELLA DE MARIA

PhD COORDINATOR:
Prof MARIA TERESA CAPUCCHIO

SCIENTIFIC DISCIPLINARY SECTOR:
ANATOMIC PATHOLOGY

ACADEMIC YEARS
2018-2021

CONTENTS

3. RESULTS

3.1 Canine osteosarcoma cell lines as valuable translational *in vitro* model

3.2 Polo-like kinase 1 as a potential target in c-Myc-overexpressing canine osteosarcoma

PREFACE

The scientific results discussed in the present thesis have led to the publication of the paper entitled "Genomic and Transcriptomic Characterization of Canine Osteosarcoma Cell Lines: A Valuable Resource in Translational Medicine" in *Frontiers in Veterinary Science*. A second paper entitled "The mitotic regular polo-like kinase 1 as potential therapeutic target for c-Myc-overexpressing canine osteosarcomas" is under review in the *Veterinary and Comparative Oncology* journal.

- **Gola**, C., Giannuzzi, D., Rinaldi, A., Iussich, S., Modesto, P., Morello, E., Buracco, P., Aresu, L., De Maria, R. Genomic and Transcriptomic Characterization of Canine Osteosarcoma Cell Lines: A Valuable Resource in Translational Medicine. Front Vet Sci. 2021 May 17;8:666838.
- **Gola** C., Licenziato L., Morello E., Iussich S., Accornero P., Modesto P., Buracco P., Aresu L., De Maria R. The mitotic regular polo-like kinase 1 as a potential therapeutic target for c-Myc-overexpressing canine osteosarcomas. Vet Comp Oncol. 2021 (under review).

As a by-product of parallel analyses, other two studies involving the PhD candidate, both as first author and as co-author studies, have been conducted.

Aside from the activation of oncogenic signalling pathways, microenvironmental stimuli, such as hypoxia, are known to play a role in cancer progression both in humans and dogs. *Ex vivo* and *in vitro* assays were performed to evaluate the prognostic value of HIF-1α and its downstream effectors, namely GLUT-1, VEGF-A and CXCR4, in canine osteosarcoma. The *in vitro* regulation of these hypoxia-regulated factors, as well as the biological effects of a chemically induced hypoxic state by $CoCl_2$ treatment, were also investigated in two canine osteosarcoma cell lines (Appendix 1). In a second paper, the functional effects of Toceranib phosphate (Palladia, Zoetis) were studied in seven primary osteosarcoma cell lines. An orthotopic mouse model was developed to further test the biological and pharmacological effects of this kinase-targeted therapy *in vivo* (Appendix 2).

1) **Gola**, C., Iussich, S., Martano, M., Gattino, F., Morello, E., Martignani, E., Maniscalco, L., Accornero, P., Buracco, P., Aresu, L., De Maria, R. (2020) Clinical significance and in vitro cellular regulation of hypoxia mimicry on HIF-1α and downstream genes in canine appendicular osteosarcoma. The Veterinary Journal, 264:105538.
2) Sánchez-Céspedes, R., Accornero, P., Miretti, S., Martignani, E., Gattino, F., Maniscalco, L., **Gola**, C., Iussich, S., Martano, M., Morello, E., Buracco, P., Aresu, L., De Maria, R. (2020) In vitro and in vivo effects of toceranib phosphate in canine osteosarcoma cell lines and associated xenograft orthotopic model. Veterinary Comparative Oncology, 18(1), 117-127.

ABSTRACT

Osteosarcoma (OSA) is a malignant mesenchymal tumour representing the most common bone neoplasia in both human and canine patients. In dogs, this tumour is characterised by a rapid growth and high metastatic rates. Despite significant improvements in surgical and chemotherapeutic treatments, most dogs perish within a year from the diagnosis, indicating a need for the identification of specific tumour targets to develop novel treatment strategies.

Canine OSA shares key features with its human counterpart, such as clinical presentation, histopathological features, biological behaviour, and response to therapies, as well as molecular features including aberrant expression and mutation of driver genes.

Furthermore, canine OSA is a spontaneously occurring tumour that accurately recapitulates human OSA tumour heterogeneity, microenvironment, and host immune response, with a 27 times higher incidence in dogs compared to humans.

Over the last decade, Next-Generation Sequencing (NGS) technologies have provided crucial insights into the mechanisms driving the pathogenesis and progression of human OSA. In the last years, deep characterization of animal models by NGS has been gradually included as well, finding its main application in comparative oncology.

Cancer cell lines are considered valuable models in basic cancer research, drug discovery, and translational medicine. Also, the recent profiling of a large panel of human cancer cell lines with omics technologies has empowered data-driven precision medicine. Despite the substantial number of studies in veterinary oncology, an analogous dataset modelling canine cancer cell lines is currently unavailable.

The first goal of this PhD program was to provide a comprehensive molecular characterization of a number of canine OSA cell lines, by an integrative analysis of Whole-Exome Sequencing and RNA sequencing data, recapitulating *in vivo* canine OSA pathogenesis and allowing future investigations on the functional implications of their mutational and transcriptomic profiles.

Given the relevant role of protein kinases in the development and growth of cancer cells, particular attention was given to the mutations affecting the kinome. The second aim of this project was to select a specific kinase inhibitor based on the mutational and transcriptomic profiling of these cell lines to evaluate its biological effects and cell line response to target therapy.

The results of my PhD provide valuable insights into the molecular mechanisms of a large number of canine OSA cell lines. Furthermore, these data strongly confirm the role of the dog as a naturally occurring model for human OSA, and assess canine OSA cell lines as a valuable translational model to empower prospective *in vitro* studies both in humans and in dogs, allowing future investigations of their functional implications and drug response.

LIST OF ABBREVIATIONS

APC	APC Regulator of WNT Signalling Pathway
AXL	AXL Receptor Tyrosine Kinase
BRCA1, **BRCA2**	BRCA1 and BRCA2 DNA Repair Associated
CCNE1	Cyclin E1
HER2/ERBB2	Erb-B2 Receptor Tyrosine Kinase 2
CDKN2A, CDKN2B	Cyclin-Dependent Kinase Inhibitor 2A and 2B
DMD	Dystrophin
FANCA	FA Complementation Group A
FBXW7	F-Box And WD Repeat Domain Containing 7
IGF-1/IGF-1R	Insulin Like Growth Factor 1 and receptor
MET	MET Proto-Oncogene Receptor Tyrosine Kinase
RON	Macrophage Stimulating 1 Receptor
EGFR	Epidermal Growth Factor Receptor
STAT3	Signal Transducer And Activator Of Transcription 3
PDGFR/PDGFR	Platelet Derived Growth Factor and receptor
MMPs	Matrix Metallopeptidases
ATM	Ataxia Telangiectasia Mutated
ATR	Ataxia Telangiectasia And Rad3-Related Protein
CHK1, CHK2	Checkpoint Kinase 1 and 2
CDK4	Cyclin Dependent Kinase 4
FOXO	Forkhead Box O1
GSK3	Glycogen Synthase Kinase
PIP2, PIP3	Prolactin Induced 2 and 3
PDK1	Pyruvate Dehydrogenase Kinase
JAK-STAT	Janus Kinase and Transducer And Activator Of Transcription
KIT	KIT proto-oncogene Receptor Kinase
KRAS	Kirsten Rat Sarcoma viral oncogene homolog
GRM4	Metabotropic glutamate receptor
NF1	Neurofibromin 1
NOTCH1	Notch Receptor 1
LRP1B	LDL Receptor Related 1B
ARID1A	AT-Rich Interaction Domain
MAPK/ERK	Mitogen-Activated Protein Kinase
MDM2	Mouse Double Minute homolog
MED12	Mediator Complex Subunit

MYC	Avian Myelocytomatosis viral homolog
NFATC2	Nuclear Factor Of T Cells 2
TET2	Tet Methylcytosine Dioxygenase
NFIB	Nuclear Factor I
NF-κB	Nuclear Factor Kappa-light-chain-enhancer activated B cells
AKT	Protein kinase B
PIK3CA	Phosphatidylinositol-4,5-Bisphosphate 3-Kinase Catalytic Alpha
PLK1	Polo Like Kinase
PTCH1	Patched 1
WRN	WRN RecQ Like
ALK	ALK Receptor Tyrosine
PMS2	PMS1 Homolog 2
RB1	Retinoblastoma 1
PTEN	Phosphatase And Tensin
RET	Ret Proto-Oncogene
RUNX2	RUNX Family Transcription 2
DLG2	Discs Large MAGUK Protein 2
SETD2	SET Domain Containing Histone Lysine Methyltransferase
mTOR	Mechanistic Target Of Kinase
SDHA	Succinate Dehydrogenase Complex Subunit A
TGFB1	Transforming Growth Factor 1
TP63	Tumour Protein P63
NTRK1	Neurotrophic Receptor Tyrosine 1
EZR	Ezrin
TP53	Tumour Protein P53
TSC2	TSC Complex Subunit
RHEB	Ras Homolog, MTORC1
VEGF/VEGFR	Vascular Endothelial Growth and receptor

1. INTRODUCTION

1.1   Innovative approaches for cancer research

Cancer is a genetic disease driven by heritable or somatic mutations that trigger uncontrollable cell growth evading host-cell control mechanisms[1]. The analysis of tumour's DNA sequence provides meaningful information to unravel the underlying pathogenic mechanisms. However, for decades the study of tumour biology was limited to a single-gene approach, which proved to be unable to describe the complexity of the disease[2].

Next-Generation Sequencing (NGS) refers to a revolutionary large-scale DNA and RNA sequencing (RNA-seq) technology that enabled an outbreak in the knowledge of cancer biology, including the characterization of molecular cancer subtypes, the identification of driver genes implicated in tumorigenesis and cancer progression, and the development of targeted therapies[3].

NGS can unveil single nucleotide variants (SNV), small insertions and deletions (indels), complex structural rearrangements and copy number aberrations (CNAs) across cancer's genome. The targeted enrichment encompassing all exons of protein-coding genes, as in whole-exome sequencing (WES), allows a higher coverage over regions of interest and potentially simplifies the bioinformatic interpretation of NGS data[4].

NGS has also revolutionized the study of the tumour transcriptome by the identification of differentially expressed genes, gene fusions, small RNAs and aberrantly spliced isoforms. Furthermore, RNA-seq unveiled the profound influence that cancer tissue microenvironment holds on gene expression[5].

In the last decade, the advances in NGS technologies together with the decrease of costs and the emergence of the dog as a valuable model for human cancer, have led to an exponential increase of studies on canine tumours to better understand the pathogenesis of disease and bridging to a new era of molecular pathology and personalised medicine. So far, WES, whole-genome sequencing (WGS) and RNA-seq have been performed on canine osteosarcoma[6-8], hemangiosarcoma[9,10], melanoma[11-13], lymphoma[14-16], mammary gland tumour[17], glioma[18], mast cell tumour[19] and transitional cell carcinoma of the urinary bladder[20,21].

Despite the many advantages provided by NGS techniques, numerous pitfalls remain, including the requirement for expertise in both the laboratory and in the bioinformatic data analysis. Furthermore, this latter requires the development of bioinformatic pipelines and workflows customized to the dog genome, since the majority of tools have been designed for humans and mice[22]. Also, the difference in annotation between the canine and human genome complicates the determination of the function of some genes and biological pathways, which may not always be pursued in dogs or needs several computational handovers.

1.2   Cell lines as valuable *in vitro* models

Cancer cell lines are considered valuable pre-clinical models in basic cancer research, drug discovery, and translational medicine[23,24].

The advent of new genomic technologies revealed that genetic heterogeneity is inherent across different tumours as well as within histological tumour subtypes and some intratumoral cell populations[25]. Interestingly, cancer cell lines retain most of the genetic properties of the tumour of origin[24], which has led to renewed interest in these as crucial tools to investigate the effects of molecular alteration on cancer biology and therapeutic response.

The molecular characterization of cancer cell lines with omics technologies in human medicine has empowered data-driven precision medicine and the usefulness of such models in medical research. Notably, recent studies built comprehensive databases depicting the genetic profile of most of cancer cell lines available, providing an important resource that facilitates the selection of the most appropriate *in vitro* model system for research[24,26].

Even though canine cancer cells have been used in oncologic research over decades, their mutational profiles have never been investigated thoroughly and cell line panels analogous to those in human medicine are currently unavailable[23]. Since the integration of genomic data with drug screening is fundamental for the development and pre-clinical evaluation of novel treatments, the deep mutational analysis of such *in vitro* models will allow the identification of new therapeutic targets and offer valuable tools in translational medicine[27,28].

In vitro canine cancer cell lines are not only fundamental for the understanding of cancer biology in veterinary patients but are also regarded as excellent comparative models of the human counterpart[23]. The implementation of comprehensive panels of canine cancer cell lines, integrating genotypic, phenotypic and pharmacologic data, and paralleling data available in human medicine, will therefore facilitate comparative analyses and create new and meaningful biological knowledge that will benefit both dogs and humans.

1.3   Comparative oncology and animal models

The considerable biological complexity of human cancer has stimulated the development of appropriate experimental models able to mimic cancer biology and represent the cellular properties of the disease in a natural and spontaneous manner. Specifically, animal models play a key role in unveiling the mechanisms and aetiology of cancer and in the development and improvement of therapeutic strategies[29].

In the past decade, the mouse has been frequently used as a model for genetic studies in mammals, due to advantages like the small size, the average lifespan of about 2 years and the short gestation

period[30]. Although crucial to investigate oncogenic mechanisms as well as responses to treatment, murine models of cancer showed significant limitations when used to study complex human diseases[31]. For instance, mouse models are unable to recreate some key characteristics that outline human cancer, such as long latency periods, tumour cell heterogeneity, genetic instability, and immune system functionality[32].

On the other side, naturally occurring tumours in pet dogs develop in the presence of an intact immune system, share a wide variety of epidemiologic, biologic, and clinical features with human cancers and are characterized by interindividual and intra-tumoral heterogeneity. Furthermore, companion animals share the same environment and risk factors as humans, asserting themselves as attractive and underused models in oncology research[27].
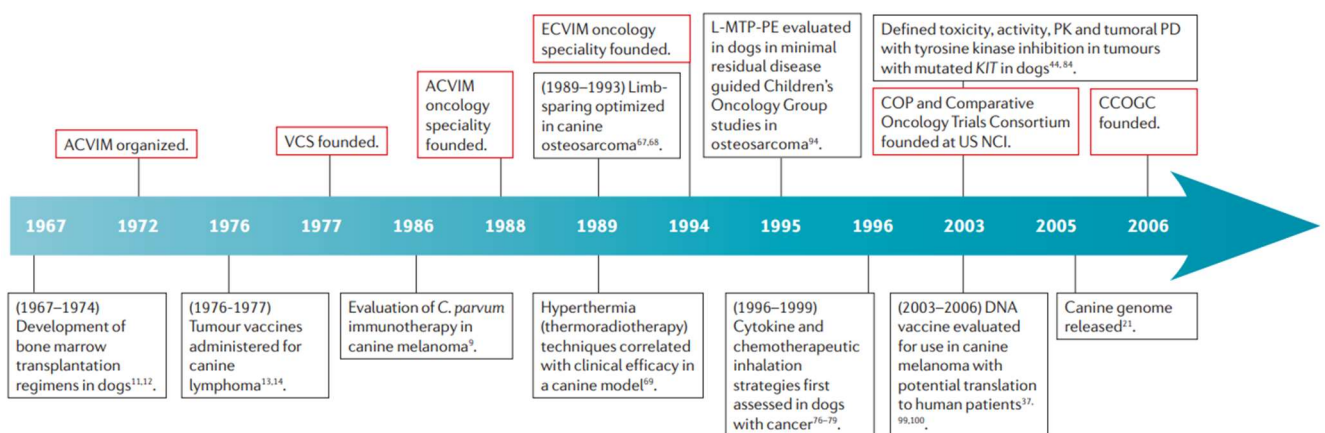
Figure 1. Historical timeline for on the use of pet dogs in cancer research[33]

Nevertheless, a deeper understanding of the genomic landscape of canine tumours that drives cancer initiation and progression, evasion of the host immune system, response to therapy and acquisition of resistance, is needed to fully realize their value as a complementary animal models[34,35].

Cross-species genomics studies represent a unique opportunity to identify common and clinically relevant regions of genomic changes that provide insight into the pathogenetic mechanisms of disease and translational drug development strategies. Multiple advantages are provided by the structure of the canine genome. For instance, dogs are highly homologous to humans in genetic and protein sequence conservation[36,37]. Indeed, in a number of canine malignancies, such as melanomas, osteosarcomas, and non-Hodgkin's lymphomas, gene expression profiles and cancer-associated genomic profiles showed numerous homologies with their human counterparts[38]. Also, druggable pathways in human oncology, including JAK-STAT, PI3K/AKT, MAPK and NF-κB, have been recognized in several canine cancer types, supporting the ongoing development of targeted therapies[21,23,39].

The constant improvement of the canine genome annotation, deposition of genomic data into public repositories and the advent of canine-specific tools have facilitated genomic, transcriptomic, and

proteomic investigations, drawing a parallel with human oncology[40]. However, further comprehensive multi-omics profiling studies are needed in canine cancer research.

General advantage	Underlying principles
Cancer develops spontaneously	Immunocompetent host
	Shared environmental factors may underlie aetiology
	Tumour heterogeneity and analogous tumour microenvironment
Analogous diagnostic and staging methods	Advanced imaging methods (ultrasound, PET/CT, MRI) available
	Staging criteria in veterinary oncology modelled after WHO criteria
	Similar biomarkers
Shortened life span	Trial outcomes reached in a shorter time frame for
	Drug toxicity and disease behaviour over lifetime of a patient
More control over confounding variables	Lifestyle choices (alcohol and tobacco consumption, drug use)
	Less variability in diet
	Hormonal status (possibility to study the disease in neutered subjects)
Ability to study therapy with minimal residual disease setting	Study of natural post-surgical disease behaviour
	Lifetime monitoring for metastatic disease
Availability of genetic and pedigree information	Canine genome defined
	American Kennel Club and other breed registration records available
Simplified trial approval process	Standard-of-care not always defined
	Animal care often provided by pet owner at home
	Pet owner consent for trial enrolment
Biosampling advantages	Ample variety and quantity of samples available
	Repeated tumour and normal tissue biopsy
	Common necropsy
Additional funding opportunities	Breed-related diseases funding
	Animal foundation funding
	Veterinary scientific community

Table 1. Advantages of pet dog cancer clinical trials[41].

1.4 Canine osteosarcoma as a model for the human disease

Osteosarcoma (OSA) is the most common primary bone malignancy in both dogs and humans[42]. However, the disease is significantly more common in dogs than in people, with an incidence rate that is averagely 27 times higher[43].

OSA has a bimodal age distribution, with a different peak of onset in the two species. In humans, OSA affects mainly children in the second decade of their life, whereas in dogs, it tends to occur in middle-aged to older subjects[44]. Furthermore, specific dog breeds, such as Rottweilers, Greyhounds, Great Danes, Saint Bernard, and Irish wolfhounds, are at disproportionate risk for the development of OSA[45]. OSA mostly occurs in the proximity of the metaphyseal growth plates of the long bones of the appendicular skeleton. Given the occurrence in anatomic sites of greater growth and the higher incidence in taller individuals, growth factors are thought to play an important role in the pathogenesis of this tumour[45]. In dogs, this association is further supported by an increased prevalence of the disease in large and giant breed dogs and the expression of the insulin-like growth factor-1 (IGF-1) receptor

and ligand in canine OSA cells[46,47]. Nevertheless, the development of neoplasia involves a complex interaction of environmental and physical factors, genetic susceptibility, and acquired molecular aberrations[45].

Canine OSA shares many features with the human counterpart, including a similar natural history of the disease, the dysregulation of several key molecular pathways, and similar responses to therapies such as surgery and chemotherapy[48,49].

In both people and dogs, OSA is characterized by a heterogeneous microscopic appearance, is divided into similar histologic subtypes, the most being the osteoblastic form, and is characterized by a high histological grade[42].

Although few canine and human patients display metastases at diagnosis by radiographic investigation, the vast majority of patients develop gross metastases despite the therapeutic management of the primary tumour, indicating that a microscopic tumour spread occurs in the early course of the disease[50].

Notwithstanding the significant improvements in surgical and chemotherapeutic treatments, about 30 to 40% of children still die from disease and over 90% of dogs perish within a year from the diagnosis, indicating a need for identification of specific tumour targets to develop novel treatment strategies[51].

Being that canine OSA recapitulates many biologic and molecular features of human OSA, with a higher incidence rate and a faster disease progression, this tumour represents a useful comparative model that can be used to interrogate novel therapies within a compressed timeline[45].

Moreover, dogs have a relatively simplified genetic determined by breeds, and empower the understanding of somatic and germline contributions to diverse cancer traits, reinforcing the role of the dog model for translational research[27,52].

Variable	Canine OSA	Human OSA
Incidence	> 10,000/year	> 1,000/year
Age of onset	Middle-aged to older dogs	Adolescent disease
	Peak onset 7-9 years	Peak onset 10-14 years
	Second small peak at 18-24 months	
Race/breed	Large or giant breed	
	Predisposed breeds: Scottish Deerhound, Rottweiler, Greyhound, Great Dane, Saint Bernards, Irish Wolfhounds	None
Site	75% in the appendicular skeleton	90% in the appendicular skeleton
	Metaphyseal region of long bones	Metaphyseal region of long bones
	Distal radius > proximal humerus > distal femur	Distal femur > proximal tibia > distal humerus
Aetiology	Generally unknown	Generally unknown
	Ionizing radiation	Ionizing radiation
	Bone infarcts	Bone infarcts
	Chronic osteomyelitis	Chronic osteomyelitis
	Metallic orthopaedic implants	Paget's disease (>40 years of age)
	Previous fracture/trauma	
Histopathology	95% high grade	85-95% high grade

Percentage clinically confined to the limb at presentation	85-90%	85-90%
Metastatic rate without chemotherapy	90% before 1 year	85-90% before 2 years
Metastatic sites	Lung > bone > soft tissues	Lung > bone > soft tissues
	Regional lymph nodes 4.4%	Regional lymph nodes 10%
Prognostic factors	Appendicular/axial tumour location	Appendicular/axial tumour location
	Proximal humeral location	Proximal humeral location
	Metastasis at diagnosis	Metastasis at diagnosis
	Incorporation of chemotherapy	Incorporation of chemotherapy
	Postoperative limb sparing infection	Postoperative limb sparing infection
	Tumour size	Tumour size
	Serum alkaline phosphatase	Local tumour recurrence
		Percentage of tumour necrosis
		Age (>65 years of age)

Table 2. Comparison of Canine and Human OSA Characteristics[45]

1.5 Molecular characterization of canine and human osteosarcoma

Given the numerous clinicopathological and molecular features shared with human osteosarcoma, canine OSA represents a highly characterized model with translational relevance to the human counterpart[40,53].

Although differences in mutational signatures are reported, the biological effects of these molecular alterations, such as tumour progression, resistance to therapy, immune evasion, resistance to apoptosis and metastasis, are superimposable in the two species[54]. This offers a unique opportunity to leverage the canine patient population in the field of pharmacogenomics and personalized therapy for both canine and human OSA[43].

The translational relevance of canine OSA was first assessed in a comparative array-based gene expression profiling, in which canine and human primary tumours show indistinguishable transcriptomic profiles[54]. Similarly, further studies documented numerous similarities between canine and human OSA with respect to structural variations and mutations involving key genes, being *TP53*, *RB1*, *MYC*, *PTEN* and *CDKN2A*[38]. Recently, NGS studies also revealed a low tumour mutational burden (~2 mutations per Mb) in both species[6] and common mutations in several pathways and driver genes[6,7].

Specifically, resistance to apoptosis following the inactivation of the p53 pathway, cell cycle progression regulated by *MYC*, loss of tumour suppressor *DLG2* and loss of DNA damage repair mechanisms such as loss of *PTEN*, were reported. The dysregulation of the tumour suppressor *SETD2*, an epigenetic modifier involved in various human tumours has only recently been identified in canine OSA[6,10,38].

As described in humans, dysregulation of the ERK and PI3K-mTOR pathways was retrieved by whole-genome sequencing and RNA-seq of canine OSA[40].

However, some differences were also identified, for instance canine OSA lacks mutational signatures of *BRCA1* or *BRCA2* deficiency involved in the homologous recombination pathway[7].

Two recent studies also characterized the genomic profile of several canine cancer cell lines, including canine OSA cell lines, and investigated their relevance in comparative oncology[23,55]. Notably, driver mutations in MAPK/ERK and PI3K/AKT signalling pathways were identified in canine OSA cell lines, and an anti-proliferative target inhibition using trametinib showed encouraging results, while alterations of the *TP53* pathway were detected in non-sensitive cell lines[55].

Factor*	Functions in canine OSA
p53	*p53* mutated and overexpressed in OSA cell lines and primary tumours
	Loss of heterozygosity of *p53* in OSA tumours
RB	*RB1* copy number loss and reduced or absent RB1 protein expression in OSA tumours
PTEN	*PTEN* deleted and downregulated in OSA cell lines
	PTEN copy number loss in OSA tumours
MYC	*MYC* copy number gain in OSA tumours
	MYC amplification detected in high percentage of Rottweilers bearing OSA
CDKN2A/B	Inherited risk gene loci (150 kb upstream of the genes *CDKN2A/B*) identified in OSA tumours from high-risk breeds
ErbB-2/HER-2	*HER2* mRNA overexpressed in OSA cell lines and tumours
IGF-1/IGF-1R	IGF-1/IGF-1R expressed in OSA cell lines (enhanced anchorage-independent growth and invasion in response to IGF-1)
RON/Met/EGFR	MET expressed in OSA cell lines (enhanced invasion/migration in response to stimulation with ligand HGF)
	MET expressed in OSA tumours
	EGFR ad Ron expressed in OSA cell lines and tumours
	Co-association of Met with EGFR and Ron in OSA cell lines
STAT3	Constitutive activation of STAT3 in OSA tumours and cell lines (enhanced cell survival and proliferation)
	Oncostatin M expressed in OSA tumours and promotes STAT3 activation, VEGF production and invasion in OSA cell lines
mTOR	mTOR activation in canine OSA cell lines
	Inhibition of mTOR pathway decreases cell survival
ezrin	High ezrin expression in OSA tumours associated with early metastasis
	Activation of ezrin through PKC enhances cell migration
PDGFs/PDGFRs	PDGF-A/B and PDGFRα/β expressed in OSA tumours
	PDGFRα/β and PDGF-A overexpressed in OSA cell lines
MMPs	OSA cell lines express high levels of MMP-2/-9
miR-134 miR-544	Decreased expression of miR-134 and miR-544 (orthologous to the human 14q32 miRNA cluster) in OSA tumours associated with shorter survival

*Bold indicated molecular and genetic factors similarly altered in human OSA

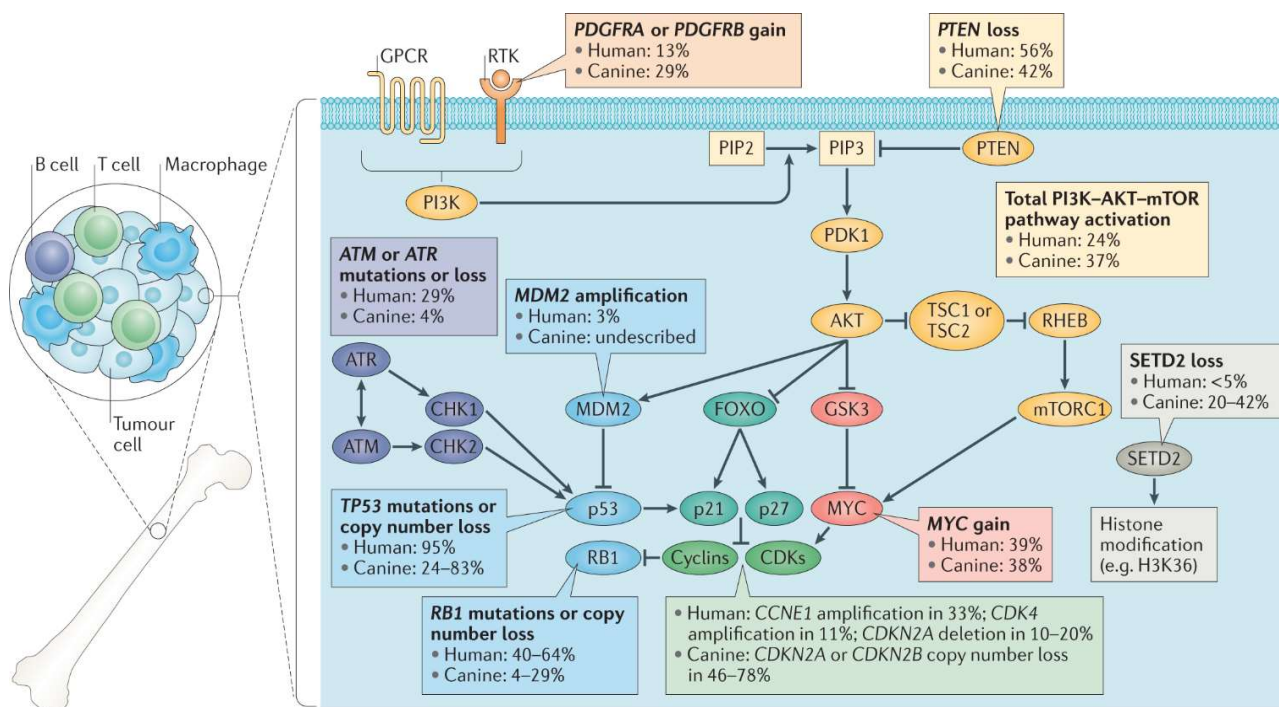Table 3. Molecular and Genetic Factors Associated with Canine OSA[45]

Figure 2. Comparative molecular features of canine and human OSA[40]

1.6   The kinome and kinase-targeted therapy in canine and human osteosarcoma

Hundreds of kinases regulate numerous intricated cellular processes, such as cell proliferation, survival, and migration, and their dysregulation contributes to various hallmarks of cancer[56].

High-throughput analyses of gene function have characterized the kinome, meaning the complete set of protein kinases encoded in the genome, in human cancers and has provided crucial insights into the functional role of specific kinases in cancer and the effect of kinome remodelling on anticancer drugs sensitivity[57]. Furthermore, recent genomic studies on kinases, have uncovered genetically inherited variants that are associated with cancer initiation, promotion, progression as well as recurrence[58].

In human medicine, the characterization of the activation status of tyrosine kinases (TKs) underlined a high frequency of mutations in well-characterized protein kinases[59]. For instance, EGFR is known to be commonly dysregulated in glioblastoma and lung adenocarcinoma; *BRAF* is mutated in over 50% of thyroid cancers and cutaneous melanomas; PDGFR α and β and c-Kit are implicated in highly malignant human tumours, including breast cancer. In addition, a number of TK receptors, such as VEGFRs, FGFRs are important in promoting tumour angiogenesis[60]. A comprehensive list of TKs receptors and non-receptor TKs implicated in human cancer is provided in the tables below (Table 4 and Table 5).

Receptor tyrosine kinase dysregulation	Associated cancer	Receptor tyrosine kinase dysregulation	Associated cancer
EGFR (HER-1)	Breast, ovary, lung, glioblastoma multiforme and others	TRKA	Papillary thyroid cancer, neuroblastoma
ERBB2 (HER-2)	Breast, ovary, stomach, lung, colon and others	TRKC	Congenital fibrosarcoma, AML
ERBB3 (HER-3)	Breast	MET	Papillary thyroid, rhabdomyosarcoma, liver, kidney
ERBB4 (HER-4)	Breast, granulosa cell tumours	RON	Colon, liver
IGF-1R	Cervix, kidney (clear cell), sarcomas and others	EPHA2	Melanoma
PDGFRα	Glioma, glioblastoma, ovary	EPHB2	Stomach, oesophagus, colon
PDGFRβ	CMML, glioma	EPHB4	Breast
CSF-1R	CMML, malignant histiocytosis, glioma, endometrium	AXL	AML
KIT/SCFR	GIST/AML, myelodysplasia, mastocytosis, seminoma, lung	TIE	Stomach, capillary haemangioblastoma
FLK2/FLT3	AML	TEK	Tumour angiogenesis
VEGFR1	Tumour angiogenesis	RYK	Ovarian cancer
VEGFR2	Tumour angiogenesis	DDR1/2	Breast, ovarian cancer
VEGF3	Tumour angiogenesis, Kaposi sarcoma, haemangiosarcoma	RET	Thyroid (papillary and medullary), multiple endocrine neoplasia
FGFR-1	AML, lymphoma, several solid tumours	ROS	Glioblastoma, astrocytoma
FGFR-2	Stomach, breast, prostate	ALK	Non-Hodgkin lymphoma
FGFR-3	Multiple myeloma		

AML, Acute myeloid leukaemia; CMML, Chronic myelomonocytic leukaemia.

Table 4. TK receptors associated with cancer development in humans[61]

Non-receptor tyrosine kinase dysregulation	Associated cancer	Non-receptor tyrosine kinase dysregulation	Associated cancer
ABL1	CML, AML, ALL, CMML	SRC	Colon, breast, pancreas, neuroblastoma
ARG	AML	YES1	Colon, melanoma
BRK	Breast	LCK	T-cell ALL, CLL
JAK1	Leukaemias	SYK	Breast
JAK2	AML, ALL, T-cell childhood ALL, atypical CML	FAK	Adhesion, invasion, and metastasis of several tumours
JAK3	Leukaemia, B-cell malignancies	PYK2	
FGR	AML, CLL, EBV-associated lymphoma		

ALL, Acute lymphoblastic leukaemia; AML, Acute myeloid leukaemia; CMML, Chronic myelomonocytic leukaemia; CLL, Chronic lymphocytic leukaemia; EBV, Epstein Barr virus.

Table 5. Non-receptor TKs associated with cancer development in humans[61]

Although tyrosine kinase dysfunction has been extensively investigated in human medicine, it is far less characterized in veterinary oncology. Nevertheless, evidence suggests that kinases are frequently dysregulated in malignant tumours affecting veterinary patients as previously reported in humans.

Several authors have identified mutations of *KIT* in canine mast cell tumours which have been associated with local recurrence and poor prognosis. Mutations of this receptor have also been identified in canine gastrointestinal stromal tumours which showed to be nearly identical to their human counterpart. Similarly, mutations in *KIT* were also identified in feline mast cell tumours[62].

In canine mammary tumours, EGFR acts as a promoter of cell migration and invasion and is associated with an aggressive tumour behaviour[63,64]. Vaccine-associated sarcoma in cats was shown to express high levels of PDGFR-β, indicating the potential for a therapeutic intervention on this latter[65].

In canine OSA, a variety of protein kinases representing potential molecular targets, such as HER2, EGFR, MET, PDGFR, c-Kit, and PKC, have been identified[66].

Given their pivotal role in carcinogenesis and tumour progression, kinases have become an attractive target for the treatment of numerous types of cancer. Single and multiple kinase inhibitors are now targeted therapeutic strategies for the treatment of human malignancies and account for a quarter of all current drug discovery research and development efforts[58].

Recent clinical trials have shown several multi-target tyrosine kinase inhibitors (TKIs) to be effective in the treatment of human OSA[67].
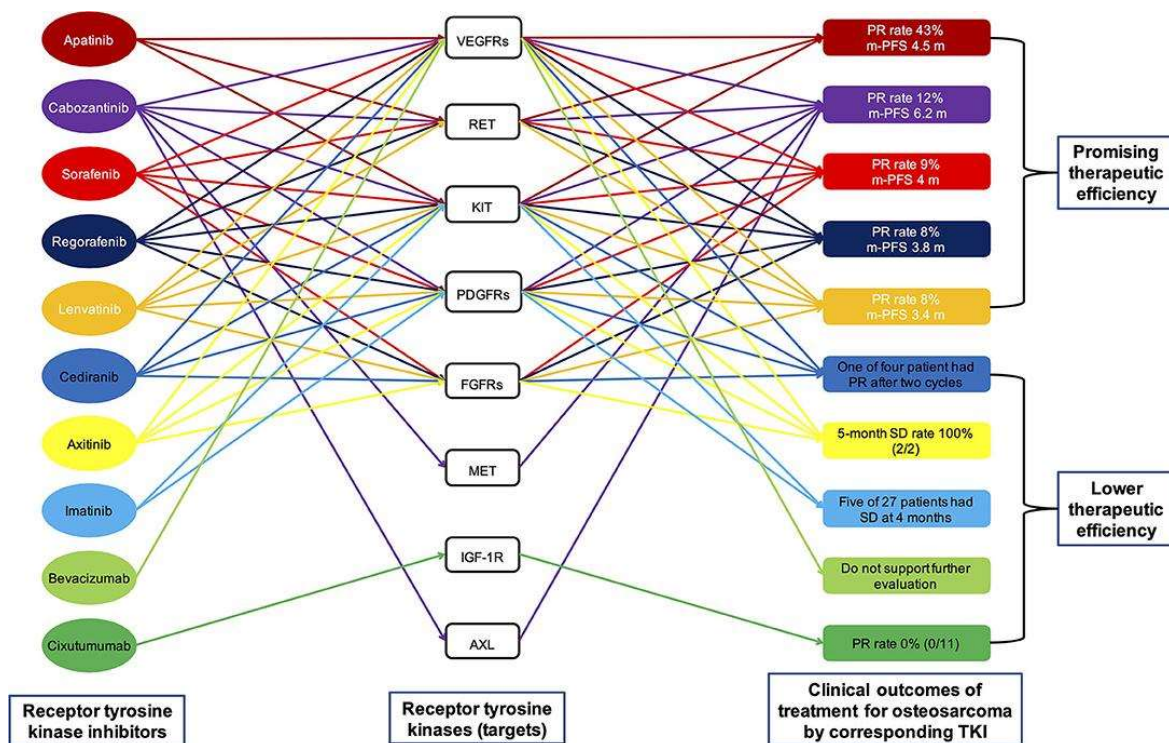

Figure 3. A visual interaction map of the different targets of the different drugs in human OSA[67] (PFS, progression-free survival; TKI, tyrosine kinase inhibitor; PR, partial response; SD, stable disease)

A study screening multiple kinase inhibitors on a panel of canine OSA tumour cell lines showed that the effective concentration and the mechanism of cell death were both cell type- and concentration-dependent. Such variability across cell lines was likely due to variable kinases expression, molecular alterations, degrees of pathway activation, or differences in the origin of the cell lines[66].

The current technologies enabling interrogation of the cancer genome allow, once again, matching the treatment to the tumour characteristics. That is, to select the optimal drug and drug dosage for each patient and thereby to improve patient outcomes.

1.7 Targeting c-Myc stability via polo-like kinase 1 target inhibition

Polo-like kinase 1 (PLK1) is a serine/threonine kinase expressed during the G_2/M-phases of the cell cycle playing a crucial role in cell cycle regulation and the mitotic process[68,69] by acting on chromosome segregation, spindle assembly and cytokinesis[70]. In particular, PLK1 transitions from centrosomes and kinetochores in the early M-phase to the midzone and cytokinetic midbody during the final stages of mitosis[69].
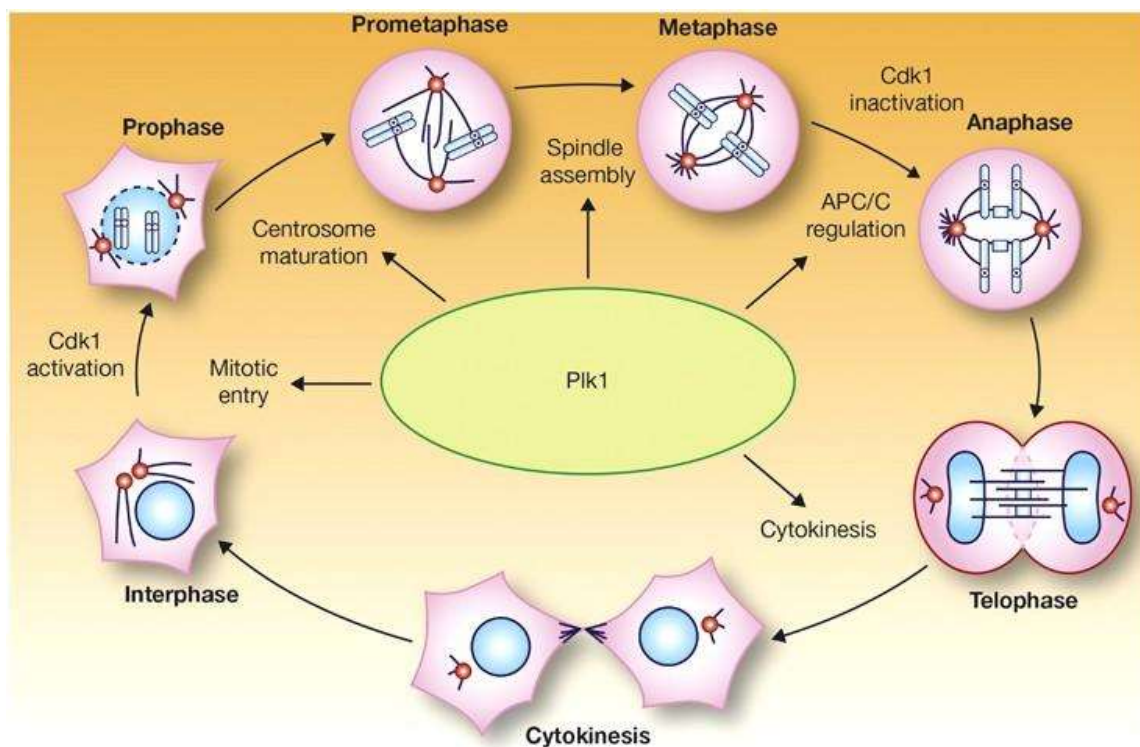

Figure 4. Functions of PLK1 during mitosis[71]

Studies have demonstrated that PLK1 is usually overexpressed in a variety of cancers in human, including OSA[72,73]. Notably, PLK1 overexpression in human OSA is responsible of chromosomal instability and aneuploidy, providing these cells an advantage to overgrow and invade tissue, and is

broadly associated with poor prognosis and disease progression[69]. Conversely, its role in dogs remains unclear.

Since PLK1 inhibition hinders tumour growth by cell cycle arrest leading to cell death[74], it is no surprise that research aims at developing small-molecule PLK1 inhibitors for cancer targeted therapy[69].

This kinase has also been implicated in the molecular crosstalk with important oncogenes, such as c-Myc[75]. c-Myc is a ubiquitous and vital transcriptional factor (TF) involved in a broad spectrum of biological processes, including cell cycle control, apoptosis, and protein synthesis[76]. Additionally, *MYC* is a central oncogenic driver in human and canine tumours being associated with tumorigenesis and sustained tumour growth[77]. In human OSA, c-Myc is frequently overexpressed in human OSA and correlated with the development of metastases and a poor prognosis[75]. Although aberrant activations of *MYC* pathway genes have been previously reported[78], only recently *MYC* activation was correlated with a short disease-free interval in canine OSA[38].

TFs have been considered undruggable targets for a long time due to the lack of defined small-molecule binding pockets[76]. However, advances in the structural characterization of TFs and insights on their interaction with other proteins changed this postulate so far uncovering new therapeutic applications of TFs as cancer drug targets.

It is within this context that functional studies demonstrated that the PLK1/Fbxw7/c-Myc axis creates a positive auto-regulatory signal, sustaining the mutual increased expression of these genes. In particular, PLK1 results essential for c-Myc protein stabilization and accumulation in the cytoplasm, hence allowing its migration into the nucleus where it promotes G_2/M transition and acts as a transcriptional factor[75].
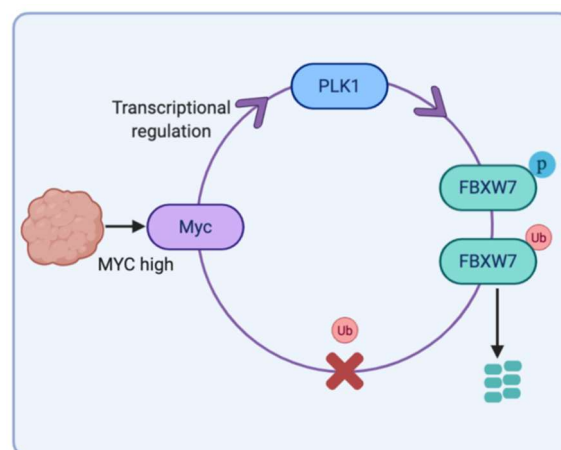

Figure 5. Regulatory Loop of PLK1/Fbxw7/c-Myc [76]

These findings underline the importance of PLK1 inhibitors as promising selective therapies against c-Myc-overexpressing canine tumours, as previously reported in a number of human cancer subtypes where the PLK1-selective inhibitors showed a specific and significant inhibitory effect on cell growth[79].
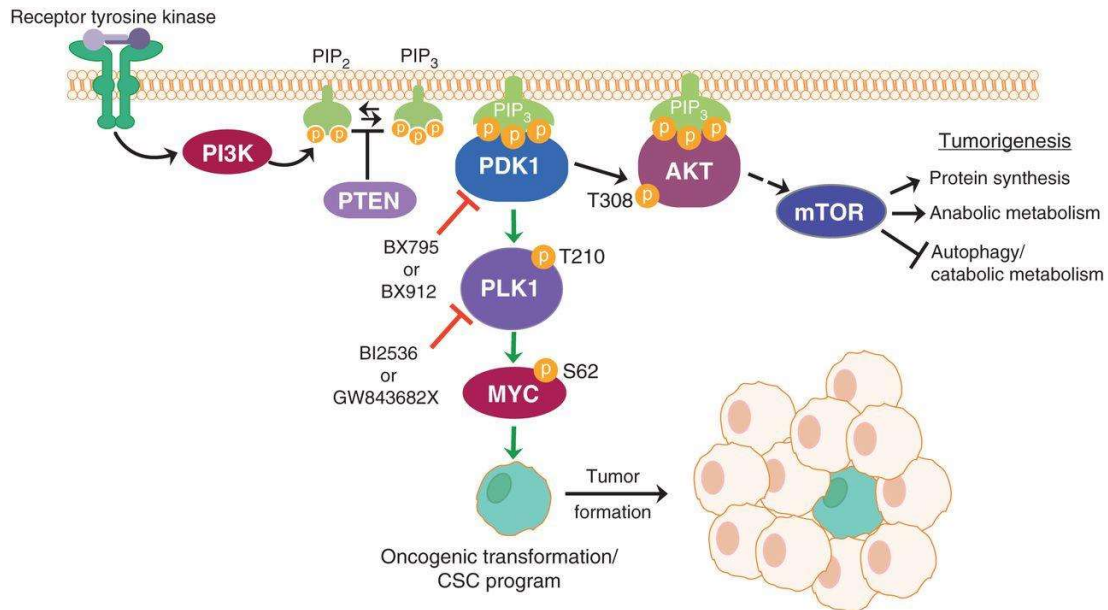
<u>Figure 6</u>. A basic depiction of PLK1-MYC interaction[80]

1.8   Objectives of the PhD research project

During this PhD program, several objectives were defined and developed within the framework of two main projects focused on the study of canine OSA.

In the first project, the purpose was to provide a comprehensive molecular characterization of a panel of canine OSA cell lines as a resource in both comparative and translational oncology, allowing future investigations on the functional implications of their genotypic and phenotypic profiles, and drug response.

An integrated analysis of WES and RNA-seq of eight canine OSA cell lines and one matched pair of primary OSA and normal tissue was performed to describe the mutational landscape of each cell lines, identify recurrently mutated genes and determine variants in putative driver genes having a likely role in canine OSA pathogenesis as well as gene expression aberrations.

Given the relevant role of protein kinases in the development and growth of cancer cells, particular attention was payed to the deregulations of the kinome, with the aim of identifying potential therapeutic target inhibitors addressing the low survival rates of patients bearing OSA.

With this in mind, the goal of the second project was to select a specific kinase inhibitor based on the mutational and transcriptomic profiling of the aforementioned canine OSA cell lines to evaluate their biological behaviour and response to therapy. In particular, we evaluated the biological effects of the selective PLK1 inhibitor, BI 2536, as regulator of cell cycle and modulator of c-Myc expression in one canine OSA cell line overexpressing both *PLK1* and *MYC* in transcriptomic analysis. Furthermore, PLK1 and c-Myc protein expression was evaluated on 53 appendicular canine OSA samples to gain insight into the potential clinical implications of these two proteins.

2. MATERIAL AND METHODS

2.1 Genomic and transcriptomic characterization of canine osteosarcoma cell lines

2.1.1 Sample collection and cell culture

Eight primary canine OSA cell lines and one matched pair of FFPE primary OSA and normal tissue were analysed.

Penny, Wall, Desmond, Sky, Lord, and Pedro cell line were previously established and validated by Maniscalco et al.[81], while D17 (ATCC®CCL183™) and D22 (ATCC®CRL-6250™) were obtained from American Type Culture Collection.

These were cultured in Dulbecco's modified Eagle's medium (DMEM; D17 and D22) and Iscove's standard medium, supplemented with 10% foetal bovine serum (FBS), 1% glutamine, 100 µg/mL penicillin and 100 µg/mL streptomycin. Cells were cultured at 37°C in a humidified atmosphere of 5% CO_2.

The FFPE samples were obtained from the same OSA from which Wall cell line was established.

2.1.2 DNA and RNA isolation from cell lines and FFPE tissues

Genomic DNA (gDNA) was isolated and purified from cell lines and the FFPE samples (Table 6) using DNeasy Blood & Tissue kit (Qiagen, Hilden, Germany) and GeneRead DNA FFPEkit (Qiagen, Hilden, Germany), respectively. gDNA concentration was determined using the Qubit 2.0 Fluorometer (Thermo Fischer, Foster City, CA, USA).

Total RNA was extracted from 6 cell lines (Penny, Wall, Desmond, Sky, D17 and D22; Table 6) using QIAzol Lysis reagent (Qiagen, Hilden, Germany) and purified. Total RNA concentration was determined using the NanoDrop ND-1000 UV-Vis spectrophotometer and its integrity was measured by the Bioanalyzer 2100 instrument (Agilent Technologies, Santa Clara, CA, USA). RNA samples with an RNA integrity number (RIN) ≥8 were considered for the RNA-seq library preparation.

The isolated DNA and RNA were stored at -20°C and -80°C, respectively, until further use.

	Whole-exome sequencing		RNA-sequencing
	Cell line	FFPE sample (matched normal)	Cell line
Penny	X	-	X
Wall	X	X	X
Sky	X	-	X
Desmond	X	-	X
Pedro	X	-	-
D17	X	-	X
D22	X	-	X
Lord	X	-	-

Table 6. NGS sequencing technologies applied in the analysis of eight canine OSA cell lines and one matched FFPE tumour sample

2.1.3 Whole-exome and RNA-sequencing library preparation and sequencing

High-quality whole-genome libraries from 10 samples (8 cells lines and 2 FFPE samples) were prepared using the KAPA HyperPlus Library Preparation Kit (Roche Sequencing and Life Science, Wilmington, MA). Exome capture was executed using Roche's SeqCap EZ Share Prime Developer Kit (Roche Sequencing and Life Science, Wilmington, MA) for non-human genomes following the SeqCap EZ HyperCap Workflow User's Guide. Probes for the exome capture were designed on the target enrichment design of 150 megabases developed by Broeckx and colleagues[82]. The developer's reagent (06684335001) was used in place of COT-1 and index-specific hybridization enhancing oligos were also used. Final concentration and size distribution were tested with the Bioanalyzer 2100 workstation (Agilent Technologies, Santa Clara, CA, USA). The libraries (fragments ranging from 300 to 400 bp) were then sequenced on an Illumina NovaSeq 6000 platform in a paired-end (150 PE) mode. The chosen target sequencing coverage was 200x.

Non-normalized libraries for RNA-seq experiments were prepared using NEBNext® Ultra™ II Directional RNA Library Prep (New England Biolabs) with Sample Purification Beads and NEBNext® Poly(A) mRNA Magnetic Isolation Module (New England Biolabs).

A single-end sequencing (75 SE) was carried out on a NextSeq 500 platform (Illumina Inc., San Diego, CA, USA). The average read depth was 10 million reads.

2.1.4 Whole-exome sequencing data analysis

Quality control prior to alignment was performed on output from Illumina software and was processed by FastQC v.0.11.9 (https://www.bioinformatics.babraham.ac.uk/projects/download.html) software. Trimmomatic was used to select high-quality reads and remove adapter sequences.

Filtered reads were mapped to the canine reference genome (CanFam3.1; Broad Institute, release 99) using BWA software[83]. To verify coverage in the exonic regions, the resulting BAM files were manually inspected using Integrative Genomic Viewer (IGV)[84].

Pre-processing for variant calling was performed following the Genome Analysis Toolkit (GATK) v.4.1 Best Practices (https://gatk.broadinstitute.org/hc/en-us/articles/360035894731-Somatic-short-variant-discovery-SNVs-Indels). Briefly, single nucleotide variants (SNVs) and small insertion and deletions (indels) were identified with GATK Mutect2 tool[85] and filtered for standard parameters of a min-alternate-count of 2, a min-alternate-frequency of 0.05 and read depth > 10.

To reduce germline artefacts, a panel of Normals (PON) was built using GATK CreateSomaticPanelOfNormals tool by downloading public available WES data from 18 non-tumour bearing and unrelated dogs (normal stroma and blood samples) from NCBI SRA database (Supplementary table 1)[55,86]. An additional filter was added to exclude known single nucleotide polymorphisms as annotated in the dbSNP 146 using the Dog Genome SNP Database (http://dogsd.big.ac.cn/)[87]. Distribution and functional consequences of variants were assessed using ANNOVAR. Additionally, missense mutations were categorized according to their pathogenicity using FidoSNP[88]. The detailed WES workflow applied to both canine OSA cell lines and the FPPE samples is summarized in the figure below (Figure 7).
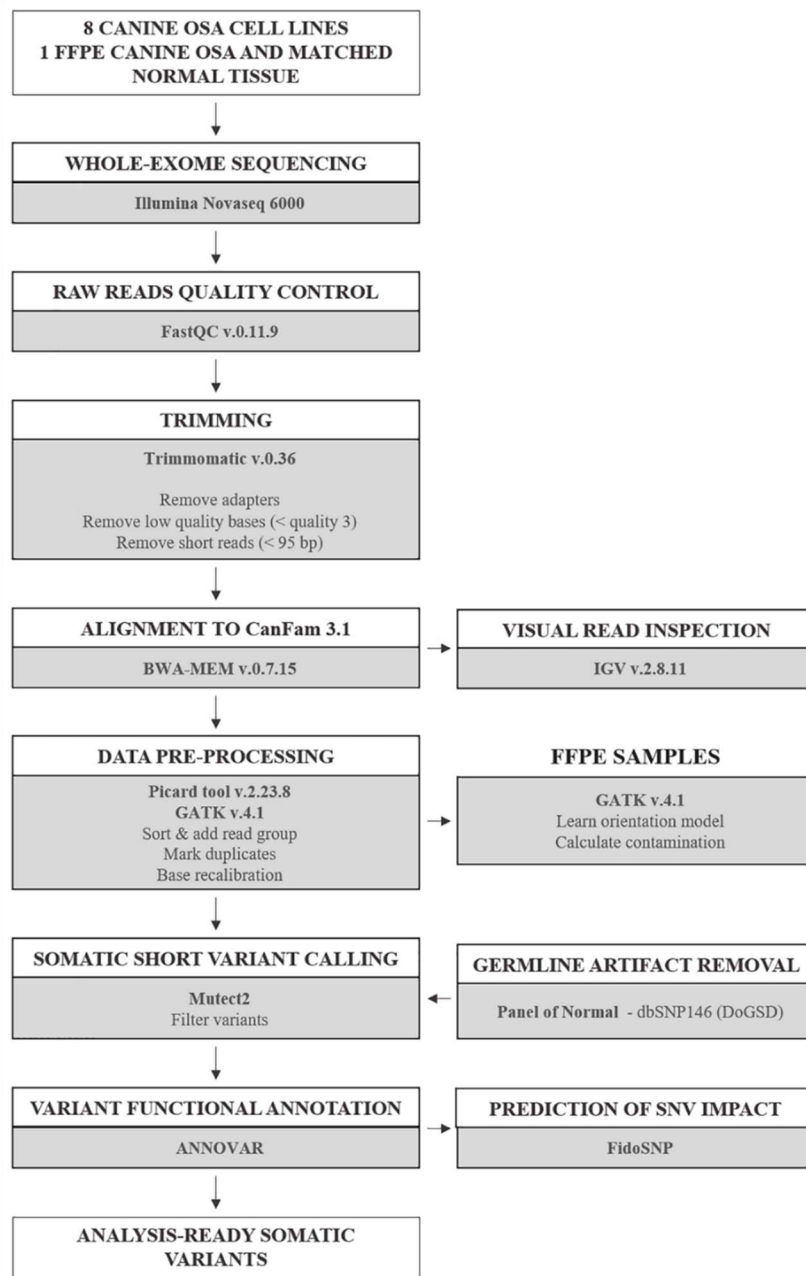
Figure 7. Workflow for whole-exome sequencing short variant discovery, sequential use of tools in evaluation of canine OSA cell lines and FFPE DNA samples.

2.1.5 RNA sequencing data analysis

All RNA-seq analyses were performed using conventional RNA-seq analysis tools[15]. Detailed information is provided in Figure 8. Briefly, post-alignment quality parameters of RNA-seq (insert length, gene-mapping bias, RNA junctions) were evaluated using RSeQC[89] in standard mode. Next, the counts of aligned reads per gene were obtained using htseq-count from the HTSeq[90] software package in single-stranded mode. Only reads that were uniquely aligned were retained. Finally, counts filtering and normalization were performed using EdgeR R package[91]. Counts per million mapped reads (CPM) were then used as unit for inter-sample comparison of gene expression.
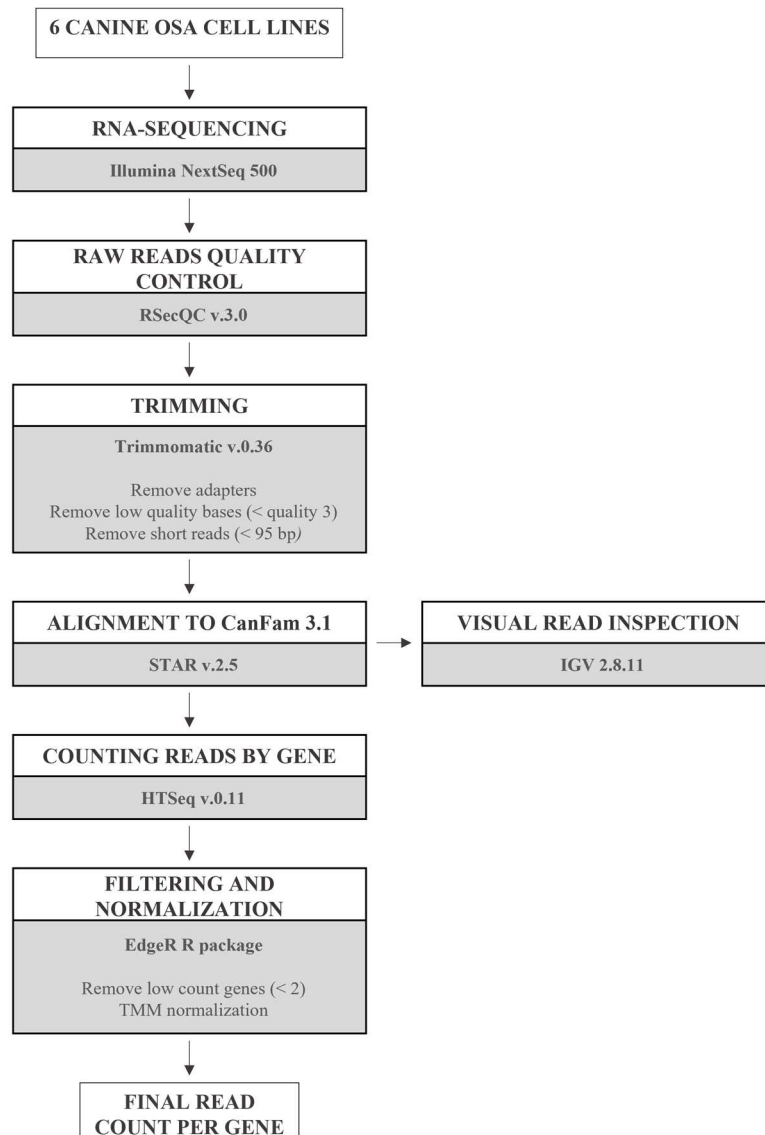
Figure 8. Workflow for RNA-seq analysis, sequential use of tools in evaluation of canine OSA cell lines.

2.1.6 Identification of recurrent variants and putative driver mutations

Annotated variants were subjected to three filtering levels with increasing stringency and designated as follows (Figure 9).

Level 1: variants included the totality of exonic-only SNV and indels retrieved from the variant call described above. These were further filtered for number of reads (min. 2), alternate allele frequency (min. 0.05) and each variant's depth of coverage (min. 10). The resulting variants were analysed to describe the mutational profile of canine OSA cell lines.

Level 2: these were nonsynonymous exonic variants selected from Level 1 to identify recurrently mutated genes having a likely role in canine OSA pathogenesis. Furthermore, variants encoding for

genes commonly mutated in human and canine OSA were also prioritized (Table 7)[6]. Level 3: these were selected from Level 2 protein-coding variants of genes listed in COSMIC Cancer Gene Census, (version 92, https://cancer.sanger.ac.uk/census)[92]. 5' UTR and splice site variants COSMIC-listed genes were also included in the analysis due to their potential impact on protein expression and function. These variants were also manually cross-checked against known oncogenic variants in human OSA available on IntOgen platform (https://www.intogen.org/search?cancer=OS)[93] to identify putative driver mutations.
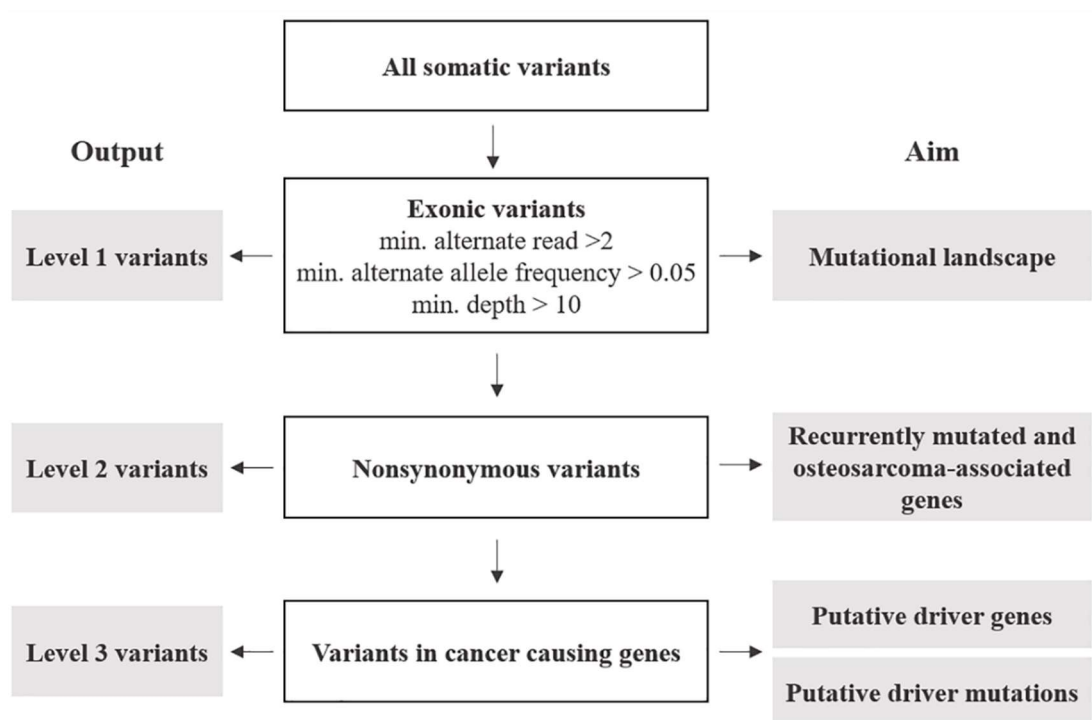

Figure 9. Post-processing of somatic variants: outline of selection criteria, categorization and analyses.

TP53	MMP2	PIK3CA	FANCA	CDH1
RB1	MMP9	FAS	RECQL4	MSH2
PTEN	RANKL	FASLG	NF1	MSH6
RHOC	CTNNB1	DLG2	TSC2	NRAS
RUNX2	PD-L1	CDK4	MLLT2	PALB2
TUSC3	COX2	CDK6	MLLT3	PTCH1
EGFR	PDGFRB	MDM2	DMD	SDHA
NOTCH1	MYC	CARD11	APC	SDHB
MET	CDKN2A	CCNE1	PMS2	GRM4
IGF1	CDKN2B	COPS3	RUNX1	NFIB
HER2	TGFB1	AKT1	KRAS	BLM
MTOR	CXCL8	E1F	NF2	WRN
NTRK1	TP63	SMAD4	RET	SETD2
EZR	BRCA1	ATM	VHL	
CXCR4	BRCA2	ATR	ALK	

Table 7. List of known OSA-associated gene in dogs and humans.

2.1.7 Validation of TP53 mutation

E273K mutation of *TP53* identified in Wall cell line and FFPE tumour sample was validated by Sanger dideoxy sequencing on Wall samples gDNA and Penny cell line (negative control). Briefly, two primers (sense 3'-ATGAGGGTGGCTAGGAGTCA -5') and (antisense 5'-CAGTGCTGGGAAAGAGAGGA-3') spanning the mutated region were designed by PRIMER3 Express software and PCR on gDNA was performed using HotStar Taq (Qiagen) at 58°C (annealing temperature) for 35 cycles. After evaluation of by agarose gel, amplification products were purified by QIAquick PCR Purification Kit (Qiagen).

2.1.8 Data availability statement

The datasets presented in this thesis can be found in online repositories. The names of the repository/repositories and accession number(s) can be found here: https://www.ncbi.nlm.nih.gov/, PRJNA701141.

2.2 Targeting c-Myc via Polo-like kinase 1 inhibition *in vitro* in canine osteosarcoma

2.2.1 Sample collection and clinical data

Fifty-three canine appendicular OSA samples were routinely collected at the Veterinary Teaching Hospital, Department of Veterinary Sciences (University of Turin), upon written consent from dog owners. All dogs were surgically treated with limb amputation or limb-sparing techniques and received adjuvant chemotherapy (doxorubicin, cisplatin, or carboplatin as single agents or combinations). Thoracic radiographs or computed tomography (CT) evaluation was performed to exclude the presence of distant metastases. Follow-up consisted of clinical evaluation and thoracic radiographs performed every 3 months during the first year and then every 6 months for a minimum of 2 years.

2.2.2 Histological diagnosis and immunohistochemistry

Formalin-fixed, paraffin-embedded (FFPE) tumour samples were stained with haematoxylin-eosin (HE) for diagnosis. The histological classification was performed according to the World Health Organization (WHO) guidelines[94] and the grading was evaluated using the Loukopoulos and Robinson grading system[95] by three independent pathologists.

Immunohistochemistry (IHC) was performed on 4μm thick paraffin sections. After endogenous peroxidase activity blocking with 0.3% H_2O_2, the sections were exposed to heat-induced antigen retrieval using citrate buffer at 98°C, pH 6 for 30 minutes and then incubated with anti-PLK1 (diluted 1:150, Invitrogen, Waltham, MA, USA) and anti-c-Myc antibodies (diluted 1:100, Santa Cruz Biotechnology, Dallas, TX, USA) for 2h at room temperature. Vectastain Elite ABC kit and ImmPACT DAB from Vector Laboratories Inc. (Burlingame, CA) were used for detection.

Immunolabeled slides were randomized and masked for blinded examination, which was performed by two independent pathologists. Immunohistochemical evaluation of PLK1 and c-Myc expression was performed using previously reported scoring systems[77,96].

2.2.3 Cell line selection and culture conditions

Four primary canine OSA cell lines were included in this study. Penny and Wall cell lines were previously established and validated by Maniscalco et al.[81], while D17 (Cat.# ATCC CCL-183) and D22 (Cat.# ATCC CRL-6250) were obtained from American Type Culture Collection. These were cultured in Dulbecco's modified Eagle's medium (DMEM; D17 and D22) and Iscove's standard

medium (Penny and Wall), supplemented with 10% foetal bovine serum (FBS), 1% glutamine, 100µg/mL penicillin, and 100µg/mL streptomycin. Cells were cultured at 37°C in a humidified atmosphere of 5% CO_2. Human breast cancer cell line T47D (Cat.# ATCC HTB-133) and human OSA cell line MG63 (Cat.# ATCC CRL-1427), previously described as being PLK1-overexpressing[78,97], were used as positive controls.

2.2.4 Morphological changes, viability, and apoptotic assays after BI 2536 treatment

The D17 cell line, overexpressing PLK1 and c-Myc proteins, was selected for *in vitro* inhibition using BI 2536 molecule[99]. Firstly, $1x10^6$ cells/well were seeded in six wells cell culture plates and treated with BI 2536 at 2.5, 5, 7.5 and 15 nm for 12, 24 and 48 hours. Morphological changes were analysed with a Leica AF6000 LX (Leica Microsystems, Wetzlar, Germany) microscope equipped with a Leica DFC350FX digital camera controlled by the LAS AF software (Leica Microsystems). Based on morphological effect, viability assay was performed using CellTiter 96® AQueous One Solution Cell Proliferation Assay (Promega, Madison, WI, USA) on 1x106 cells/well at 2.5, 5, 7.5 and 15 nM for 12 and 24 hours. Similarly, caspase activity for apoptosis detection was evaluated using Caspase-Glo® 3/7 Assay System (Promega, Madison, WI, USA) according to the datasheet after 12- and 24-hours treatment at 2.5, 5 and 7.5 nM. The untreated D17 cell line was used as control while the medium was used as blank to subtract background signal. All experiments were performed in triplicate and repeated three times.

2.2.5 PLK1 and c-Myc expression in canine osteosarcoma cell lines

Whole-exome sequencing and RNA-seq data from a previous study[98] on the aforementioned canine OSA cell lines were further analysed to identify non-synonymous mutations or gene expression aberrations affecting *PLK1* and *MYC* genes.

The expression of PLK-1 and c-MYC in treated or untreated cells was evaluated by Western Blot (WB) and RT-qPCR. Proteins from all the cell lines were extracted in lysis buffer (1% Triton X-100, 10% glycerol, 50 mM Tris, 150 mM sodium chloride, 2 mM EDTA, pH 8.0 and 2 mM magnesium chloride) containing protease inhibitor cocktail (Sigma). Twenty micrograms of total protein from all previous cell lines were separated by SDS-PAGE (10% or 15%) and transferred onto a nitrocellulose membrane (Thermo Fisher Scientific; Waltham, MA USA). After washing, membranes were incubated in TBS/BSA 10% (bovine serum albumin) at room temperature for 1 h and incubated overnight at 4°C with PLK1 (diluted 1:1000, Invitrogen, Waltham, MA, USA) and c-Myc antibodies (diluted 1:1000, Cell Signaling Technology, Danvers, MA, USA). β-tubulin was used as an internal control

(diluted 1:10000, T5201, Sigma-Aldrich). After incubation with horseradish peroxidase (HRP)-linked secondary antibody diluted 1:15,000 in TBS-Tween, membranes were washed 6 times in TBS-Tween and incubated with Clarity Western ECL Substrate (BioRad Laboratories). The proteins were visualized by briefly exposing the membrane to an autoradiographic CL-XPosure Film (Thermo Fisher Scientific). WB results were then acquired with an Epson scanner.

Total RNA was isolated from all cell lines by using QIAzol Lysis reagent (Qiagen). QuantiTect Reverse Transcription kit (Qiagen) was used to retro-transcribe 1 µg of total RNA into cDNA. RT-qPCR was performed by using the IQ SYBR Green Supermix (BioRad) and the IQ5 detection system (BioRad). Primer sequences to determine PLK1 and MYC transcripts were designed using Primer Express v. 1.5 software and are listed in Supplementary Table 2. GAPDH showed stable expression levels under all experimental conditions and was selected as housekeeping gene. Gene expression was calculated using the formula $2^{-\Delta\Delta Ct}$ (fold increase), where $\Delta\Delta Ct = \Delta Ct$ (sample) $- \Delta Ct$ (control) and ΔCt was calculated by subtracting the Ct of the target genes from the Ct of the housekeeping gene. RT-qPCR was performed in both technical and experimental triplicates.

2.2.6 Cell cycle analysis by FACS

The biological effect of BI 2536 on the cell cycle was evaluated by 7-Aminoactinomycin D (7AAD) staining and FACS analysis. Briefly, D17 cells were exposed to 2.5, 5, 7.5 and 15 nM of BI 2536 for 16h, detached with trypsin-EDTA, washed with PBS, fixed for 1h at 4°C with 50% ice-cold ethanol added drop-by-drop with continuous vortexing. Samples were then spun at 500 x g for 7 min, resuspended in 1 mL of PBS with 25 µg/mL 7AAD and stained overnight at 4°C. The samples were analysed using a Cytoflex (Beckman Coulter) equipped with a 488 nm (Blue) excitation laser and a 690/50 nm (Red) emission filter. For each sample, 25.000 to 50.000 events were analysed, and each experiment was repeated 3 or more times. The percentages of cells in the different phases of their cycle were calculated using the Flowing Software version 2.5.1 (https://bioscience.fi/services/cell-imaging/flowing-software/).

2.2.7 Statistical analysis

Correlations of PLK1 and c-Myc expression with clinical and histopathological data, as well as the mutual correlation of these factors, were analysed by Fischer's exact test. Additionally, Kaplan-Meyer analyses were performed to examine the correlations of all variables with the time elapsed between surgery and the detection of metastases and/or local recurrence (disease-free interval; DFI) and the time elapsed between surgery and death (overall survival; OS) using the log-rank test, using R

statistical software (R Core Team, 2018). Dogs who died for unrelated causes or were lost during the follow-up were censored.

Data from viability and apoptotic assays, gene expression and cell cycle analyses were analysed by two-way ANOVA to investigate the effect of BI2536 treatment. Data were analysed with GraphPad Prism (version 8.0.0, GraphPad Software). A P value of less than 0.05 was considered statistically significant.

3. RESULTS

3.1 Canine osteosarcoma cell lines as valuable translational *in vitro* model

3.1.1 The mutational profile of primary canine osteosarcoma cell lines

DNA extracted from 8 canine OSA cell lines underwent WES and an average of 158 million reads per sample (range 143-164) was obtained.

The mean depth of reads mapping to the canine reference genome (CanFam3.1) was 187.7 (range 128-219), with over 99% of the targeted exome uniquely aligned. The optimal coverage was achieved for 6 out of 8 cell lines. For each cell line, all reads passed the quality control (Phred quality score) ≥ 30. The FFPE samples (tumour and matched normal) achieved a mean depth of 54.71.

The median tumour mutational burden of all Level 1 somatic variants was 9.6 mutations/Mb (range 3.9-16.9); in the Wall FFPE sample, the mutational burden reached 17.7 mutations/Mb (Figure 10). On average, 19.6% (range 13.3-26 %) and 17.1% of Level 1 variants of canine OSA cell line and Wall FFPE sample, respectively, were annotated as synonymous and were consequently excluded from downstream analyses.

In all our cell lines, missense mutations were the most frequently represented somatic coding mutation type, accounting for an average of 38.7% across all exonic variants. Frameshifts insertion and deletions were 15.8% and 12.5% of the variants, respectively (Figure 10). In Wall FFPE sample nonsynonymous variants, frameshift and non-frameshift deletions were the most represented mutation types (36.3%, 20.5% and 10.3%, respectively).

The most common base change identified in all samples was C > T transition (Figure 10).
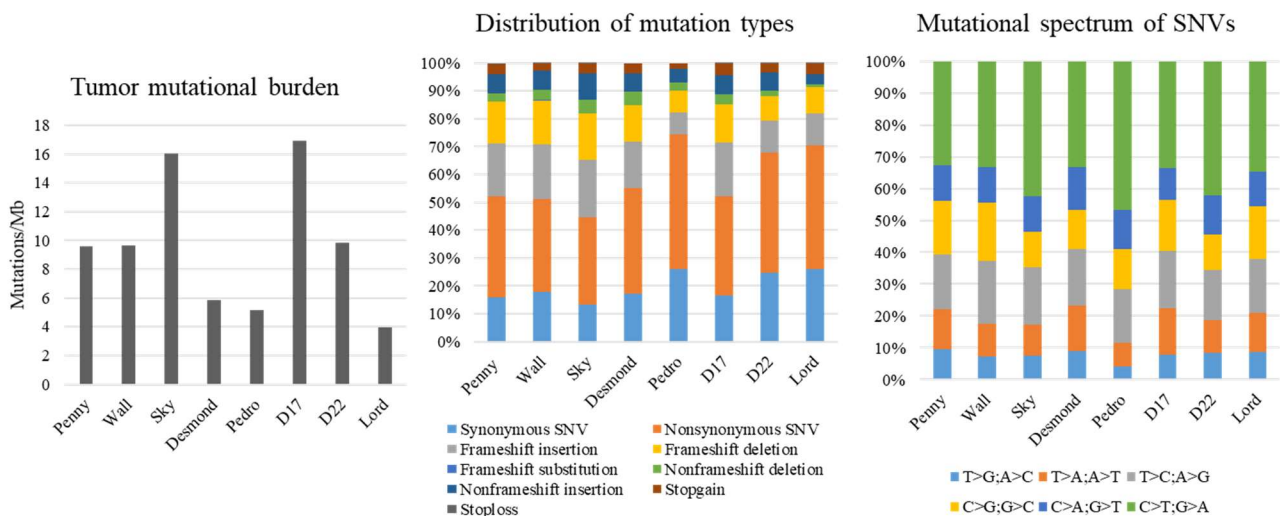

Figure 10. Mutational landscape of canine OSA cell lines, Level 1 variants. Tumour mutational burden; distribution of mutation types; mutational spectrum of single-nucleotide variants.

The analysis of the WES data using Mutect2 revealed a total of 11,554 exonic variants (Level 1), 7,981 of these were identified as nonsynonymous (Level 2) and encoded for 4,045 genes (Figure 11). The number of genes in each sample ranged from 318 (Lord) to 1,345 (D17) and reached the maximum of 1,533 genes in Wall FFPE sample (Figure 12).

Using FidoSNP pathogenicity prediction tool, 50.5% (1,929/3,819 SNVs) of all missense point mutations were categorized as deleterious.
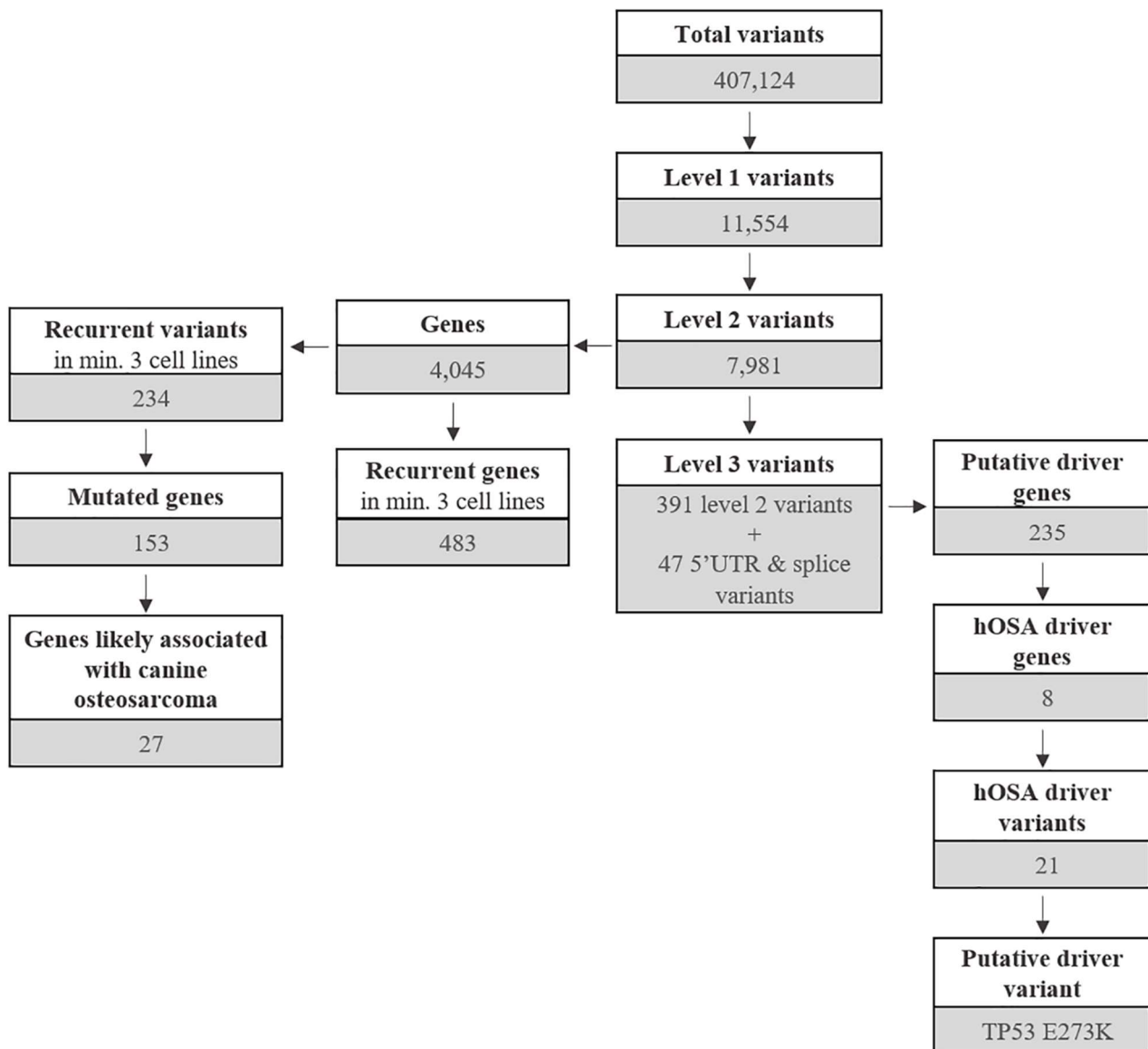

Figure 11. Outline of mutated genes and variants distribution across Level 1, 2 and 3 variants.
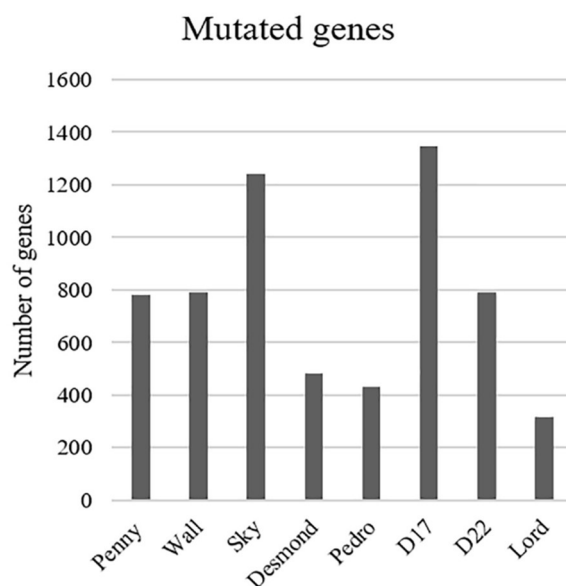
Figure 12. Distribution of the mutated genes across the cell lines.

3.1.2 Canine osteosarcoma cell lines show mutations in several known oncogenes and tumour suppressor genes

As mentioned above, 4,045 genes with 7,981 protein-modifying variants were identified. Overall, 483 genes were recurrently mutated in at least 3 cell lines. Taking into account the recurrent variants across all cell lines, a total of 234 variants were retrieved in three or more samples, and 51.4% of all SNVs (54/105) were categorized as pathogenic. When recurrent variants were collapsed to genes, 153 recurrently mutated genes were identified (Figure 11).

In addition, genes were filtered using the list of OSA-associated genes retrieved from literature (Table 7). Finally, a total of 27 genes likely implicated in OSA pathogenesis were identified across all our cell lines. Among them, *PDGFRB, PTCH1* and *WRN* were retrieved in at least three cell lines; whereas oncogenes and tumour suppressor genes, such as *TP53, ALK, MYC, MET*, were retrieved in only one cell line each (Figure 13).

The number of mutated genes ranged from 2 (Desmond and Lord) to 10 genes (Sky) (Figure 14). Overall, these osteosarcoma-associated genes were encoded by 51 variants, and 53.3% of all SNVs (16/30) were categorized as pathogenic.
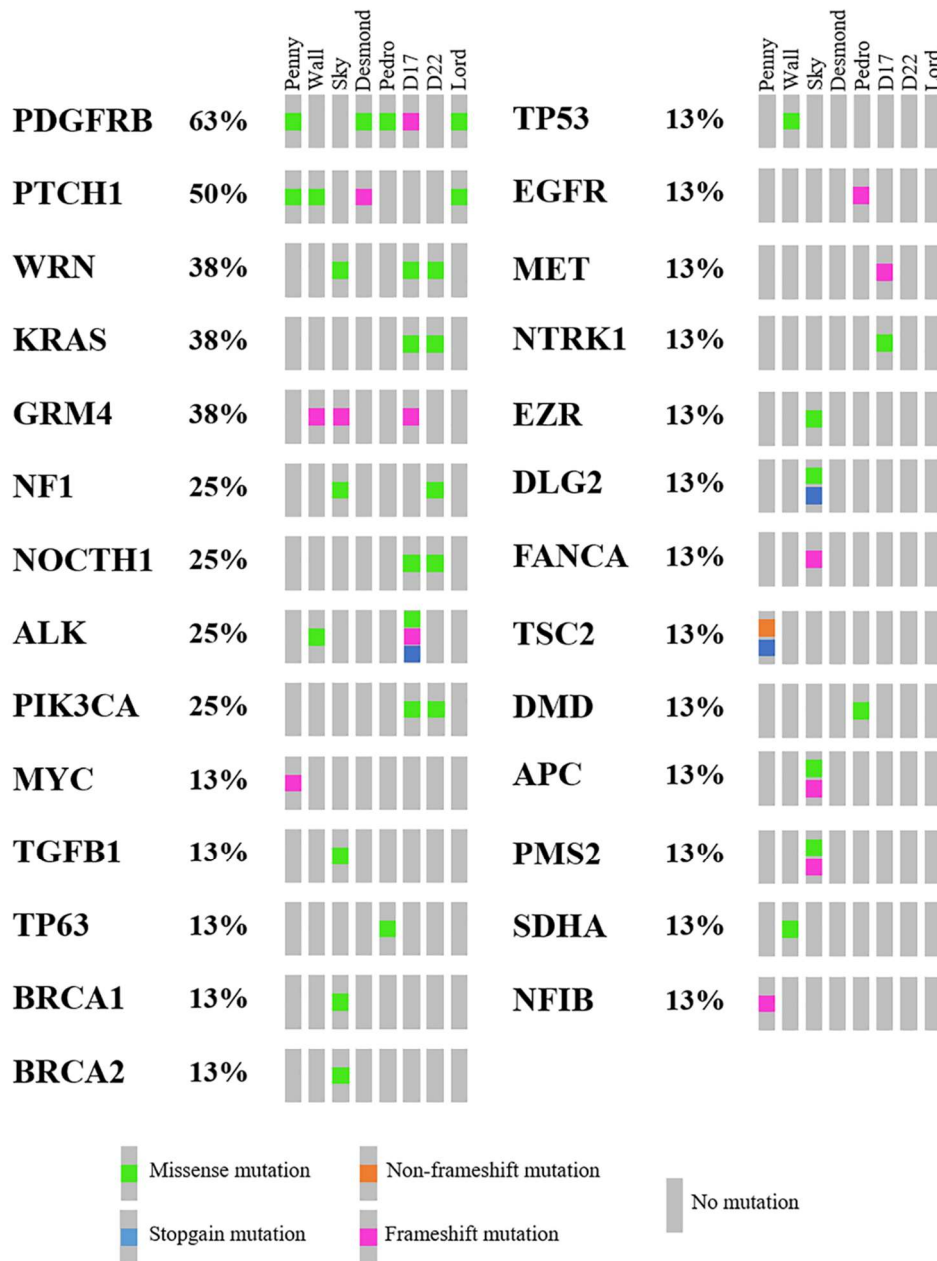
Figure 13. Oncoplot of genes likely involved in canine OSA pathogenesis retrieved in Level 2 analysis, including the mutational incidence and the mutational type across the cell line panel.
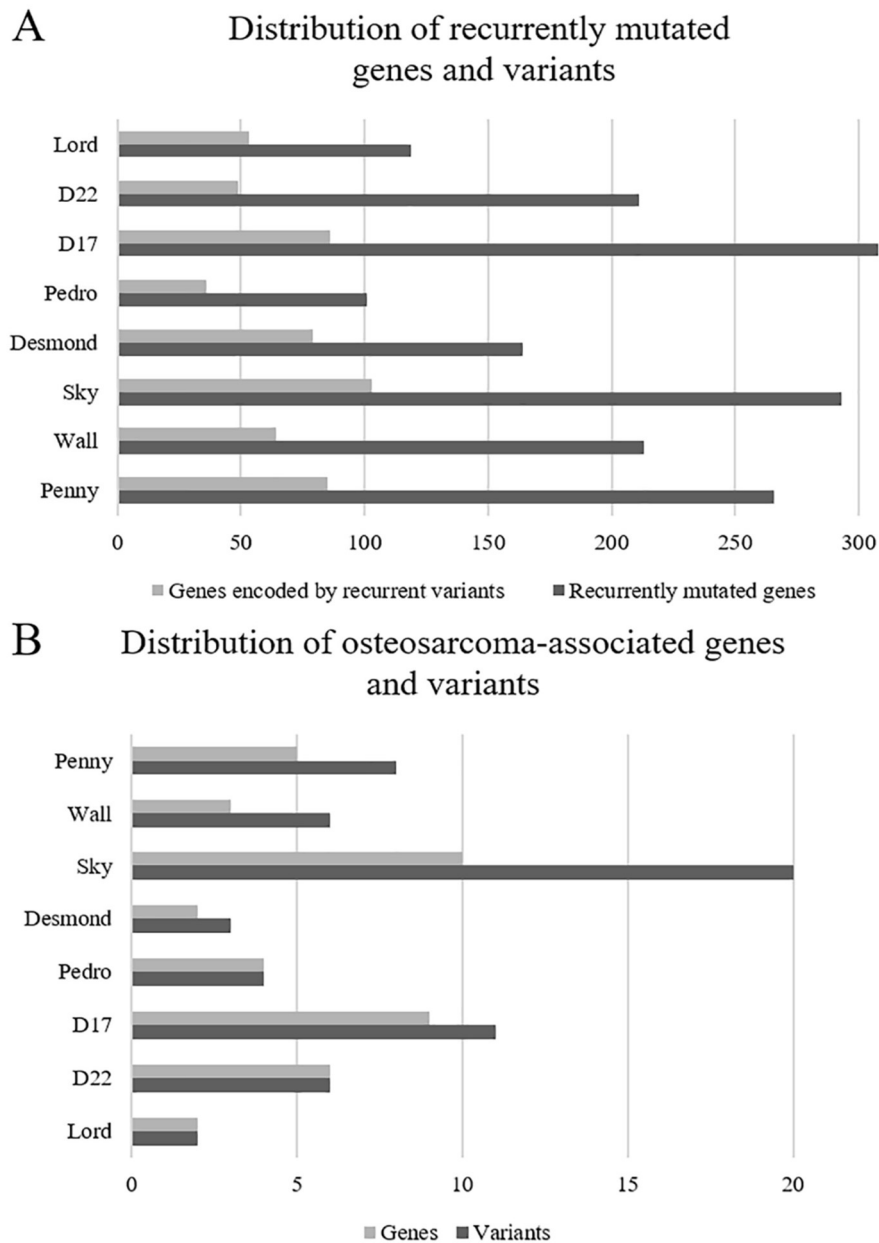
Figure 14. (A) Distribution of recurrently mutated genes and variants across all the canine OSA cell lines. (B) Distribution of OSA-associated genes and corresponding variants across all the canine OSA cell lines.

Comparing these 27 genes to the top twenty most frequently mutated genes in human cancers (Cancer Genome Atlas; https://portal.gdc.cancer.gov/), four overlapping genes were identified. Namely, *PIK3CA, KRAS, APC* and *NF1* ranked 2nd, 6th, 10th and 13th in human cancer, respectively. At last, four genes were also identified in Wall FFPE sample but did not overlap those of the corresponding cell line (Table 8).

Genes	Wall		Genes	Wall	
	Cell line	FFPE		Cell line	FFPE
PDGFRB	-	-	BRCA2	-	X
PTCH1	X	X	EGFR	-	-
WRN	-	-	MET	-	-
NOTCH1	-	-	NTRK1	-	-
PIK3CA	-	-	EZR	-	X
NF1	-	X	DLG2	-	-
KRAS	-	-	FANCA	-	-
ALK	X	-	TSC2	-	-
GRM4	-	-	DMD	-	-
TP53	X	X	APC	-	-
MYC	-	-	PMS2	-	X
TGFB1	-	-	SDHA	X	-
TP63	-	-	NFIB	-	-
BRCA1	-	-			

Table 8. Variants retrieved in genes likely involved in canine OSA pathogenesis (n= 27; Level 2 analysis) in Wall cell line and matching FFPE tumour sample.

3.1.3 Canine osteosarcoma cell lines share several driver genes with human osteosarcoma

COSMIC Cancer Gene Census was used to identify candidate driver variants (Level 3) in known cancer-causing genes in humans.

Level 3 included 438 variants coding for 235 genes, regardless of their incidence across the cell line panel (Figure 11). A total of 19 genes were uniquely encoded by 5' UTR or splice variants.

Overall, 190 genes were indicated as having a relevant and documented activity that promotes oncogenic transformation. In particular, 28 were designated as fusion genes, 74 as tumour suppressors, 63 as oncogenes and 25 functioned as both. The distribution of putative driver mutations across all cell lines is depicted in Figure 15.

Distribution of putative driver variants and genes
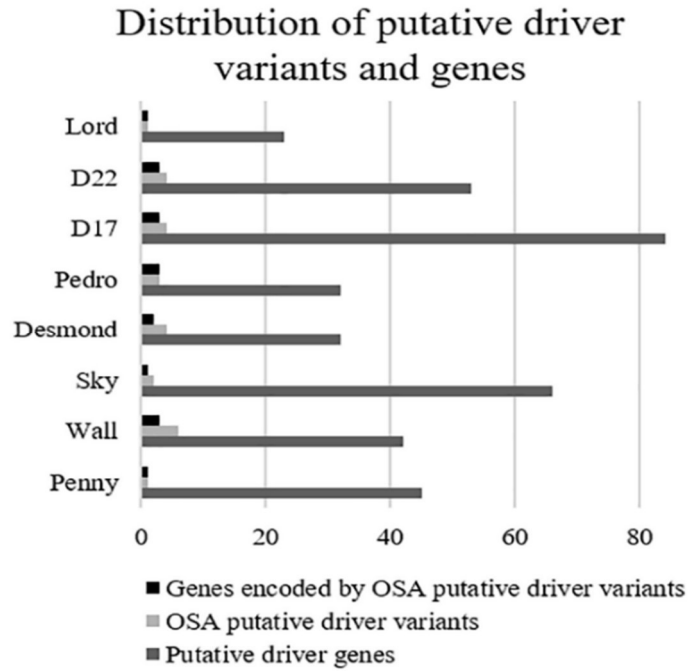
Figure 15. Distribution of putative driver variants and encoded genes across canine OSA cell lines.

About 88% of the SNVs encoding for these genes were categorized as pathogenic. When compared to the top 20 cancer driver genes involved in human OSA (COSMIC Cancer Browser), 8 genes, encoded by 21 variants, were retrieved in Level 3 genes (Table 9). Among these, well-known oncogenes, and tumour suppressor genes, such as *TP53, PTCH1, MED12 and PI3KCA*, were identified.

Gene	Mutation	Cell lines								FFPE
		Penny	Wall	Sky	Desmond	Pedro	D17	D22	Lord	Wall
PTCH1	c.17A>G	-	-	-	-	-	-	-	X	-
	c.3850C>T	X	-	-	-	-	-	-	-	-
	c.4014insT	-	X	-	-	-	-	-	-	X
	c.4023delA	-	X	-	-	-	-	-	-	X
	c.4200_4201insAGTCCCCG	-	X	-	X	-	-	-	-	X
	c.4203_4210del	-	X	-	X	-	-	-	-	X
LRP1B	c.12056A>T	-	-	-	X	-	-	-	-	-
	c.3112A>C	-	-	-	-	-	-	X	-	-
	c.3105_3106insATTGGGCCTGTGATGGTGA	-	-	-	-	-	-	X	-	-
ARID1A	c.6276A>T	-	X	-	-	-	-	-	-	X
	c.4863_4862insCCCCCCA	-	-	X	-	-	-	-	-	-
	c.4858_4852del	-	-	X	-	-	-	-	-	-
	c.1877G>A	-	-	-	-	X	-	-	-	-
NFATC2	c.510G>A	-	-	-	-	X	-	-	-	-
TET2	c.1349G>C	-	-	-	-	-	X	-	-	-
	c.2817_2818insCTGTGACTTCCTCCCTGGTCAGACA	-	-	-	-	-	X	-	-	-
	c.2894_2897del	-	-	-	-	X	-	-	-	-
PIK3CA	c.2217G>T	-	-	-	-	-	X	X	-	-
TP53	c.818C>T	-	X	-	-	-	-	-	-	X
MED12	c.2089_2090insATGGACTGCCCTTCCCCTCAC	-	-	-	X	-	-	-	-	-
	c.2581G>A	-	-	-	-	-	X	X	-	-

Table 9. List of putative driver genes and variants across all the cell lines

3.1.4 Canine osteosarcoma TP53 putative driver mutation matches a known human-equivalent mutation hotspot

All putative driver variants were cross-referenced with human OSA driver mutations available on IntOgen. Only Wall cell line and FFPE tumour sample harboured a putative driver mutation, namely the *TP53*[E273K] mutation (c.818C>T) corresponding to the human *TP53*[E285K] mutation hotspot. This putative driver mutation was further validated in homozygosis in Wall cell line and tumour sample by Sanger sequencing (Figure 16).
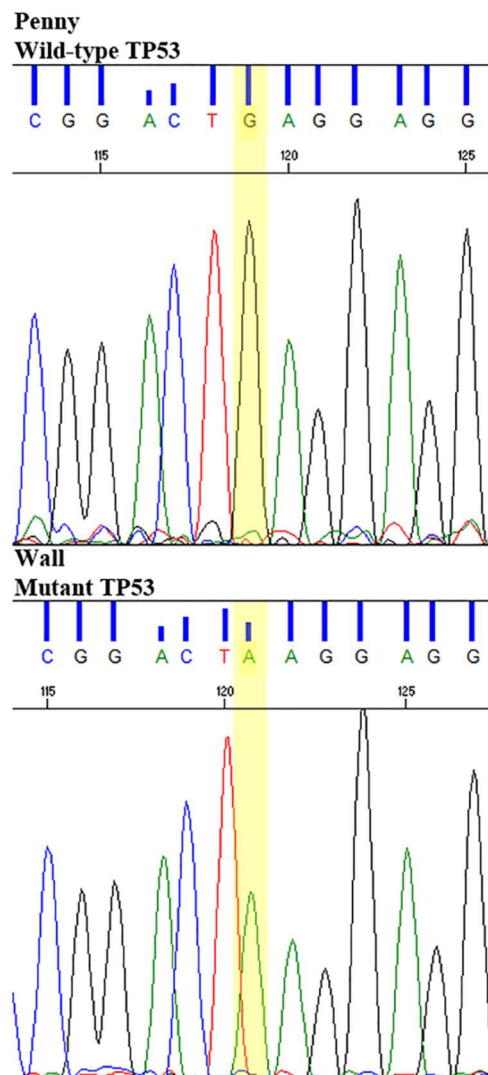

Figure 16. Sanger sequencing of TP53[E273K] mutation in Wall cell line and primary FFPE tumour, compared to wild-type TP53 Penny cell line and the reference canine TP53 sequence.

3.1.5 The oncogenic potential of TP53 and MET gene expression aberrations

RNA-seq generated over 10 million reads per sample. Quality control and trimming procedures retained the vast majority of the sequences, and unique alignment to the canine reference genome was successful for 86% of the cleaned reads.

Normalized gene expression of the OSA-associated genes described above was then profiled within the same gene across all samples.

In particular, *TP53* gene expression was increased in Wall cell line, which harboured a hotspot mutation, as well as in D17 and D22, which retained a wild-type gene status. Interestingly, D17 and D22 showed a 9-fold and 5.5-fold increase of *MDM2* and *MDM4* transcript levels, respectively, compared to the other cell lines. Conversely, *MDM2* transcript level was decreased by 2 to 20 times in Wall cell line compared to the rest of the cell lines (Table 10).

Transcriptional upregulation of *MET* by 19-fold was observed in D17 cell line, which harboured a frameshift insertion on this gene, and to the same extent in D22 which retained a wild-type gene status. Notably, genes involved in the downstream MAPK/ERK pathway, such as *MAPK1*, *MEK* and *MYC* showed increased transcript levels, although no mutations were detected in WES analysis (Table 10).

Conversely, downstream signalling components of mutated cancer-associated genes, such as *PTCH1, MED12, PDGFRB* and *PIK3CA*, did not show any transcript level change.

Gene		Cell lines					
		Penny	**Wall**	**Sky**	**Desmond**	**D17**	**D22**
P53 pathway	**TP53**	969	1618	799	580	2612	2178
	MDM2	542	249	865	511	4888	4951
	MDM4	542	249	865	511	4888	4951
MET pathway	**MET**	37	28	115	48	1163	1018
	PIK3CA	26	48	87	66	20	23
	AKT1	1314	2913	2694	1993	3974	3962
	MTOR	364	863	513	305	588	526
	MAPK1	517	745	1142	534	1841	1306
	MEK	466	1571	634	409	955	858
	RAF1	323	259	489	391	707	695
	MYC	529	562	566	302	1653	1152

Table 10. Transcriptional landscape of the P53 regulatory pathway and the MET pathway.
Normalized gene expression reported in counts per million reads (CPM).

3.2 Polo-like kinase 1 as a potential target in c-Myc-overexpressing canine osteosarcoma

3.2.1 Clinicopathological data

This retrospective study included 53 dogs with appendicular OSA. The clinicopathological characteristics and follow-up data are provided in Table 11.

Both dogs bearing third grade OSAs and developing lung metastases showed a significantly shorter DFI and OS than dogs with lower grade OSAs and dogs without lung metastasis, respectively (Figure 17). Although not significant, the development of metastases was observed in 79% of dogs affected by third grade OSA compared to OSAs with a lower histological grade (data not shown).

Age (years)	Mean	7.5
	Median	8
	Range	2-13
Gender, n (%)	Female	24 (45.3)
	Male	29 (54.7)
Breed, n (%)	Crossbreed	13 (24.5)
	Boxer	6 (11.3)
	Rottweiler	5 (9.4)
	German Shepherd	5 (9.4)
	Great Dane	4 (7.6)
	Others	20 (37.8)
Weight (kg)	Mean	39.9
	Median	38
	Range	7.5-71
Localisation , n (%)	Forelimb	33 (62.3)
	Hindimb	20 (37.7)
Follow-up (days) DFI	Mean	214
	Median	178
	Range	34-1493
OS	Mean	302
	Median	203
	Range	36-1493
Histological type, n (%)	Osteoblastic OSA	33 (62.3)
	Chondroblastic OSA	8 (15.1)
	Fibroblastic OSA	6 (11.3)
	Miscellaneous	6 (11.3)
Grading, n (%)	I Grade	11 (20.8)
	II Grade	22 (41.5)
	III Grade	20 (37.7)

Table 11. Clinicopathological characteristics of the dogs included in the study
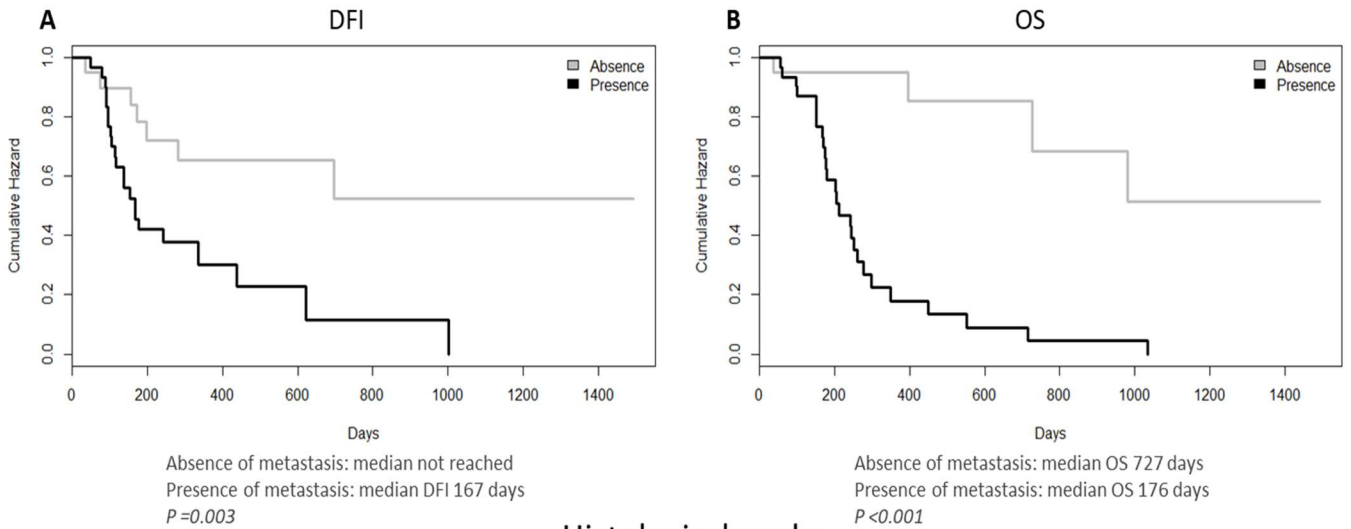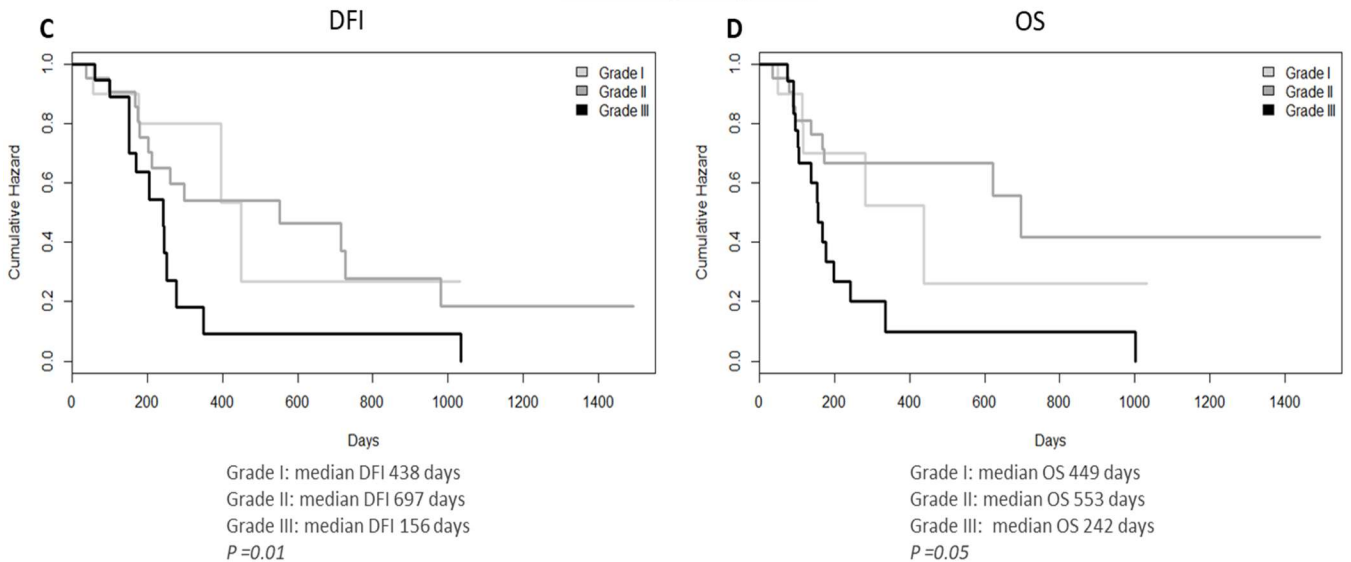
Figure 17. Kaplan-Meier curve. (A) Disease-free interval (DFI) and (B) overall survival (OS), in dogs developing metastases compared to those without metastases; (C) DFI and (D) OS, in dogs with I, II, III grade osteosarcomas.

3.2.2 c-Myc is a negative prognostic marker in canine osteosarcoma

A high c-Myc expression by immunohistochemistry was correlated with a significantly shorter OS when compared to samples with a low c-Myc expression (Figure 18). No other significant correlations with clinicopathological findings were found for both PLK1 and c-Myc. A summary of IHC results of PLK1 and c-Myc is provided in Table 12, and representative images are shown in Figure 19.

c-Myc expression

Low c-Myc expression: median DFI 336 days
High c-Myc expression : median DFI 197 days
P =0.2

Low c-Myc expression: median OS 553 days
High c-Myc expression : median OS 203 days
P =0.03

Figure 18. Kaplan-Meier curve. (A) DFI and (B) in dogs bearing high c-Myc-expressing osteosarcomas compared to low-c-Myc-expressing osteosarcomas.

Figure 19. Immunohistochemistry. (A) Low and (B) high PLK1 expression in canine osteosarcoma samples; (C) Low and (D) high c-Myc expression in canine osteosarcoma samples. (Scale bar = 50 μm)

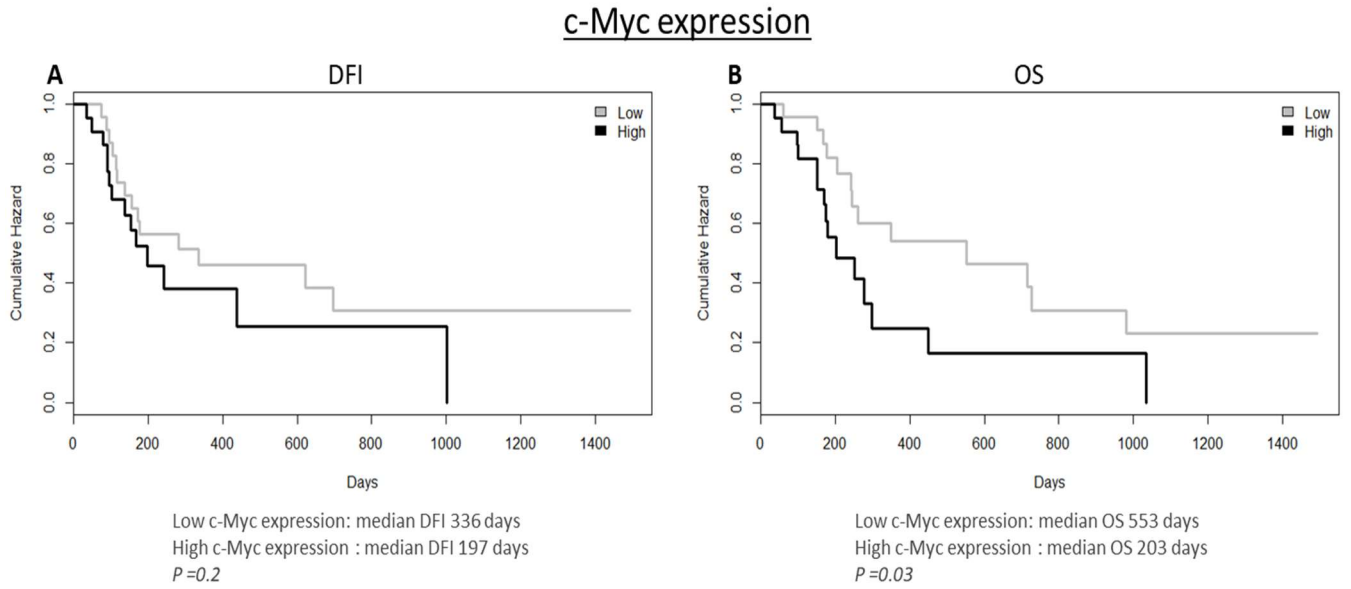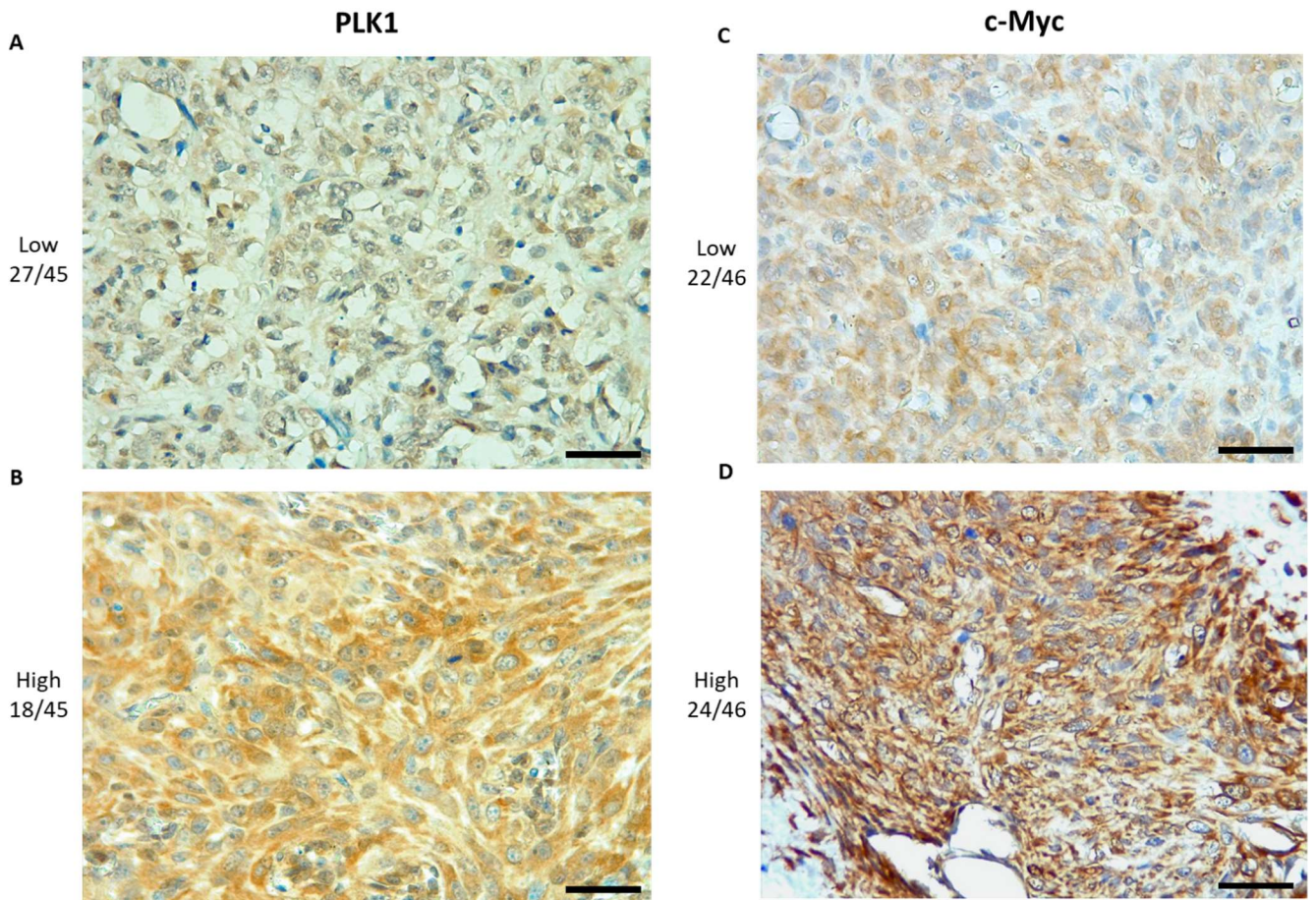| Marker		Score	Total
PLK1, n (%)	Low	29 (61.7)	47
	High	18 (38.3)	
c-Myc, n (%)	Low	24 (50)	
	High	24 (50)	48

Table 12. Immunohistochemical scoring of PLK1 and c-Myc.

3.2.3 PLK1 and c-Myc are broadly expressed in D17 and D22 cell lines

Whole-exome sequencing data revealed that *MYC* gene was mutated in Penny cell line only, while PLK1 did not show any mutation in none of the four cell lines analysed here. Transcriptional upregulation of PLK1 by 2.5-fold was observed in D17, D22 and Wall cell lines compared to Penny cell line. Furthermore, D17 and D22 cell lines showed a 2.5-fold increase of MYC transcript levels compared to Wall and Penny cell lines.

All canine OSA cell lines, although at different levels, showed both PLK1 and c-Myc expression. Overall, PLK1 and c-Myc protein expression resulted higher in the D17 and D22 cell lines when compared to the Penny and Wall cell lines as well as to human MG-63 and T47D cell lines (Figure 20). Quantitative PCR results confirmed these findings. Indeed, all canine OSA cell lines expressed higher *MYC* and *PLK1* transcripts than canine osteoblasts, whereas D17 cells showed a 2 to 3 times greater amount of *PLK1* and *MYC* transcripts when compared to the other cell lines (Figure 20).
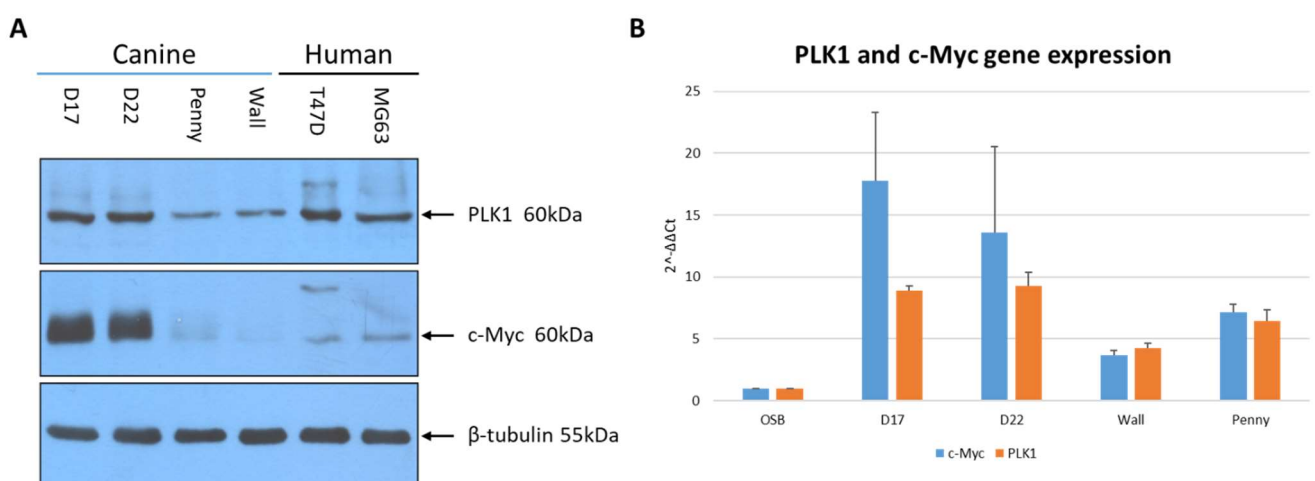

Figure 20. (A) Western Blot analysis of PLK1 and c-Myc protein expression in untreated canine osteosarcoma cell lines (D17, D22, Penny and Wall) and human osteosarcoma and breast cancer cell lines (MG-63 and TD47D, respectively). β-tubulin was used as housekeeping gene. (B) Quantitative RT-qPCR. Fold increase of

both PLK1 and c-Myc transcripts in D17, D22, Penny and Wall cell lines, compared to a canine osteoblast cell line. The error bars indicate the standard deviation of experimental triplicates.

3.2.4 BI 2536 induces G_2/M cell-cycle arrest and apoptosis in D17 cell line

According to the aforementioned results, the D17 cell line was selected to evaluate the in vitro effects of BI 2536 on cell morphology, viability, and apoptosis. As shown in Figure 21, BI 2536 treatment resulted in a significant change in cell morphology within 24 hours characterized by an increased number of rounded-up and floating cells, suggestive for a mitotic arrest. This phenomenon was more evident with higher BI 2536 concentrations and longer incubation times. FACS analysis was performed to further confirm this finding and examine the impact of BI 2536 treatment on the cell cycle. Cell cycle analysis displayed a decrease of the cell population in the G_0/G_1 phase from 20.5%±2.4 in untreated cells to 7.4±2% in cells treated with 15 nM BI 2536 for 16h (*P<0.0001*). Furthermore, a peak consisting of an average of 37.8%±2.4 of cells and corresponding to the G_2/M phase was observed in both untreated cells and under PLK1 inhibition. A third peak increasing from 18.3±2.4% in control cells up to 47.2±7.7% in cells under 15 nM treatment was also identified *(P<0.0001)* (Figure 22). At the same time, cell in mitotic arrest increased along with the concentration of the treatment. Notably, a peak in correspondence of to the G_2/M phase in untreated cells was also present and showed little changes at different concentrations of BI 2536 treatment. However, a third peak increasing from 18.3±2.4% in control cells up to 47.2±7.7% in cells treated with 15 nM was identified (P<0.0001).

Cell viability and apoptosis assays were then performed. As shown in Figure 23 after 24h of BI 2536 treatment in D17 we found a concentration-dependent reduction of cell viability up to 61.2% when compared to untreated cells. Concurrently, a significant concentration-dependent increase in apoptosis after 24h treatment at 5 and 7.5 nM in D17 cells treated with BI 2536 was found (*P<0.0001*).
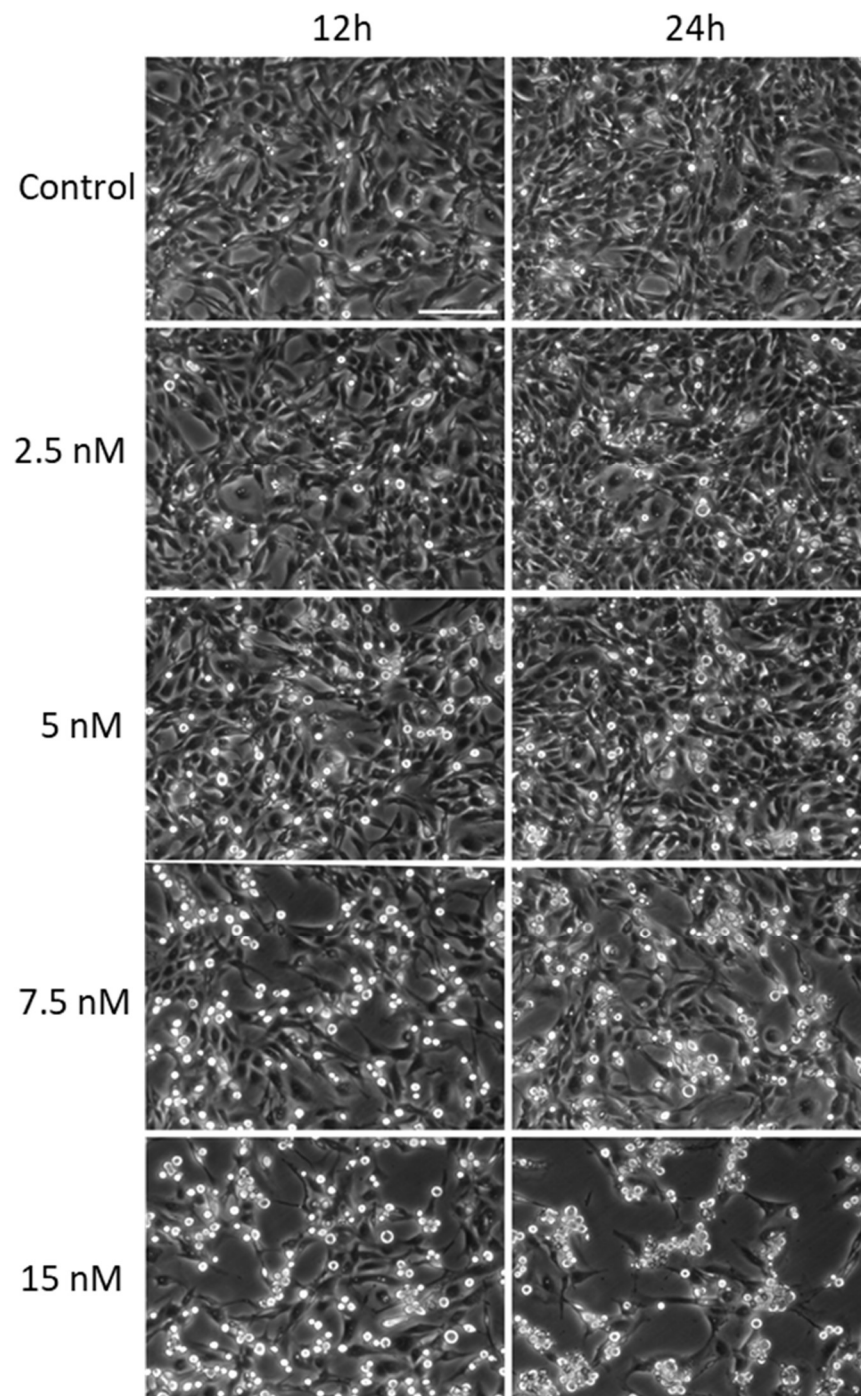
Figure 21. Cell morphology changes of the D17 cell line under BI 2536 treatment at different concentrations or untreated, for 12 and 24 hours.

Cell cycle
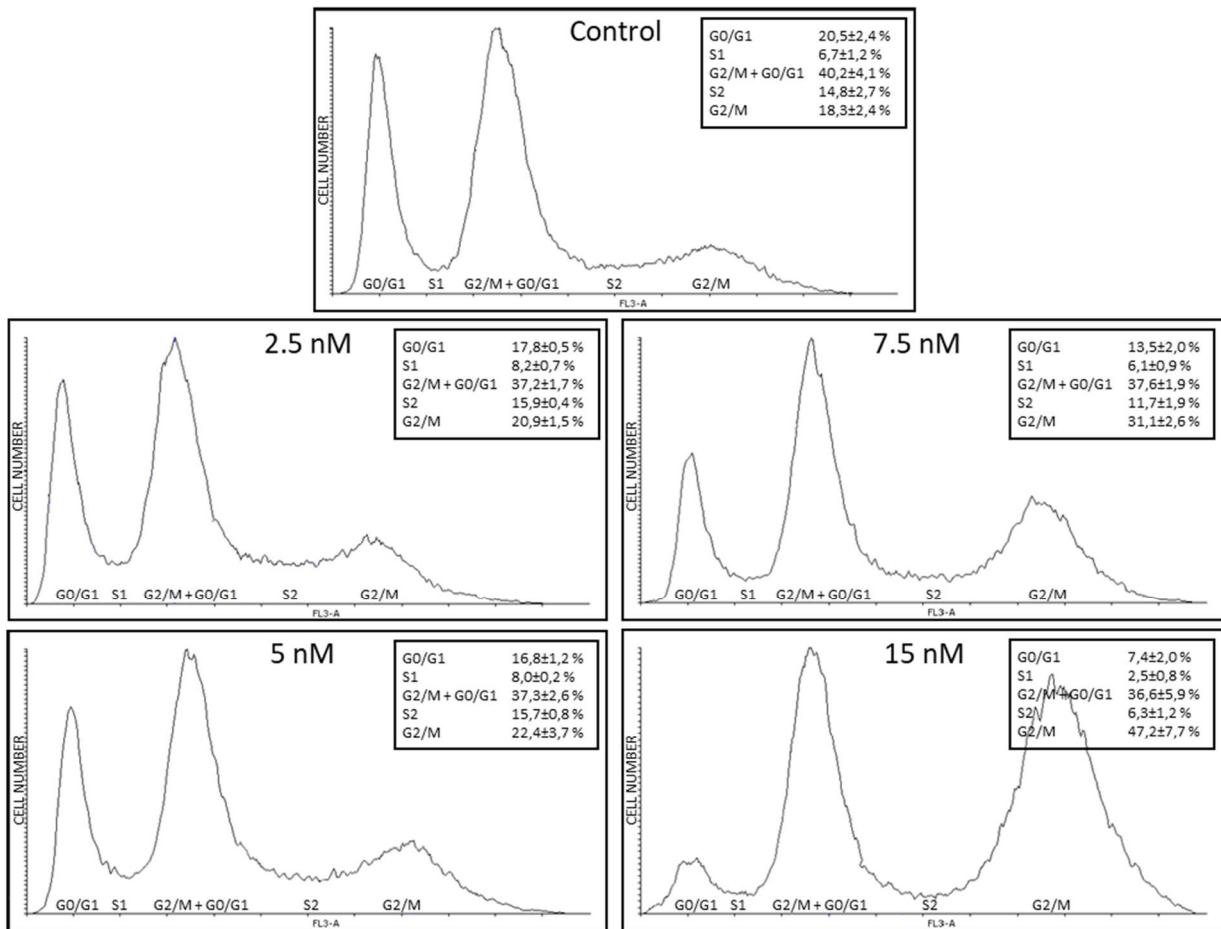
Figure 22. Cell cycle analysis of the D17 cell line under BI 2536 treatment at different concentrations or untreated, for 16 hours.
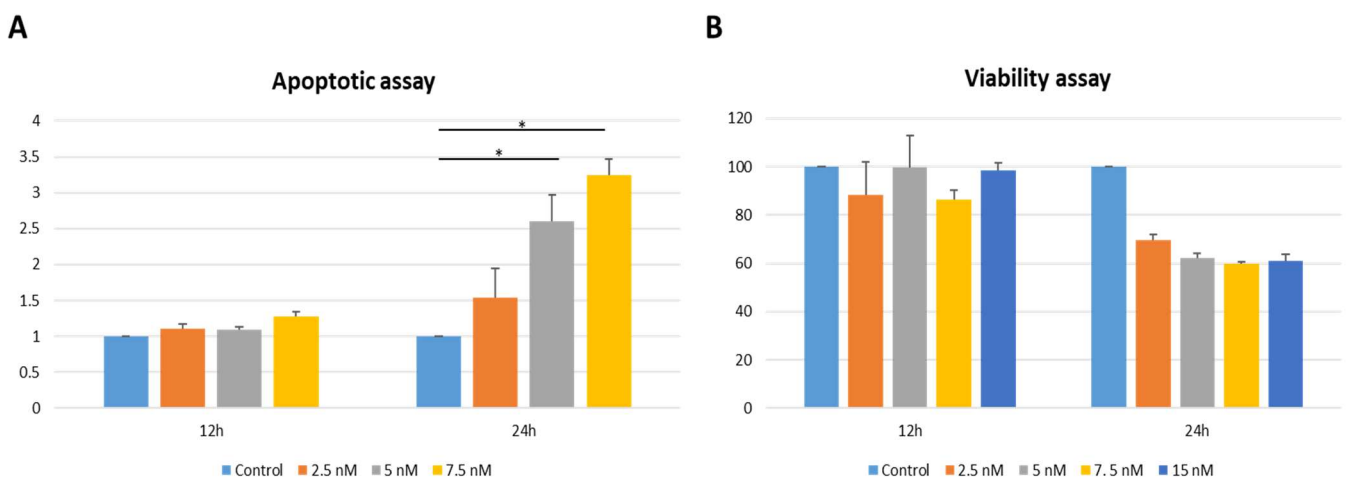
Figure 23. (A) Apoptotic assay. Relative quantification of apoptosis in the D17 cell line treated with BI 2536 at different exposure times and different concentrations, or untreated. (* p=0.001). (B) Viability assay. Percentage of viable cells in the D17 cell line treated with BI 2536 at different exposure times and different

concentrations, or untreated. Data were normalized using the D17 untreated cell line in both assays; the error bars indicate the standard deviation of experimental triplicates.

3.2.5 PLK1 inhibition *in vitro* reduces c-Myc protein expression

To investigate the effect of PLK1 inhibition on c-Myc expression, WB and RT-qPCR were performed on D17 cells exposed to BI 2536. As depicted in Figure 24 after 24h of treatment with BI 2536, cells showed an evident concentration-dependent decrease of c-Myc protein expression while PLK1 showed no significant variation. Conversely, no significant variation in neither *PLK1* nor *MYC* gene expression was observed.
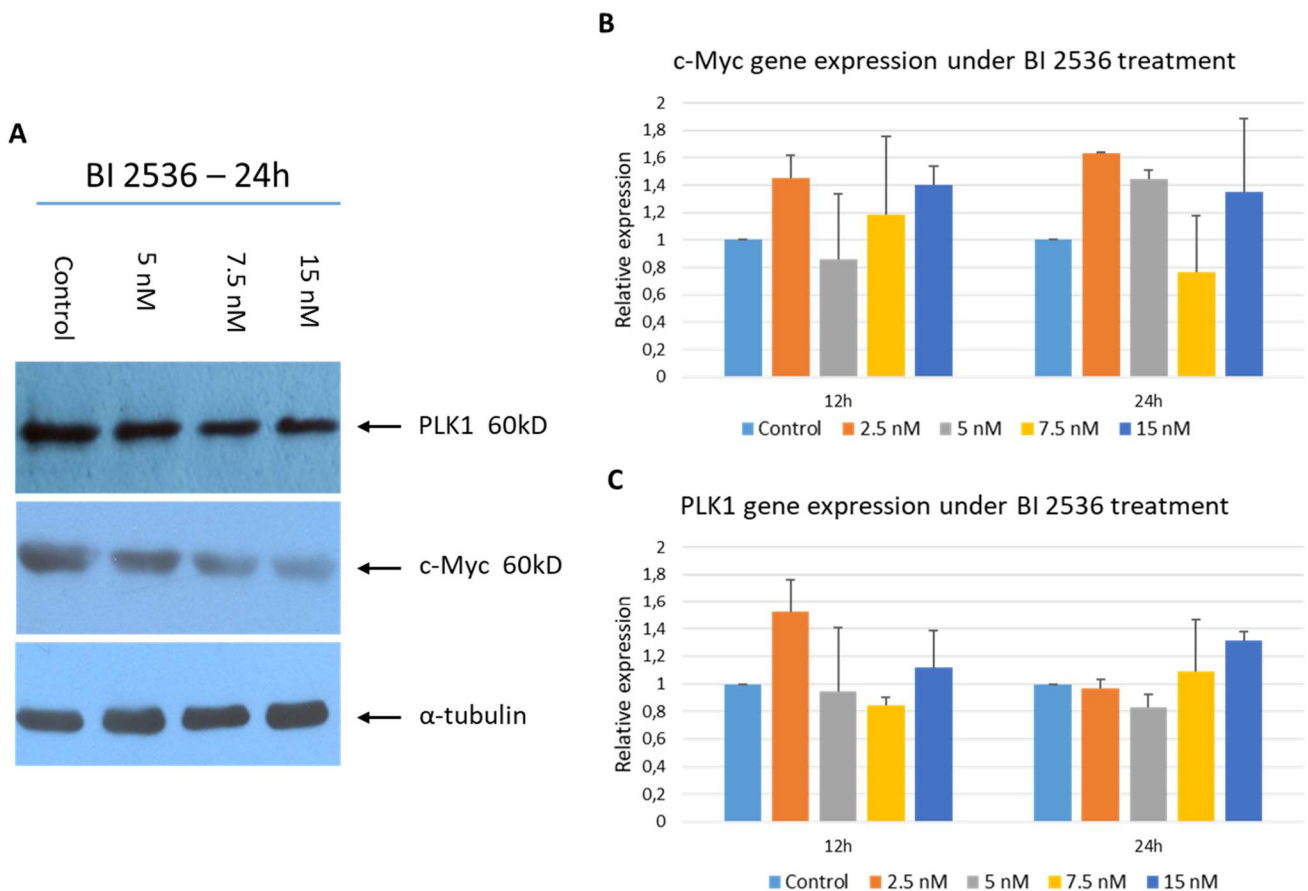
Figure 24. (A) Western Blot analysis of PLK1 and c-Myc protein expression in the D17 cell line treated with BI 2536 for 24h at different concentrations or untreated. β-tubulin was used as housekeeping gene. (B) Quantitative RT-qPCR. Fold increase of c-Myc and (C) PLK1 transcripts in the D17 cell line, after 12 and 24h treatment with BI 2536 at different concentrations. Gene expression was normalized using the D17 untreated cell line; the error bars indicate the standard deviation of experimental triplicates.

4. DISCUSSION

Naturally occurring tumours in dogs represent a widely assessed and powerful model for understanding human cancer biology and exploring novel therapeutic strategies.

In the recent years, the advent of omics technologies deepened our understanding of the cancer biology empowering data-driven precision medicine and culminating in improved clinical outcomes[100].

The selection of the most appropriate in vitro model system able to mimic at a genetic level the disease, is crucial for screening new therapeutic agents and biomarkers. In this perspective, cancer cell lines are crucial for translating data obtained from sequencing experiments into clinical practice. This statement has been substantiated by recent studies demonstrating that cancer cell lines embody most of the genetic alterations that were found in the corresponding tumour samples[24].

However, despite the long history and the substantial quantity of research performed on canine cancer cells, *in vitro* panels have not yet been developed to the scale that has occurred in human medicine[23].

With these new tools, the possibilities for comparative and translational applications with human cancer research are becoming readily apparent. Dogs with cancer can potentially benefit from new discoveries made in human oncology, and conversely, human research can benefit through the integration of canine cancer models for pre-clinical validation studies.

The integrative analysis of WES and RNA-seq data provides for the first time a complete molecular characterization of a large number of canine OSA cell lines recapitulating in vivo canine OSA pathogenesis and allowing future investigations on potential therapeutic targets and biomarkers. To date, this dataset represents the largest explored for a single tumour in dogs.

Overall, the mutational burden in our canine OSA cell lines ranged between 3.9 and 16.9 mutations/Mb, but was lower than the one described by Das and colleagues[55]. However, the diversity of the cell lines and the differences in library preparation kits, exome capture designs, and downstream stringency filters may have caused this discrepancy. Consistent with previous reports in canine OSA cell lines and human OSA, the mutational type distribution showed a prevalence of missense mutations, and C>T transitions dominated this mutational spectrum[55,101].

Among genes having a likely role in canine OSA as putative driver genes, mutations of *TP53* in Wall and *WRN* in Sky, D17 and D22 cell lines were retrieved. In particular, the putative driver *TP53*[E273K] mutation was identified in Wall cell line and tumour sample, and further validated by Sanger sequencing. As most of the *TP53* mutations, *TP53*[E273K] occurred in the mutational hotspot corresponding to the DNA-binding domain[102] and matched the human pathogenic hotspot mutation E285K[6]. Both canine *TP53*[E273K] and its human equivalent were previously reported in canine OSA and

human OSA[6]. According to the IARC *TP53* Database[103], this mutant allele is listed among the top 15 most common mutations in human cancers predicted to disrupt protein structure and function[104]. In our experiment, the presence of this mutation in both Wall tumour tissue and the derived cell line demonstrates a genetic fidelity with the primary tumour that remained stable during cell line establishment[24,105].

Looking at gene expression, the mutant *TP53* transcript levels in Wall were twice as high as in Penny, Sky and Desmond cell lines. This is in accordance with the literature where *TP53* missense mutations are reported to moderately affect the transcription but produce a full-length protein with a scarce ability to bind specific DNA sequence motifs and activate downstream target genes[104,106].

Concurrently, *MDM2*, a well-known *TP53* transcriptional target, showed a lower expression in Wall compared with the other wild-type *TP53* cell lines. This data suggests that *TP53* mutation in Wall cell line might cause a loss of function rather than an altered mRNA expression[107]. Overall, this indicates that $TP53^{E273K}$ is a likely pathogenic driver mutation and contextually, the Wall cell line represents a valuable translational model for prospective *in vitro* studies in both humans and dogs[108].

Remarkably, D17 and D22 cell lines showed an increase of *TP53* transcript compared to Wall, while retaining a wild-type gene status. In association, *MDM2* and *MDM4* transcripts levels were increased, suggesting that TP53 function might be impaired by their oncogenic and deregulated inhibiting activity in these cell lines[109]. In accordance with our findings, *TP53* overexpression in D17 was also detected in a recent report by Modesto and colleagues[110].

Surprisingly, a recent study showed that missense mutations in *TP53* in canine OSA were associated with longer DFI compared to wild-type *TP53* tumours, likely due to an increased response to chemotherapy[38].

Besides *TP53*, putative driver genes such as *PTCH1, MED12* and *PIK3CA* were also identified. *PTCH1* was mutated in 4 out of 8 cell lines. Physiologically, Hh ligand binding to the Ptch1 receptor relieves its inhibitory effect on the canonical Hedgehog pathway, which activation plays a role in both human OSA and canine OSA[111,112]. Despite a low *PTCH1* transcript level in these cell lines, no constitutive expression of Hedgehog pathway target genes was detected.

Similarly, *MED12* and *PIK3CA*, which are known to contribute to human OSA initiation and progression via the Wnt and PI3K/Akt pathways[113,114], did not show gene expression aberrations in the mutated cell lines, suggesting a biological irrelevant role in our cell lines.

Contrary to previous reports in dogs, no somatic mutations nor gene expression aberrations affecting *CDKN2A* and *SETD2* were identified[6,7]. Regarding *CDKN2A*, it is generally affected by germline mutations and copy number aberrations, which were not investigated here[6,7,115]. Whereas *SETD2* mutations were only recently identified in human OSA and canine OSA, and their biological role remains to be elucidated[6,7,116].

Across genes identified as recurrently mutated in our dataset, the two tyrosine kinase receptors *PDGFRB* and *MET* were retrieved. Both genes are known to play an important role in the development and progression of many canine cancers and were thoroughly investigated in canine OSA as well[49,81,117,118].

In five cell lines, *PDGFRB* harboured both frameshift and missense mutations, but only Desmond showed an increased gene transcript level. Nevertheless, no overexpression of *PDGFRB* downstream signalling molecules was detected, suggesting that these mutations did not affect gene transcription in Desmond. Gardner and colleagues reported previously that *PDGFRB* loci are affected by copy number gains rather than point mutations, however, no correlation with gene expression was found[6]. *MET* oncogene was highly expressed in D17 and D22 cell line but resulted mutated only in D17 cell line. However, the frameshift insertion mutation was unlikely associated with overexpression since several stop codons were retrieved in the transcript analysis. Nevertheless, *MET* is regulated by several mechanisms, including amplifications and epigenetic aberrations[119]. In D17 and D22 cell lines overexpression of *MET* downstream genes, including *MAPK1* and *MEK*, was observed, suggesting a possible activation of MAPK/ERK pathway[117,120,121].

MYC gene was mutated in Penny cell line only. However, increased transcript levels were identified in D17 and D22 cell lines, and likely related to the aforementioned *MET* signalling.

MYC is a member of a proto-oncogenic TF family, which is deregulated in the majority of human and canine tumours, including human OSA. c-Myc aberrant expression is associated with aggressive tumour behaviour and poor prognosis[77,122], while its inactivation results in sustained tumour regression in murine models[123,124]. Nowadays, c-Myc represents a long-pursued target and a top-listed putative target in anticancer therapy[125,126].

Among the multiple approaches blocking c-Myc oncogenic activity, PLK1 inhibition by selective compounds, such as BI 2536 and BI 6727 (Volarsetib), represent an attractive therapeutic strategy in the treatment of c-Myc-driven tumours[75,127]. Indeed, both these molecules induce c-Myc protein degradation by inhibiting PLK1/Fbxw7/c-Myc axis via the suppression of Fbxw7 auto poly-ubiquitination[76].

RNA sequencing analyses from a previous study showed an aberrant expression of both *MYC* and *PLK1* in two canine OSA cell lines (D17 and D22) although no mutations were detected WES analysis[98]. Similarly, two recent studies reported an aberrant gene expression of *MYC* in canine OSA samples[6,55]. In human OSA cell lines, c-Myc overexpression is known to promote cell invasion via MAPK/ERK signalling[122].With this in mind, we aimed at investigating the role of PLK1 and c-Myc in canine OSA and evaluating the biological effects of BI 2536 on a well-established canine OSA cell line overexpressing both *PLK1* and *MYC* oncogene.

We first examined PLK1 and c-Myc protein expression in surgically removed canine OSA samples. C-Myc overexpression was associated with shorter OS in canine patients compared to those with low c-Myc expression. This finding outlines the prognostic value of this marker in canine OSA, as previously assessed in human OSA[128-130], and open therapeutic implication targeting c-Myc inhibition[131]. Conversely, PLK1 was broadly expressed in canine OSA samples without showing any significant correlation with the clinicopathological factors. These data are in accordance with the human literature where PLK1 is an exploitable therapeutic target in c-Myc overexpressing tumours[76], but not a prognostic factor.

To gain insight into the effects of PLK inhibition in canine OSA cells, the *PLK1* and *MYC* overexpressing D17 cell line was treated with the BI 2536 molecule[132]. Our results showed that PLK1 inhibition induced visible morphological changes after 24 hours in a dosage-dependent manner. Under BI 2536 treatment, notably at 15 nM, cells appeared rounded and detached from the plate; this biological effect has been previously described as indicative of mitotic arrest[133] and was confirmed by our cell cycle analysis. Indeed, PLK1 inhibition induced a constitutive block of the D17 cell line in the G_2/M phase at 15 nM after 16 hours. It is worth noting that, in untreated D17 cells, the peak corresponding to the G_2/M phase of the cell cycle is likely due to superimposed polyploid cells in G_0/G_1. The third peak, which increases significantly under BI 2536 treatment, likely represents the aforementioned polyploid cells blocked in G_2/M, thus confirming the widely recognized crucial role of PLK1 in the precise regulation of cell division[78]. These data are consistent with a previous study on human OSA, in which BI 2536 suppressed cell growth and induced mitotic arrest and cellular aneuploidy in the human osteosarcoma MG-63 cell line[78]. These results were further corroborated by the decreased cell proliferation and induction of apoptosis in treated tumour cells under matching *in vitro* conditions, underlining the potential antitumour activity of PLK1 inhibition[78]. Finally, to demonstrate whether BI 2536 treatment promotes c-Myc cytoplasmic degradation, WB and RT-qPCR against PLK1 and c-Myc were performed. Consistently with previous data, the experiment induced a concentration-dependent decrease in c-Myc levels, notably at 7.5 and 15 nM, without affecting PLK1 expression[75]. Finally, under BI 2536, no significant variations of *PLK1* nor *MYC* transcripts were observed. The discrepancy between c-Myc protein and mRNA levels is consistent with the post-transcriptional inhibitory mechanisms of BI 2536 treatment, based on proteasomal, rather than transcriptional regulation of this factor[75].

Not surprisingly, all assays showed a dosage-dependent efficacy of PLK1 inhibition on cell cycle progression after 16h treatment which is the time required for cells to proceed through the mitotic process[134].

The association between the constitutive block of cells in the G_2/M phase and the evident decrease in c-Myc protein levels under BI 2536 treatment underlines the regulatory role of PLK1 in this signalling axis and strongly confirms the critical role of c-Myc inactivation in cell cycle arrest[135].

Data obtained in this study are similar to those retrieved in human cancer research, where PLK1 inhibitory molecules find an application in the treatment of several neoplasia[136,137] encouraging clinical trials with drugs indirectly targeting c-Myc[76]. Our results highlight the effectiveness of PLK1 selective inhibition on c-Myc and its downstream effects on cell proliferation and viability of canine OSA cells. Furthermore, as described in human OSA[127], targeting the MYC-driven signalling via the PLK1/Fbxw7/c-Myc axis might represent a promising therapeutic strategy for the treatment of canine patients bearing OSAs.

Overall, the results obtained in this project strongly confirm the crucial role of the dog as a naturally occurring model, both *in vitro* and *in vivo*, in comparative studies for human malignancies. Our data provide valuable insights into the molecular mechanisms of a large number of canine OSA cell lines, allowing future investigations of their functional implications and drug response.

The correlation of genomic and transcriptomic data with drug sensitivity will not only generate comprehensive datasets allowing the selection of accurate in vitro models for pre-clinical testing of novel therapeutics, but also contribute to the development of personalized therapeutic approaches, such as the PLK1 target inhibition in c-Myc overexpressing tumours. Furthermore, the availability of superimposable cancer cell line panels in veterinary and human medicine, will facilitate comparative analyses in oncology research.

Some limitations to this study need to be addressed in future studies. The lack of matched normal samples prevented the characterization of copy number aberrations in this study. Consequently, the effect of germline mutations was not considered in these analyses, and no evaluation of their impact in gene expression was performed. Similarly, differential gene expression analysis was not conducted, limiting the application of RNA-seq results to comparison of expression levels between samples as complementary data to the somatic mutations identified by WES. Finally, further investigation of putative driver mutations, such as *TP53*[E273K], in canine OSA samples can be of value in determining their relevance in a biological context.

In future, the integration of new sequencing approaches, such as methylation analysis and single-cell RNA-seq, and the addition of new primary canine OSA and matched normal cell lines will reveal a more complete biological picture of these models for canine OSA, deepening our understanding of the mechanisms contributing to individual therapeutic sensitivity.

Given that PLK1 also represents a central hub regulating functionality and interplay of several cell cycle checkpoints other than c-Myc, studies investigating the effects of PLK1 inhibition on the checkpoint activity and the interaction with other signalling pathways are critical to explore new combination therapies addressing the adverse effects and limitations of monotherapy.

At last, these integrative approaches must be explored to detect data-driven target therapies that not only may have an application *in vitro* but may also benefit both dogs and humans.

5. REFERENCES

1. Hanahan D, Weinberg RA. Hallmarks of cancer: the next generation. *Cell.* 2011;144(5):646-674.
2. Shendure J, Balasubramanian S, Church GM, et al. DNA sequencing at 40: past, present and future. *Nature.* 2017;550(7676):345-353.
3. Morganti S, Tarantino P, Ferraro E, D'Amico P, Duso BA, Curigliano G. Next Generation Sequencing (NGS): A Revolutionary Technology in Pharmacogenomics and Personalized Medicine in Cancer. *Adv Exp Med Biol.* 2019;1168:9-30.
4. Kamps R, Brandao RD, Bosch BJ, et al. Next-Generation Sequencing in Oncology: Genetic Diagnosis, Risk Prediction and Cancer Classification. *Int J Mol Sci.* 2017;18(2).
5. Piskol R, Ramaswami G, Li JB. Reliable identification of genomic variants from RNA-seq data. *Am J Hum Genet.* 2013;93(4):641-651.
6. Gardner HL, Sivaprakasam K, Briones N, et al. Canine osteosarcoma genome sequencing identifies recurrent mutations in DMD and the histone methyltransferase gene SETD2. *Commun Biol.* 2019;2:266.
7. Sakthikumar S, Elvers I, Kim J, et al. SETD2 Is Recurrently Mutated in Whole-Exome Sequenced Canine Osteosarcoma. *Cancer Res.* 2018;78(13):3421-3431.
8. Chu S, Skidmore ZL, Kunisaki J, et al. Unraveling the chaotic genomic landscape of primary and metastatic canine appendicular osteosarcoma with current sequencing technologies and bioinformatic approaches. *PLoS One.* 2021;16(2):e0246443.
9. Wang G, Wu M, Durham AC, et al. Molecular subtypes in canine hemangiosarcoma reveal similarities with human angiosarcoma. *PLoS One.* 2020;15(3):e0229728.
10. Megquier K, Turner-Maier J, Swofford R, et al. Comparative Genomics Reveals Shared Mutational Landscape in Canine Hemangiosarcoma and Human Angiosarcoma. *Mol Cancer Res.* 2019;17(12):2410-2421.
11. Hendricks WPD, Zismann V, Sivaprakasam K, et al. Somatic inactivating PTPRJ mutations and dysregulated pathways identified in canine malignant melanoma by integrated comparative genomic analysis. *PLoS Genet.* 2018;14(9):e1007589.
12. Brachelente C, Cappelli K, Capomaccio S, et al. Transcriptome Analysis of Canine Cutaneous Melanoma and Melanocytoma Reveals a Modulation of Genes Regulating Extracellular Matrix Metabolism and Cell Cycle. *Sci Rep.* 2017;7(1):6386.
13. Giannuzzi D, Marconato L, Elgendy R, et al. Longitudinal transcriptomic and genetic landscape of radiotherapy response in canine melanoma. *Vet Comp Oncol.* 2019;17(3):308-316.
14. Elvers I, Turner-Maier J, Swofford R, et al. Exome sequencing of lymphomas from three dog breeds reveals somatic mutation patterns reflecting genetic background. *Genome Res.* 2015;25(11):1634-1645.
15. Giannuzzi D, Giudice L, Marconato L, et al. Integrated analysis of transcriptome, methylome and copy number aberrations data of marginal zone lymphoma and follicular lymphoma in dog. *Vet Comp Oncol.* 2020;18(4):645-655.
16. Giannuzzi D, Marconato L, Cascione L, et al. Mutational landscape of canine B-cell lymphoma profiled at single nucleotide resolution by RNA-seq. *PLoS One.* 2019;14(4):e0215154.
17. Kim KK, Seung BJ, Kim D, et al. Whole-exome and whole-transcriptome sequencing of canine mammary gland tumors. *Sci Data.* 2019;6(1):147.
18. Amin SB, Anderson KJ, Boudreau CE, et al. Comparative Molecular Life History of Spontaneous Canine and Human Gliomas. *Cancer Cell.* 2020;37(2):243-257.e247.
19. Vozdova M, Kubickova S, Pal K, Fröhlich J, Fictum P, Rubes J. Recurrent gene mutations detected in canine mast cell tumours by next generation sequencing. *Vet Comp Oncol.* 2020;18(4):509-518.
20. Ramsey SA, Xu T, Goodall C, et al. Cross-species analysis of the canine and human bladder cancer transcriptome and exome. *Genes Chromosomes Cancer.* 2017;56(4):328-343.
21. Cronise KE, Das S, Hernandez BG, et al. Characterizing the molecular and immune landscape of canine bladder cancer. *Vet Comp Oncol.* 2021.
22. van Steenbeek FG, Hytönen MK, Leegwater PA, Lohi H. The canine era: the rise of a biomedical model. *Anim Genet.* 2016;47(5):519-527.

23. Fowles JS, Dailey DD, Gustafson DL, Thamm DH, Duval DL. The Flint Animal Cancer Center (FACC) Canine Tumour Cell Line Panel: a resource for veterinary drug discovery, comparative oncology and translational medicine. *Vet Comp Oncol.* 2017;15(2):481-492.

24. Mirabelli P, Coppola L, Salvatore M. Cancer Cell Lines Are Useful Model Systems for Medical Research. *Cancers (Basel).* 2019;11(8).

25. Zhang J, Späth SS, Marjani SL, Zhang W, Pan X. Characterization of cancer genomic heterogeneity by next-generation sequencing advances precision medicine in cancer treatment. *Precis Clin Med.* 2018;1(1):29-48.

26. Huang YH, Vakoc CR. A Biomarker Harvest from One Thousand Cancer Cell Lines. *Cell.* 2016;166(3):536-537.

27. Rowell JL, McCarthy DO, Alvarez CE. Dog models of naturally occurring cancer. *Trends Mol Med.* 2011;17(7):380-388.

28. Riccardo F, Aurisicchio L, Impellizeri JA, Cavallo F. The importance of comparative oncology in translational medicine. *Cancer Immunol Immunother.* 2015;64(2):137-148.

29. Onaciu A, Munteanu R, Munteanu VC, et al. Spontaneous and Induced Animal Models for Cancer Research. *Diagnostics (Basel).* 2020;10(9).

30. Gordon IK, Khanna C. Modeling opportunities in comparative oncology for drug development. *Ilar j.* 2010;51(3):214-220.

31. Mak IW, Evaniew N, Ghert M. Lost in translation: animal models and clinical trials in cancer treatment. *Am J Transl Res.* 2014;6(2):114-118.

32. Talmadge JE, Singh RK, Fidler IJ, Raz A. Murine models to evaluate novel and conventional therapeutic strategies for cancer. *Am J Pathol.* 2007;170(3):793-804.

33. Paoloni M, Khanna C. Translation of new cancer treatments from pet dogs to humans. *Nat Rev Cancer.* 2008;8(2):147-156.

34. Ostrander EA, Dreger DL, Evans JM. Canine Cancer Genomics: Lessons for Canine and Human Health. *Annu Rev Anim Biosci.* 2019;7:449-472.

35. LeBlanc AK, Mazcko CN, Khanna C. Defining the Value of a Comparative Approach to Cancer Drug Development. *Clin Cancer Res.* 2016;22(9):2133-2138.

36. Lindblad-Toh K, Wade CM, Mikkelsen TS, et al. Genome sequence, comparative analysis and haplotype structure of the domestic dog. *Nature.* 2005;438(7069):803-819.

37. Parker HG, Shearin AL, Ostrander EA. Man's best friend becomes biology's best in show: genome analyses in the domestic dog. *Annu Rev Genet.* 2010;44:309-336.

38. Das S, Idate R, Regan DP, et al. Immune pathways and TP53 missense mutations are associated with longer survival in canine osteosarcoma. *Commun Biol.* 2021;4(1):1178.

39. Cletzer E, Klahn S, Dervisis N, LeRoith T. Identification of the JAK-STAT pathway in canine splenic hemangiosarcoma, thyroid carcinoma, mast cell tumor, and anal sac adenocarcinoma. *Vet Immunol Immunopathol.* 2020;220:109996.

40. LeBlanc AK, Mazcko CN. Improving human cancer therapy through the evaluation of pet dogs. *Nat Rev Cancer.* 2020;20(12):727-742.

41. Henry CJ. Unleashing the power of comparative oncology models in nanomedicine research. *European Journal of Nanomedicine.* 2015;7(2):129-133.

42. Morello E, Martano M, Buracco P. Biology, diagnosis and treatment of canine appendicular osteosarcoma: similarities and differences with human osteosarcoma. *Vet J.* 2011;189(3):268-277.

43. Simpson S, Dunning MD, de Brot S, Grau-Roma L, Mongan NP, Rutland CS. Comparative review of human and canine osteosarcoma: morphology, epidemiology, prognosis, treatment and genetics. *Acta Vet Scand.* 2017;59(1):71.

44. Makielski KM, Mills LJ, Sarver AL, et al. Risk Factors for Development of Canine and Human Osteosarcoma: A Comparative Review. *Vet Sci.* 2019;6(2).

45. Fenger JM, London CA, Kisseberth WC. Canine osteosarcoma: a naturally occurring disease to inform pediatric oncology. *Ilar j.* 2014;55(1):69-85.

46. Maniscalco L, Iussich S, Morello E, et al. Increased expression of insulin-like growth factor-1 receptor is correlated with worse survival in canine appendicular osteosarcoma. *Vet J.* 2015;205(2):272-280.

47. MacEwen EG, Pastor J, Kutzke J, et al. IGF-1 receptor contributes to the malignant phenotype in human and canine osteosarcoma. *J Cell Biochem.* 2004;92(1):77-91.

48. Boerman I, Selvarajah GT, Nielen M, Kirpensteijn J. Prognostic factors in canine appendicular osteosarcoma - a meta-analysis. *BMC Vet Res.* 2012;8:56.
49. Gustafson DL, Duval DL, Regan DP, Thamm DH. Canine sarcomas as a surrogate for the human disease. *Pharmacol Ther.* 2018;188:80-96.
50. Diessner BJ, Marko TA, Scott RM, et al. A comparison of risk factors for metastasis at diagnosis in humans and dogs with osteosarcoma. *Cancer Med.* 2019;8(6):3216-3226.
51. Guim TN, Bianchi MV, De Lorenzo C, et al. Relationship Between Clinicopathological Features and Prognosis in Appendicular Osteosarcoma in Dogs. *J Comp Pathol.* 2020;180:91-99.
52. Karlsson EK, Baranowska I, Wade CM, et al. Efficient mapping of mendelian traits in dogs through genome-wide association. *Nat Genet.* 2007;39(11):1321-1328.
53. Jarvis S, Koumadoraki E, Madouros N, Sharif S, Saleem A, Khan S. Non-rodent animal models of osteosarcoma: A review. *Cancer Treat Res Commun.* 2021;27:100307.
54. Paoloni M, Davis S, Lana S, et al. Canine tumor cross-species genomics uncovers targets linked to osteosarcoma progression. *BMC Genomics.* 2009;10:625.
55. Das S, Idate R, Cronise KE, Gustafson DL, Duval DL. Identifying Candidate Druggable Targets in Canine Cancer Cell Lines Using Whole-Exome Sequencing. *Mol Cancer Ther.* 2019;18(8):1460-1471.
56. Ardito F, Giuliani M, Perrone D, Troiano G, Lo Muzio L. The crucial role of protein phosphorylation in cell signaling and its use as targeted therapy (Review). *Int J Mol Med.* 2017;40(2):271-280.
57. Fleuren ED, Zhang L, Wu J, Daly RJ. The kinome 'at large' in cancer. *Nat Rev Cancer.* 2016;16(2):83-98.
58. Bhullar KS, Lagaron NO, McGowan EM, et al. Kinase-targeted cancer therapies: progress, challenges and future directions. *Mol Cancer.* 2018;17(1):48.
59. Lahiry P, Torkamani A, Schork NJ, Hegele RA. Kinase mutations in human disease: interpreting genotype-phenotype relationships. *Nat Rev Genet.* 2010;11(1):60-74.
60. Du Z, Lovly CM. Mechanisms of receptor tyrosine kinase activation in cancer. *Mol Cancer.* 2018;17(1):58.
61. Bavcar S, Argyle DJ. Receptor tyrosine kinase inhibitors: molecularly targeted drugs for veterinary cancer therapy. *Vet Comp Oncol.* 2012;10(3):163-173.
62. London CA. Tyrosine kinase inhibitors in veterinary medicine. *Top Companion Anim Med.* 2009;24(3):106-112.
63. Kaszak I, Ruszczak A, Kanafa S, Kacprzak K, Król M, Jurka P. Current biomarkers of canine mammary tumors. *Acta Vet Scand.* 2018;60(1):66.
64. Ranieri G, Pantaleo M, Piccinno M, et al. Tyrosine kinase inhibitors (TKIs) in human and pet tumours with special reference to breast cancer: a comparative review. *Crit Rev Oncol Hematol.* 2013;88(2):293-308.
65. Lawrence J, Saba C, Gogal R, Jr., et al. Masitinib demonstrates anti-proliferative and pro-apoptotic activity in primary and metastatic feline injection-site sarcoma cells. *Vet Comp Oncol.* 2012;10(2):143-154.
66. Mauchle U, Selvarajah GT, Mol JA, Kirpensteijn J, Verheije MH. Identification of anti-proliferative kinase inhibitors as potential therapeutic agents to treat canine osteosarcoma. *Vet J.* 2015;205(2):281-287.
67. Tian Z, Niu X, Yao W. Receptor Tyrosine Kinases in Osteosarcoma Treatment: Which Is the Key Target? *Front Oncol.* 2020;10:1642.
68. Cholewa BD, Liu X, Ahmad N. The role of polo-like kinase 1 in carcinogenesis: cause or consequence? *Cancer Res.* 2013;73(23):6848-6855.
69. Colicino EG, Hehnly H. Regulating a key mitotic regulator, polo-like kinase 1 (PLK1). *Cytoskeleton (Hoboken).* 2018;75(11):481-494.
70. de Cárcer G, Manning G, Malumbres M. From Plk1 to Plk5: functional evolution of polo-like kinases. *Cell Cycle.* 2011;10(14):2255-2262.
71. Gjertsen BT, Schöffski P. Discovery and development of the Polo-like kinase inhibitor volasertib in cancer therapy. *Leukemia.* 2015;29(1):11-19.
72. Takai N, Hamanaka R, Yoshimatsu J, Miyakawa I. Polo-like kinases (Plks) and cancer. *Oncogene.* 2005;24(2):287-291.
73. Cheng L, Wang C, Jing J. Polo-like kinase 1 as a potential therapeutic target for osteosarcoma. *Curr Pharm Des.* 2015;21(10):1347-1350.

74. Liu X, Erikson RL. Polo-like kinase (Plk)1 depletion induces apoptosis in cancer cells. *Proc Natl Acad Sci U S A.* 2003;100(10):5789-5794.

75. Xiao D, Yue M, Su H, et al. Polo-like Kinase-1 Regulates Myc Stabilization and Activates a Feedforward Circuit Promoting Tumor Cell Survival. *Mol Cell.* 2016;64(3):493-506.

76. Wang C, Zhang J, Yin J, et al. Alternative approaches to target Myc for cancer treatment. *Signal Transduct Target Ther.* 2021;6(1):117.

77. Feng W, Dean DC, Hornicek FJ, et al. Myc is a prognostic biomarker and potential therapeutic target in osteosarcoma. *Ther Adv Med Oncol.* 2020;12:1758835920922055.

78. Morales AG, Brassesco MS, Pezuk JA, et al. BI 2536-mediated PLK1 inhibition suppresses HOS and MG-63 osteosarcoma cell line growth and clonogenicity. *Anticancer Drugs.* 2011;22(10):995-1001.

79. Liu XS, Liu X. Targeting Plk1 in cutaneous T-cell lymphomas (CTCLs). In: *Cell Cycle.* Vol 10. United States2011:1523.

80. Cunningham JT, Ruggero D. New connections between old pathways: PDK1 signaling promotes cellular transformation through PLK1-dependent MYC stabilization. Cancer Discov. 2013;3(10):1099-1102.

81. Maniscalco L, Iussich S, Morello E, et al. PDGFs and PDGFRs in canine osteosarcoma: new targets for innovative therapeutic strategies in comparative oncology. Vet J. 2013;195(1):41-47.

82. Broeckx BJ, Hitte C, Coopman F, et al. Improved canine exome designs, featuring ncRNAs and increased coverage of protein coding genes. *Sci Rep.* 2015;5:12810.

83. Li H, Durbin R. Fast and accurate short read alignment with Burrows-Wheeler transform. *Bioinformatics.* 2009;25(14):1754-1760.

84. Robinson JT, Thorvaldsdóttir H, Wenger AM, Zehir A, Mesirov JP. Variant Review with the Integrative Genomics Viewer. *Cancer Res.* 2017;77(21):e31-e34.

85. Benjamin D, Sato T, Cibulskis K, Getz G, Stewart C, Lichtenstein L. Calling Somatic SNVs and Indels with Mutect2. *bioRxiv.* 2019:861054.

86. Broeckx BJG, Derrien T, Mottier S, et al. An exome sequencing based approach for genome-wide association studies in the dog. *Sci Rep.* 2017;7(1):15680.

87. Bai B, Zhao WM, Tang BX, et al. DoGSD: the dog and wolf genome SNP database. *Nucleic Acids Res.* 2015;43(Database issue):D777-783.

88. Capriotti E, Montanucci L, Profiti G, et al. Fido-SNP: the first webserver for scoring the impact of single nucleotide variants in the dog genome. *Nucleic Acids Res.* 2019;47(W1):W136-w141.

89. Wang L, Wang S, Li W. RSeQC: quality control of RNA-seq experiments. *Bioinformatics.* 2012;28(16):2184-2185.

90. Anders S, Pyl PT, Huber W. HTSeq--a Python framework to work with high-throughput sequencing data. *Bioinformatics.* 2015;31(2):166-169.

91. Robinson MD, McCarthy DJ, Smyth GK. edgeR: a Bioconductor package for differential expression analysis of digital gene expression data. *Bioinformatics.* 2010;26(1):139-140.

92. Tate JG, Bamford S, Jubb HC, et al. COSMIC: the Catalogue Of Somatic Mutations In Cancer. *Nucleic Acids Res.* 2019;47(D1):D941-d947.

93. Martínez-Jiménez F, Muiños F, Sentís I, et al. A compendium of mutational cancer driver genes. *Nat Rev Cancer.* 2020;20(10):555-572.

94. Misdorp W, Van der Heul RO. Tumours of bones and joints. Bull World Health Organ. 1976;53(2-3):265-282.

95. Loukopoulos P, Robinson WF. Clinicopathological relevance of tumour grading in canine osteosarcoma. J Comp Pathol. 2007;136(1):65-73.

96. Kaczorowski M, Borowiec T, Donizy P, et al. Polo-like kinase-1 immunoreactivity is associated with metastases in cutaneous melanoma. J Cutan Pathol. 2017;44(10):819-826.

97. Birk M, Bürkle A, Pekari K, Maier T, Schmidt M. Cell cycle-dependent cytotoxicity and mitotic spindle checkpoint dependency of investigational and approved antimitotic agents. Int J Cancer. 2012;130(4):798-807.

98. Gola C, Giannuzzi D, Rinaldi A, et al. Genomic and Transcriptomic Characterization of Canine Osteosarcoma Cell Lines: A Valuable Resource in Translational Medicine. Front Vet Sci. 2021;8:666838.

99. Steegmaier M, Hoffmann M, Baum A, et al. BI 2536, a potent and selective inhibitor of polo-like kinase 1, inhibits tumor growth in vivo. Curr Biol. 2007;17(4):316-322.

100. Pauli C, Hopkins BD, Prandi D, et al. Personalized In Vitro and In Vivo Cancer Models to Guide Precision Medicine. Cancer Discov. 2017;7(5):462-477.

101. Lawrence MS, Stojanov P, Polak P, et al. Mutational heterogeneity in cancer and the search for new cancer-associated genes. Nature. 2013;499(7457):214-218.

102. Olivier M, Hollstein M, Hainaut P. TP53 mutations in human cancers: origins, consequences, and clinical use. *Cold Spring Harb Perspect Biol.* 2010;2(1):a001008.

103. Bouaoun L, Sonkin D, Ardin M, et al. TP53 Variations in Human Cancers: New Lessons from the IARC TP53 Database and Genomics Data. *Hum Mutat.* 2016;37(9):865-876.

104. Baugh EH, Ke H, Levine AJ, Bonneau RA, Chan CS. Why are there hotspot mutations in the TP53 gene in human cancers? *Cell Death Differ.* 2018;25(1):154-160.

105. Goodspeed A, Heiser LM, Gray JW, Costello JC. Tumor-Derived Cell Lines as Molecular Models of Cancer Pharmacogenomics. *Mol Cancer Res.* 2016;14(1):3-13.

106. Donehower LA, Soussi T, Korkut A, et al. Integrated Analysis of TP53 Gene and Pathway Alterations in The Cancer Genome Atlas. Cell Rep. 2019;28(11):3010.

107. Pfister NT, Prives C. Transcriptional Regulation by Wild-Type and Cancer-Related Mutant Forms of p53. Cold Spring Harb Perspect Med. 2017;7(2).

108. Duffy MJ, Synnott NC, Crown J. Mutant p53 as a target for cancer treatment. Eur J Cancer. 2017;83:258-265.

109. Wade M, Li YC, Wahl GM. MDM2, MDMX and p53 in oncogenesis and cancer therapy. Nat Rev Cancer. 2013;13(2):83-96.

110. Modesto P, Fernandez JLC, Martini I, et al. Characterization of D-17 Canine Osteosarcoma Cell Line and Evaluation of Its Ability to Response to Infective Stressor Used as Alternative Anticancer Therapy. *Animals (Basel).* 2020;10(11).

111. Czarnecka AM, Synoradzki K, Firlej W, et al. Molecular Biology of Osteosarcoma. Cancers (Basel). 2020;12(8).

112. Baldanza VE, Rogic A, Yan W, et al. Evaluation of canonical Hedgehog signaling pathway inhibition in canine osteosarcoma. PLoS One. 2020;15(4):e0231762.

113. Matsuoka K, Bakiri L, Wolff LI, et al. Wnt signaling and Loxl2 promote aggressive osteosarcoma. Cell Res. 2020;30(10):885-901.

114. Zhang J, Yu XH, Yan YG, Wang C, Wang WJ. PI3K/Akt signaling in osteosarcoma. Clin Chim Acta. 2015;444:182-192.

115. Morrow JJ, Khanna C. Osteosarcoma Genetics and Epigenetics: Emerging Biology and Candidate Therapies. Crit Rev Oncog. 2015;20(3-4):173-197.

116. Jiang C, Ma S, Hu R, et al. Effect of CXCR4 on Apoptosis in Osteosarcoma Cells via the PI3K/Akt/NF-kappabeta Signaling Pathway. Cell Physiol Biochem. 2018;46(6):2250-2260.

117. De Maria R, Miretti S, Iussich S, et al. met oncogene activation qualifies spontaneous canine osteosarcoma as a suitable pre-clinical model of human osteosarcoma. J Pathol. 2009;218(3):399-408.

118. Takagi S, Takemoto A, Takami M, Oh-Hara T, Fujita N. Platelets promote osteosarcoma cell growth through activation of the platelet-derived growth factor receptor-Akt signaling axis. Cancer Sci. 2014;105(8):983-988.

119. Zhang J, Babic A. Regulation of the MET oncogene: molecular mechanisms. Carcinogenesis. 2016;37(4):345-355.

120. Patanè S, Avnet S, Coltella N, et al. MET overexpression turns human primary osteoblasts into osteosarcomas. Cancer Res. 2006;66(9):4750-4757.

121. Zhang Y, Xia M, Jin K, et al. Function of the c-Met receptor tyrosine kinase in carcinogenesis and associated therapeutic opportunities. Mol Cancer. 2018;17(1):45.

122. Han G, Wang Y, Bi W. C-Myc overexpression promotes osteosarcoma cell invasion via activation of MEK-ERK pathway. Oncol Res. 2012;20(4):149-156.

123. Pelengaris S, Littlewood T, Khan M, Elia G, Evan G. Reversible activation of c-Myc in skin: induction of a complex neoplastic phenotype by a single oncogenic lesion. *Mol Cell.* 1999;3(5):565-577.

124. Pelengaris S, Khan M, Evan GI. Suppression of Myc-induced apoptosis in beta cells exposes multiple oncogenic properties of Myc and triggers carcinogenic progression. *Cell.* 2002;109(3):321-334.
125. Chen H, Liu H, Qing G. Targeting oncogenic Myc as a strategy for cancer treatment. *Signal Transduct Target Ther.* 2018;3:5.
126. Allen-Petersen BL, Sears RC. Mission Possible: Advances in MYC Therapeutic Targeting in Cancer. *BioDrugs.* 2019;33(5):539-553.
127. Mo H, He J, Yuan Z, et al. PLK1 contributes to autophagy by regulating MYC stabilization in osteosarcoma cells. *Onco Targets Ther.* 2019;12:7527-7536.
128. Gamberi G, Benassi MS, Bohling T, et al. C-myc and c-fos in human osteosarcoma: prognostic value of mRNA and protein expression. Oncology. 1998;55(6):556-563.
129. Wu X, Cai ZD, Lou LM, Zhu YB. Expressions of p53, c-MYC, BCL-2 and apoptotic index in human osteosarcoma and their correlations with prognosis of patients. Cancer Epidemiol. 2012;36(2):212-216.
130. Chen J, Guo X, Zeng G, Liu J, Zhao B. Transcriptome Analysis Identifies Novel Prognostic Genes in Osteosarcoma. Comput Math Methods Med. 2020;2020:8081973.
131. Whitfield JR, Beaulieu ME, Soucek L. Strategies to Inhibit Myc and Their Clinical Applicability. *Front Cell Dev Biol.* 2017;5:10.
132. Steegmaier M, Hoffmann M, Baum A, et al. BI 2536, a potent and selective inhibitor of polo-like kinase 1, inhibits tumor growth in vivo. Curr Biol. 2007;17(4):316-322.
133. Cheng CY, Liu CJ, Huang YC, Wu SH, Fang HW, Chen YJ. BI2536 induces mitotic catastrophe and radiosensitization in human oral cancer cells. Oncotarget. 2018;9(30):21231-21243.
134. Arata Y, Takagi H. Quantitative Studies for Cell-Division Cycle Control. Front Physiol. 2019;10:1022.
135. Bretones G, Delgado MD, León J. Myc and cell cycle control. Biochim Biophys Acta. 2015;1849(5):506-516.
136. Doz F, Locatelli F, Baruchel A, et al. Phase I dose-escalation study of volasertib in pediatric patients with acute leukemia or advanced solid tumors. Pediatr Blood Cancer. 2019;66(10):e27900.
137. Montaudon E, Nikitorowicz-Buniak J, Sourd L, et al. PLK1 inhibition exhibits strong anti-tumoral activity in CCND1-driven breast cancer metastases with acquired palbociclib resistance. Nat Commun. 2020;11(1):4053.

6. SUPPLEMENTARY

Supplementary Table 1

Panel of Normals: public available WES data from 18 non-tumour bearing and unrelated dogs (normal stroma and blood samples) from NCBI SRA database.

BioSample	Assay Type	Breed	Age	sex	Organism	LibraryLayout	Reference
SAMN10380236	WES	Golden Retriever	6.5 years	female	Canis lupus familiaris	PAIRED	13
SAMN10380231	WES	Shetland Sheepdog	8 years	female	Canis lupus familiaris	PAIRED	13
SAMN10380230	WES	Mix	10.4 years	male	Canis lupus familiaris	PAIRED	13
SAMN10380229	WES	Mix	11.8 years	male	Canis lupus familiaris	PAIRED	13
SAMN10380235	WES	Rottweiler	10.3 years	female	Canis lupus familiaris	PAIRED	13
SAMN10380234	WES	Bernese Mountain Dog	6.8 years	male	Canis lupus familiaris	PAIRED	13
SAMN10380233	WES	Greyhound	10.3 years	female	Canis lupus familiaris	PAIRED	13
SAMN10380232	WES	Labrador	9.5 years	male	Canis lupus familiaris	PAIRED	13
SAMN10380238	WES	Golden Retriever	10.5 years	male	Canis lupus familiaris	PAIRED	13
SAMN10380237	WES	Rhodesian Ridgeback	10.3 years	female	Canis lupus familiaris	PAIRED	13
SAMN10380240	WES	Golden Retriever	9.7 years	female	Canis lupus familiaris	PAIRED	13
SAMN10380239	WES	Cocker Spaniel	12.9 years	female	Canis lupus familiaris	PAIRED	13
SAMN10380241	WES	Boxer	3.8 years	female	Canis lupus familiaris	PAIRED	13
SAMN06885761	WES	Labrador	missing	missing	Canis lupus familiaris	PAIRED	24
SAMN06885765	WES	Labrador	missing	missing	Canis lupus familiaris	PAIRED	24
SAMN06885739	WES	Poodle	missing	missing	Canis lupus familiaris	PAIRED	24
SAMN06885749	WES	Poodle	missing	missing	Canis lupus familiaris	PAIRED	24
SAMN06885753	WES	Poodle	missing	missing	Canis lupus familiaris	PAIRED	24

Supplementary Table 2.
Primer sequences employed in RT-qPCR

Gene	Primer	Sequence
PLK1	Forward	3' GCATTGACGCTGTGTAGCTG 5'
	Reverse	5' AGCAACCGGAAGCCTCTTAC 3'
c-Myc	Forward	3' CCCTCCACCAGGAAGGACTA 5'
	Reverse	5' CGTTGTGTGTTCGCCTCTTG 3'
GAPDH	Forward	3' GGCACAGTCAAGGCTGAGAA 5'
	Reverse	5' CCAGCATCACCCCATTTGAT 3'

7. APPENDIX

- **Gola**, C., Iussich, S., Martano, M., Gattino, F., Morello, E., Martignani, E., Maniscalco, L., Accornero, P., Buracco, P., Aresu, L., De Maria, R. (2020) Clinical significance and in vitro cellular regulation of hypoxia mimicry on HIF-1α and downstream genes in canine appendicular osteosarcoma. The Veterinary Journal, 264:105538.

- Sánchez-Céspedes, R., Accornero, P., Miretti, S., Martignani, E., Gattino, F., Maniscalco, L., **Gola**, C., Iussich, S., Martano, M., Morello, E., Buracco, P., Aresu, L., De Maria, R. (2020) In vitro and in vivo effects of toceranib phosphate in canine osteosarcoma cell lines and associated xenograft orthotopic model. Veterinary Comparative Oncology, 18(1), 117-127.

Clinical significance and in vitro cellular regulation of hypoxia mimicry on HIF-1α and downstream genes in canine appendicular osteosarcoma

C. Gola[a,1], S. Iussich[a,1], S. Noury[b], M. Martano[c], F. Gattino[a], E. Morello[a], E. Martignani[a], L. Maniscalco[a], P. Accornero[a], P. Buracco[a], L. Aresu[a], R. De Maria[a,*]

[a] Department of Veterinary Science, University of Turin, Grugliasco (TO), Italy
[b] Hassan II Institute of Agronomy and Veterinary Medicine, Rabat, Morocco
[c] Department of Veterinary Science, University of Parma, Parma (PR)

ARTICLE INFO

ABSTRACT

Cellular adaptation to a hypoxic microenvironment is essential for tumour progression and is largely mediated by HIF-1α and hypoxia-regulated factors, including CXCR4, VEGF-A and GLUT-1. In human osteosarcoma, hypoxia is associated with resistance to chemotherapy as well as with metastasis and poor survival, whereas little is known about its role in canine osteosarcoma (cOSA). This study aimed primarily to evaluate the prognostic value of several known hypoxic markers in cOSA. Immunohistochemical analysis for HIF-1α, CXCR4, VEGF-A and GLUT-1 was performed on 56 appendicular OSA samples; correlations with clinicopathological features and outcome was investigated. The second aim was to investigate the in vitro regulation of markers under chemically induced hypoxia ($CoCl_2$). Two primary canine osteosarcoma cell lines were selected, and Western blotting, immunofluorescence and qRT-PCR were used to study protein and gene expression.

Dogs with high-grade OSA (35.7%) were more susceptible to the development of metastases ($P = 0.047$) and showed high HIF-1α protein expression ($P = 0.007$). Moreover, HIF-1α overexpression (56%) was correlated with a shorter disease-free interval (DFI; $P = 0.01$), indicating that it is a reliable negative prognostic marker. The in vitro experiments identified an accumulation of HIF-1α in cOSA cells after chemically induced hypoxia, leading to a significant increase in GLUT-1 transcript ($P = 0.02$). HIF-1α might be a promising prognostic marker, highlighting opportunities for the use of therapeutic strategies targeting the hypoxic microenvironment in cOSA. These results reinforce the role of the dog as a comparative animal model since similar hypoxic mechanisms are reported in human osteosarcoma.

© 2020 Elsevier Ltd. All rights reserved.

Introduction

Osteosarcoma (OSA) is the most common primary malignant bone tumour in dogs (Morello et al., 2011; Simpson et al., 2017) and is characterised by highly aggressive behaviour (Schott et al., 2018). Despite the current standard of care, most dogs succumb to disease with median overall survival ranging between 3 and 6 months (Morello et al., 2011). In addition, canine OSA (cOSA) shares several clinical, histopathological and molecular features with its human counterpart, including aberrant expression and mutations of driver genes (Boerman et al., 2012; Gustafson et al., 2018).

Two recent genetic studies have provided crucial insights regarding the wide variety of pathways implicated in the pathogenesis of cOSA and the most frequent mutation hotspots, such as the TP53, RB1, PTEN, CDKN2A, WT1, MYC and MET genes. Recurrent mutations in SETD2, a known tumour-suppressor gene with no previously recognised role in cOSA, have also been described (Sakthikumar et al., 2018; Gardner et al., 2019). In addition, transcriptomic studies highlighted that several micro-environmental stimuli and hypoxia signatures were also enriched in cOSA (Majmundar et al., 2010; Agani and Jiang, 2013; D'Ignazio et al., 2017).

Hypoxia affects multiple physiological functions of somatic cells (Mahdi et al., 2019) and enables adaptive cellular responses to the reduced blood supply in tumours (Schito and Semenza, 2016; Parks et al., 2017). In this context, hypoxic metabolic reprogramming confers an aggressive and metastatic phenotype and resistance to therapy in several tumours (Ouyang et al., 2016). The master regulator of the hypoxic response is hypoxia-inducible factor-1α (HIF-1α; Semenza, 2014). Briefly, decreased oxygenation induces HIF-1α stabilisation, which consequently triggers the

Table 1
Primary antibodies used in this study.

Antibody	Application	Dilution	Code	Source	Validation on canine tissues
HIF-1α	IHC	1:100	A300-286A	Bethyl Laboratories	Mammary tumour (P)
	WB	1:1000	CS-14179	Cell Signaling Technology	Skin (N)
	IF	1:100	610958	BD Transduction Lab.	
GLUT-1	IHC	1:80	NB120-15309	Novus Biologicals	Placenta (P)
	WB	1:500	NB120-15309	Novus Biologicals	Testis (N)
CXCR4	IHC	1:300	NB100-56437	Novus Biologicals	Mammary tumour (P)
	WB	1:750	NB100-56437	Novus Biologicals	Skin (N)
VEGF-A	IHC	1:25	SC-65617	Santa Cruz Biotechnology	N/A
	WB	1:25	SC-65617	Santa Cruz Biotechnology	
α-Tubulin	WB	1:10,000	T-5168	Sigma Aldrich	

IHC, immunohistochemistry; WB, western blot; IF, immunofluorescence; P, positive controls; N, negative controls; N/A, not available.

transcription of specific hypoxia-response genes. The most relevant genes are involved in cell proliferation, angiogenesis, glucose metabolism and cell migration (Hansen et al., 2011; Rankin et al., 2016) and include vascular endothelial growth factor (VEGF), glucose transporter 1 (GLUT-1) and chemokine receptor type 4 (CXCR4; Eales et al., 2016; Rankin and Giaccia, 2016).

In tumours, VEGF acts as a central mediator of angiogenesis, stimulating new blood vessel growth and allowing oxygen and metabolite access (Shibuya, 2013). In cOSA, VEGF upregulation is correlated with a more aggressive phenotype and poor prognosis (Sottnik et al., 2011; Zhao et al., 2015). GLUT-1 mediates glucose transport across the cell membrane and plays a key role in glucose uptake in many cell types including cancer cells (Ramapriyan et al., 2019). GLUT-1 is correlated with a poor prognosis in hOSA, whereas its role in cOSA remains unclear (Petty et al., 2008; Fan et al., 2017). Finally, CXCR4 coordinates cell directional migration to facilitate cell survival during the hypoxic state and is involved in lung metastasis development both in canine and human OSA (Guo et al., 2014; Byrum et al., 2016).

Despite the expanding knowledge about tumour hypoxia and associated therapy resistance mechanisms, few data are available on the role of hypoxia in cOSA. Here, we performed clinical and in vitro investigations to evaluate the prognostic value of HIF-1α and related hypoxic factors in cOSA and to investigate the biological modifications of an induced hypoxic state.

Materials and methods

Sample collection and clinical data

OSA specimens were obtained from 56 dogs diagnosed with appendicular OSA at the Department of Veterinary Sciences (University of Turin) under informed consent from the pet owner. All dogs underwent surgery with limb amputation or limb-sparing techniques and received adjuvant chemotherapy consisting of doxorubicin, cisplatin, or carboplatin as single agents or combinations. Dogs without macroscopic lung or lymph node metastases at presentation were included in the study. Metastatic disease was evaluated by thoracic radiography or computed tomography (CT). Follow-up consisted of clinical evaluation and thoracic radiographs performed every 3 months during the first year and then every 6 months for a minimum of 2 years.

Histological and immunohistochemical analysis

FFPE tumour samples were stained with haematoxylin-eosin for diagnosis. Tumours were classified by the predominant histological pattern according to the World Health Organization (WHO) guidelines (Misdorp and Van der Heul, 1976).

Histological grading was evaluated using the Loukopoulos and Robinson grading system (Loukopoulos and Robinson, 2007) by three independent pathologists (SI, ML, LA). The authors converted this grading into a 2-tier grading system by combining grades I and II (low-grade OSAs) and grade III (high-grade OSAs), according to a recent article (Schott et al., 2018). Immunohistochemistry (IHC) was performed on 4 μm thick paraffin sections. After blocking peroxidase activity (0.3% H_2O_2 in deionised water for 30 min) and heat-induced antigen retrieval (30 min with citrate buffer at 98 °C, pH 6), sections were incubated with primary antibodies against HIF-1α, VEGF-A, CXCR4 and GLUT-1 overnight at 4 °C (Table 1). Sections undergoing HIF-1α immunohistochemical staining were

Table 2
Clinicopathological and immunohistochemical characteristics of the study population.

Variables	Total		
Age (years)	56	Mean	7.5
		Median	8
		Range	2–13
Sex, n (%)	56	Female	25 (44.6)
		Male	31 (55.4)
Breed, n (%)	56	Crossbreed	14 (25)
		Boxer	7 (12.5)
		Rottweiler	6 (10.7)
		German Shepherd	5 (8.9)
		Great Dane	4 (7.2)
		Others	20 (35.7)
Weight (kg)	56	Mean	40.6
		Median	38
		Range	7.5–68
Localisation, n (%)	56	Forelimb	35 (62.5)
		Hindlimb	21 (37.5)
Histological type, n (%)	56	Osteoblastic	35 (62.5)
		Chondroblastic	9 (16.1)
		Fibroblastic	6 (10.7)
		Miscellaneous	6 (10.7)
Grading, n (%)	56	Low grade	36 (64.3)
		High grade	20 (35.7)
Follow-up (days)	54[a]	Mean	119
Disease-free interval		Median	180
		Range	34–1493
		Mean	135
Overall survival		Median	207
		Range	36–193
Metastasis development, n (%)	54[a]	No	21 (38.9)
		Yes	33 (61.1)
HIF-1α, n (%)	50[b]	Negative	22 (44)
		Positive	28 (56)
GLUT-1, n (%)	55[b]	Score 0	7 (12.7)
		Score 1	27 (49.1)
		Score 2	21 (38.2)
CXCR4, n (%)	52[b]	Score 0	11 (21.2)
		Score 1	41 (78.8)
VEGF-A, n (%)	54[b]	Score 0	4 (7.4)
		Score 1	28 (51.9)
		Score 2	22 (40.7)

[a] Two dogs were lost to follow-up and were excluded from the survival analysis.
[b] Immunohistochemical staining was not assessable for the remaining samples.

pretreated with Triton X-100 (Sigma Aldrich; 0.1%) for 10 min at room temperature. All antibodies were validated for cross-reactivity with canine positive controls (Supplementary Fig. 1).

Detection was performed using the Vectastain Elite ABC Kit (Vector Laboratories).

Immunolabeled slides were randomised and masked for blinded examination, which was performed by three independent pathologists. Immunohistochemical evaluation was performed using scoring systems previously reported in the literature (Petty et al., 2008; El Naggar et al., 2012; Ren et al., 2016; Liu et al., 2017; Supplementary Tables 1 and 2).
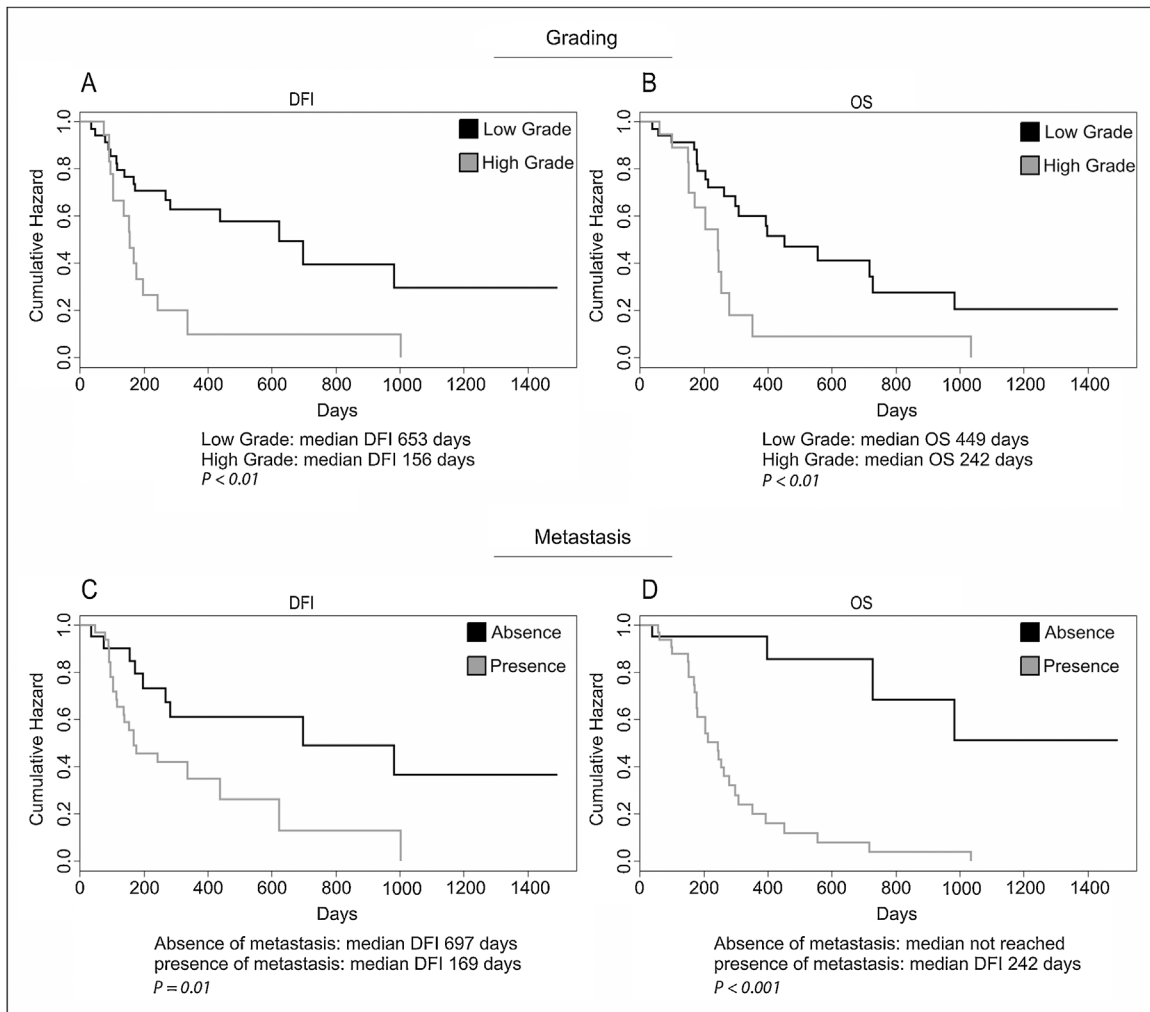
Fig. 1. Kaplan–Meier curve. Disease-free interval (DFI; A) and overall survival (OS; B) in dogs with high-grade osteosarcomas (OSA) compared to dogs with low-grade OSA; DFI (C) and OS (D) in dogs that developed metastases during follow-up compared to those that did not develop metastases.

Cell line validation and culture conditions

Two canine OSA cell lines (Wall and Penny), previously characterised and validated by the authors (Maniscalco et al., 2013), were cultured in Iscove's medium supplemented with 10% foetal bovine serum (FBS), 1% glutamine, 100 μg/mL penicillin and 100 μg/mL streptomycin at 37 °C and 5% CO_2.

Proliferation assay after $CoCl_2$ treatment

A total of 2200 cells/well of Penny and Wall cell lines were cultured in a 96-well CellCarrier Ultra Plate (Perkin Elmer) in chemically induced hypoxic conditions for 12, 24 and 48 h using concentrations of 50, 100 and 200 μM $CoCl_2$ (Sigma Aldrich, 15862-1ML-F; Rana et al., 2019). The same cell lines grown in normal medium without $CoCl_2$ represented the normal control for each condition. All experiments were performed in triplicate and repeated three times.

The Ensight module for well imaging (Perkin Elmer) was used for direct cell counting with digital phase-contrast images without any staining.

Western blot analysis

Proteins from Penny and Wall cell lines, treated with 200 μM of $CoCl_2$ for 12, 24 and 48 h or untreated, were extracted in lysis buffer (1% Triton X-100, 10% glycerol, 50 mM Tris, 150 mM sodium chloride, 2 mM EDTA, pH 8.0 and 2 mM magnesium chloride) containing protease inhibitor cocktail (P8340 Sigma). Twenty micrograms of total protein was separated by SDS-PAGE (10% or 15%) and transferred onto a PVDF membrane. After washing, membranes were incubated in TBS/BSA 10% (bovine serum albumin) at room temperature for 1 h and incubated overnight at 4 °C with HIF-1α, GLUT-1, CXCR4 and VEGF-A antibodies (Table 1). The α-Tubulin was used as an internal control. After incubation with horseradish peroxidase (HRP)-linked secondary antibody diluted 1:10,000 in PBS-Tween, membranes were washed in PBS-Tween for 30 min and incubated with enhanced chemiluminescence reagent (Clarity Wester ECL Substrate, BioRad). The T47D cell line (Cat.# ATCC HTB-133) with and without $CoCl_2$ treatment was used as a control and cross-reactivities of antibodies were validated (Supplementary Fig. 2).

Immunofluorescence

To investigate the effects of $CoCl_2$ on HIF-1α nuclear translocation, immunofluorescence staining for HIF-1α was performed in Penny cells exposed to the highest $CoCl_2$ concentration (200 μM) for 12, 24 and 48 h. Briefly, 2×10^4 cells were plated in four-well chamber slides (Lab-Tek II Chamber Slide System; Nalge Nunc International) and incubated until they reached 70% confluence. After treatment, cells were fixed with methanol:acetone (1:1) for 30 s. After washing three times with Tris-HCl (0.1 M, pH 7.6), cells were blocked with 10% normal goat serum for 1 h at room temperature and then incubated with anti-HIF-1α antibody (Table 1) overnight at 4 °C. After washing with Tris-HCl, cells were incubated with a fluorescent secondary Alexa Fluor 488-conjugated goat anti-rabbit IgG antibody (1:500 dilution, Thermo Fisher) for 1 h in the dark. After cell nuclei were stained with DAPI (0.5 μg/mL in Tris-HCl, Sigma-Aldrich) for 10 min, they were washed three times with Tris-HCl, and then the sections were covered with mounting medium (PermaFluor, Thermo Scientific) and kept overnight in the dark. Immunofluorescence signals were assessed using a Leica AF6000 LX (Leica Microsystems) inverted microscope equipped with a Leica DFC350 FX digital camera. T47D cells (Cat.# ATCC HTB-133) with and without $CoCl_2$ treatment were used as controls and cross-reactivity of antibody was validated (Supplementary Fig. 3).
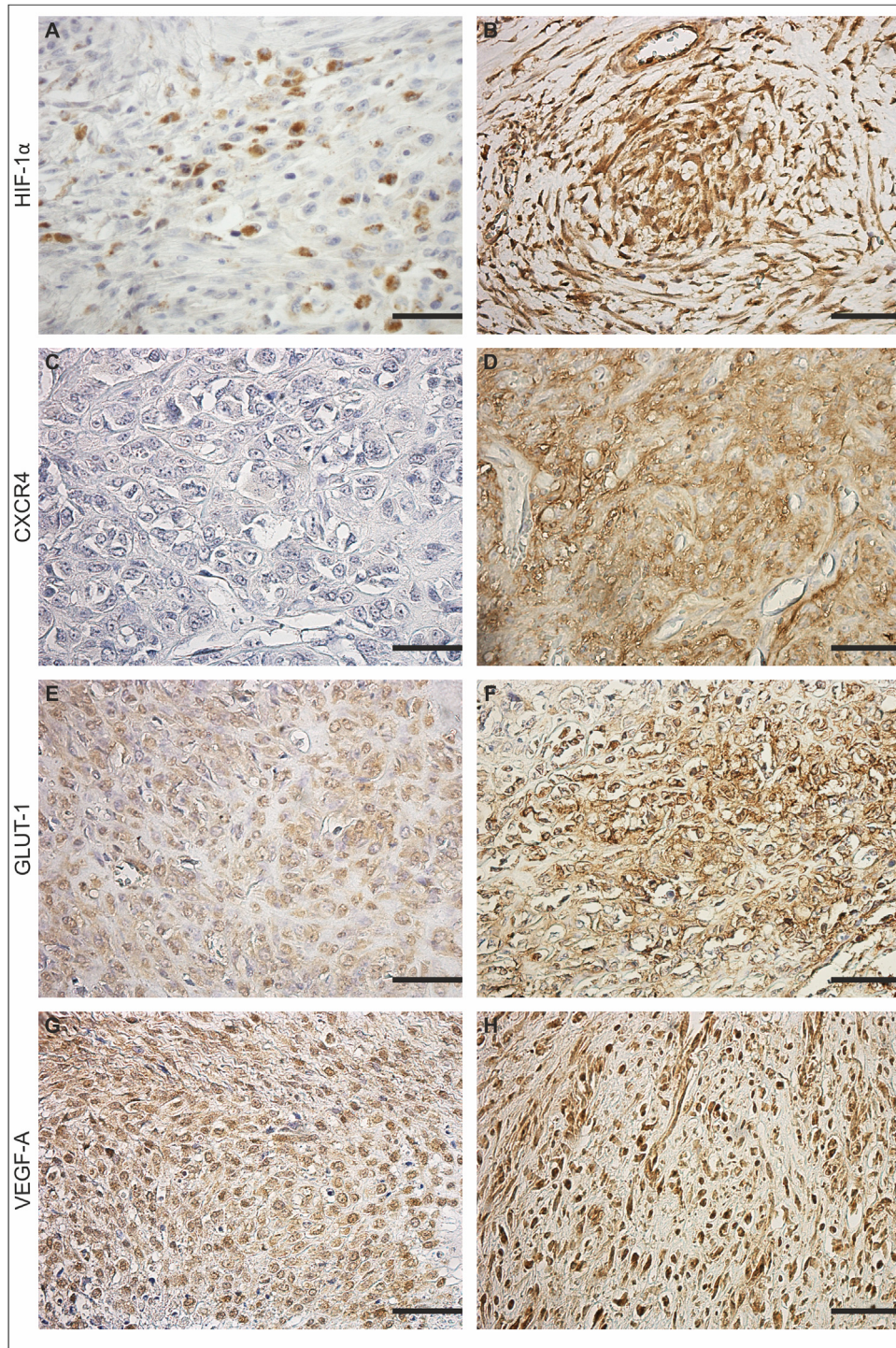
Fig. 2. Immunohistochemical staining in osteosarcoma (OSA). (A) Cytoplasmic (negative) immunohistochemical (IHC) staining of HIF-1α; (B) nuclear (positive) IHC staining of HIF-1α; (C) negative IHC staining of CXCR4; (D) positive IHC staining of CXCR4; (E) weak IHC staining of GLUT-1; (F) strong IHC staining of GLUT-1; (G) moderate IHC staining of VEGF-A; (H) strong IHC staining of VEGF-A (scale bar = 100 μm).

RNA extraction and quantitative PCR (q-PCR)

Total RNA was extracted from Penny and Wall cell lines treated with CoCl$_2$, or without treatment as a control, by using QIAzol Lysis reagent (Qiagen). cDNA was synthesised starting from 1 μg of total RNA using the QuantiTect Reverse Transcription kit (Qiagen). To determine the relative amounts of specific HIF-1α, GLUT-1 CXCR4 and VEGF-A transcripts, the cDNA was subjected to RT-qPCR using the IQ SYBR Green Supermix (BioRad) and the IQ5 detection system (BioRad). The RPS18s was selected as a housekeeping gene among others (HPRT, GAPDH, RP13a, RP18s and RP32) based on its stability and efficiency value.

Primer sequences were designed using Primer Express v. 1.5 software and are listed in Supplementary Table 3. Gene expression was calculated using the formula $2^{-\Delta\Delta Ct}$ (fold increase), where $\Delta\Delta Ct = \Delta Ct$ (sample) – ΔCt (control) and ΔCt was calculated by subtracting the Ct of the target genes from the Ct of the housekeeping gene. qPCR was performed in both technical and experimental triplicates.

Table 3
Correlations between clinical parameters and hypoxia-related markers expression.

	Total n (%) (n = 56)	HIF-1α[a] (n = 50)			GLUT-1[a] (n = 55)				CXCR4[a] (n = 52)			VEGF-A[a] (n = 54)			
		Neg	Pos	P	0	1	2	P	0	1	P	0	1	2	P
Age															
<5 years	9 (16.1)	5	3		2	5	2		1	8		1	5	3	
>5 years	47 (83.9)	17	25	0.25	5	22	19	0.45	11	33	0.36	3	23	19	0.83
Sex															
Female	25 (44.6)	12	11		2	11	11		3	21		0	11	12	
Male	31 (55.4)	10	1	0.29	5	16	10	0.49	8	20	0.16	4	17	10	0.11
Localisation															
Forelimb	35 (62.5)	13	19		5	16	13		7	25		3	16	14	
Hindlimb	21 (37.5)	9	9	0.53	2	11	8	0.84	4	16	0.87	1	12	8	0.75
Histotype															
Osteoblastic	35 (62.5)	15	17		3	21	11		8	25		4	20	14	
Chondroblastic	9 (16.1)	3	5		2	2	4		1	7		0	8	1	
Fibroblastic	6 (10.7)	3	2		2	2	2		1	5		0	4	2	
Others	6 (10.7)	1	4	0.59	0	2	4	0.39	1	4	0.62	0	3	3	0.72
Grading															
Low grade	36 (64.3)	19	14		7	18	11		5	28		2	21	12	
High grade	20 (35.7)	3	14	0.007*	0	9	10	0.07*	6	13	0.16	2	7	10	0.26
Metastasis[b]															
No development	21 (38.9)	11	9		2	10	9		4	26		1	10	10	
Development	33 (61.1)	11	17	0.29	5	17	10	0.63	7	24	0.9	3	18	10	0.49

Neg, negative; Pos, positive.
[a] Immunohistochemical staining was not assessable for the remaining samples.
[b] Two dogs were lost to follow-up.
* $P < 0.05$.
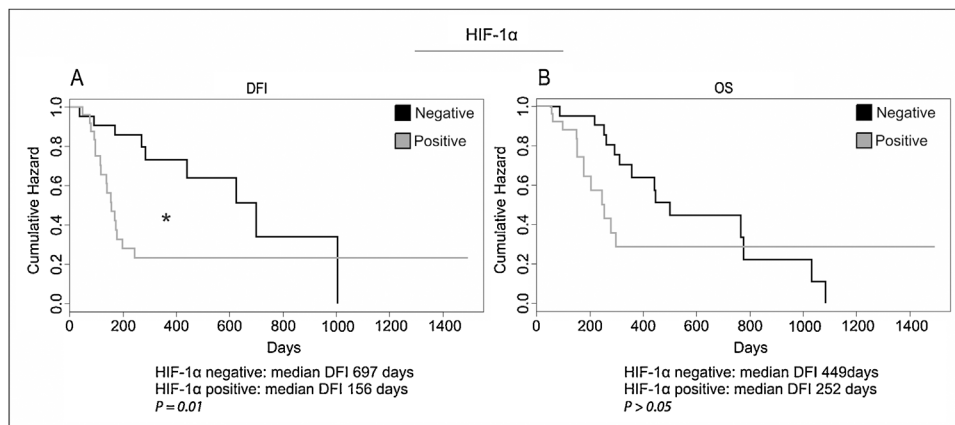
Fig. 3. Kaplan–Meier curve. Disease-free interval (A) and overall survival (B) in dogs with HIF-1α-positive osteosarcomas compared to those with HIF-1α-negative osteosarcomas.
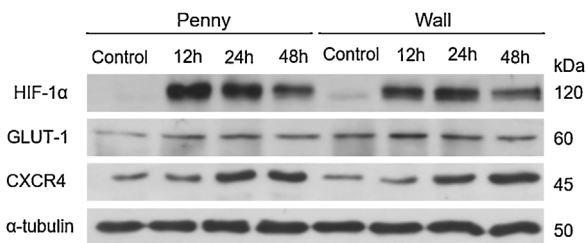
Fig. 4. Western blot analysis of HIF-1α, CXCR4 and GLUT-1 protein expression in osteosarcoma Wall and Penny cell lines treated with $CoCl_2$ (12 h, 24 h and 48 h treatment) or untreated (control). α-Tubulin was used for normalisation.

Statistical analysis

Correlations of HIF-1α, VEGF-A, CXCR4 and GLUT-1 expression with clinical and histopathological data were examined by using contingency tables (χ^2 test). The mutual correlation of these hypoxic markers was also analysed by χ^2 test.

Additionally, a univariate statistical analysis was used to examine the correlations of all variables with the DFI (time elapsed between surgery and the detection of metastases and/or local recurrence) and OS (time elapsed between surgery and death) using the log-rank test and by calculating the Kaplan–Meier survival curves. Dogs who died for unrelated causes or were lost during the follow-up were censored.

All variables showing an association ($P < 0.1$) with OS and DFI by univariate analysis (Supplementary Table 4) were introduced to multivariate logistic regression. Univariate and multivariate analyses were performed using statistical software[2].

Proliferation assay and gene expression data for treated and untreated cell lines were analysed by two-way ANOVA to investigate the effect of $CoCl_2$. Data were analysed with GraphPad Prism (version 8.0.0, GraphPad Software). A P value of less than 0.05 was considered statistically significant.

[2] See: R Core Team, 2018. R: A language and environment for statistical computing. R Foundation for Statistical Computing, Vienna, Austria. http://www.R-project.org/ (Accessed 2 September 2020).
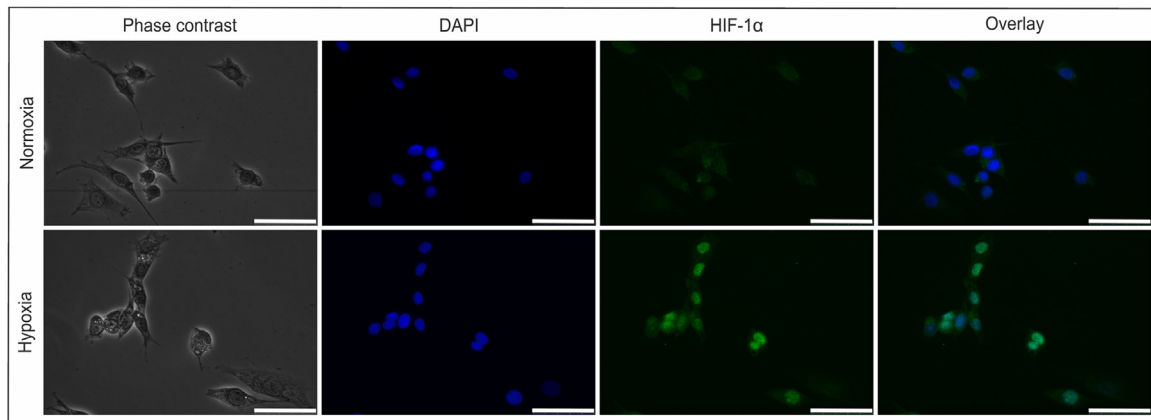
Fig. 5. Immunofluorescence assay. HIF-1α expression in Penny cells without hypoxic treatment (normoxia — first row); HIF-1α expression in Penny cells treated with CoCl$_2$ (hypoxia — second row; scale bar = 50 μm).

Results

Clinicopathological data

Fifty-six dogs with appendicular OSA were included in the study. The clinicopathological characteristics and follow-up data are provided in Table 2 and Supplementary Table 4. Metastasis was observed in 15 of 19 dogs with high-grade OSA and in 18 of 35 dogs with low-grade OSA, and it was revealed that dogs with high-grade OSA were more likely to develop metastases (P = 0.047). The median DFI and OS of dogs without lung metastasis were significantly longer than those of dogs developing lung metastasis (Fig. 1). Finally, dogs diagnosed with high-grade cOSA showed a shorter DFI and OS than dogs with low-grade cOSA (Fig. 1). However, in multivariate analysis, neither tumour grading nor the development of metastasis showed significant correlations with DFI or OS.

HIF-1α as a new prognostic marker

The results of immunohistochemical examinations for HIF-1α, GLUT-1, CXCR4 and VEGF-A are summarised in Table 2, and representative images are shown in Fig. 2. High-grade cOSA was significantly associated with increased HIF-1α expression (Table 3), whereas HIF-1α-positive cOSA showed a significantly shorter DFI than HIF-1α-negative samples (Fig. 3). The expression of GLUT-1 was significantly correlated with the expressions of CXCR4 and HIF-1α (P = 0.02; Supplementary Table 5). In the multivariate analysis, HIF-1α expression remained to be significantly associated with DFI (P = 0.04).

CoCl$_2$ treatment does not affect cellular proliferation in the Penny cell line

To determine whether CoCl$_2$ affected cell proliferation and viability in Penny and Wall cell lines, direct cell counting was performed. The treatment did not significantly affect Penny cell line growth, although an increase in cell population was detectable (Supplementary Fig. 4). Conversely, the proliferation rate in the Wall cell line decreased significantly in a time- and dose-dependent manner.

Hypoxia upregulates HIF-1α, GLUT-1 and CXCR4 protein expression

To determine whether HIF-1α, GLUT-1, CXCR4 and VEGF-A expression was triggered by experimental hypoxic conditions,

Western blot analysis was performed. When treated with CoCl$_2$, both Penny and Wall cell lines showed a moderate increase in HIF-1α, GLUT-1 and CXCR4 protein (Fig. 4). Expression of HIF-1α showed a peak at 12 h after treatment, whereas CXCR4 was detectable after longer incubation times (Fig. 4). VEGF-A protein was not detectable at any considered times (Supplementary Fig. 5).

Hypoxia triggers HIF-1α activation in vitro

The Penny cell line was selected for further experiments given the relevant HIF-1α protein expression. An immunofluorescence assay was performed to verify HIF-1α activation and nuclear translocation under hypoxia mimicry. Under normoxia, HIF-1α was weakly detectable in the cellular cytoplasm, but significant nuclear translocation was recorded after CoCl$_2$ treatment (Fig. 5).

Hypoxia increases GLUT-1 transcript

To gain insight into the transcriptional mechanisms of the hypoxia response in cOSA, qRT-PCR was performed. Increasing exposure times and concentrations of CoCl$_2$ significantly affected GLUT-1 mRNA expression in Penny and Wall cell lines. Although not significant, a mild increase in VEGF-A transcript was always detected in the Penny cell line. Conversely, no modification was observed for HIF-1α and CXCR4 mRNA (Fig. 6).

Discussion

OSA is one of the most aggressive tumours in dogs and is characterised by rapid growth and high metastasis rates, leading to a poor prognosis (Simpson et al., 2017). Although very detailed studies have recently identified mutation hotspots and aberrant oncogenic signalling pathways affecting this tumour (Sakthikumar et al., 2018; Gardner et al., 2019), therapeutic approaches are still very limited and not curative. Therefore, it has become critical to investigate the mechanisms driving pathogenesis and progression.

Solid tumours frequently outgrow the oxygen supply modifying the microenvironment. Limited blood circulation and lack of nutrients cause a selective pressure towards cells with a consequent diminished apoptotic potential and increased migratory capabilities via the activation of hypoxia-related factors (Majmundar et al., 2010; Hiraga, 2018; Yeldag et al., 2018). Within this context, the role of hypoxia has been deeply investigated in hOSA, whereas it little is known about its role in cOSA (Guo et al., 2014; Zhao et al., 2015; Zhang et al., 2018).
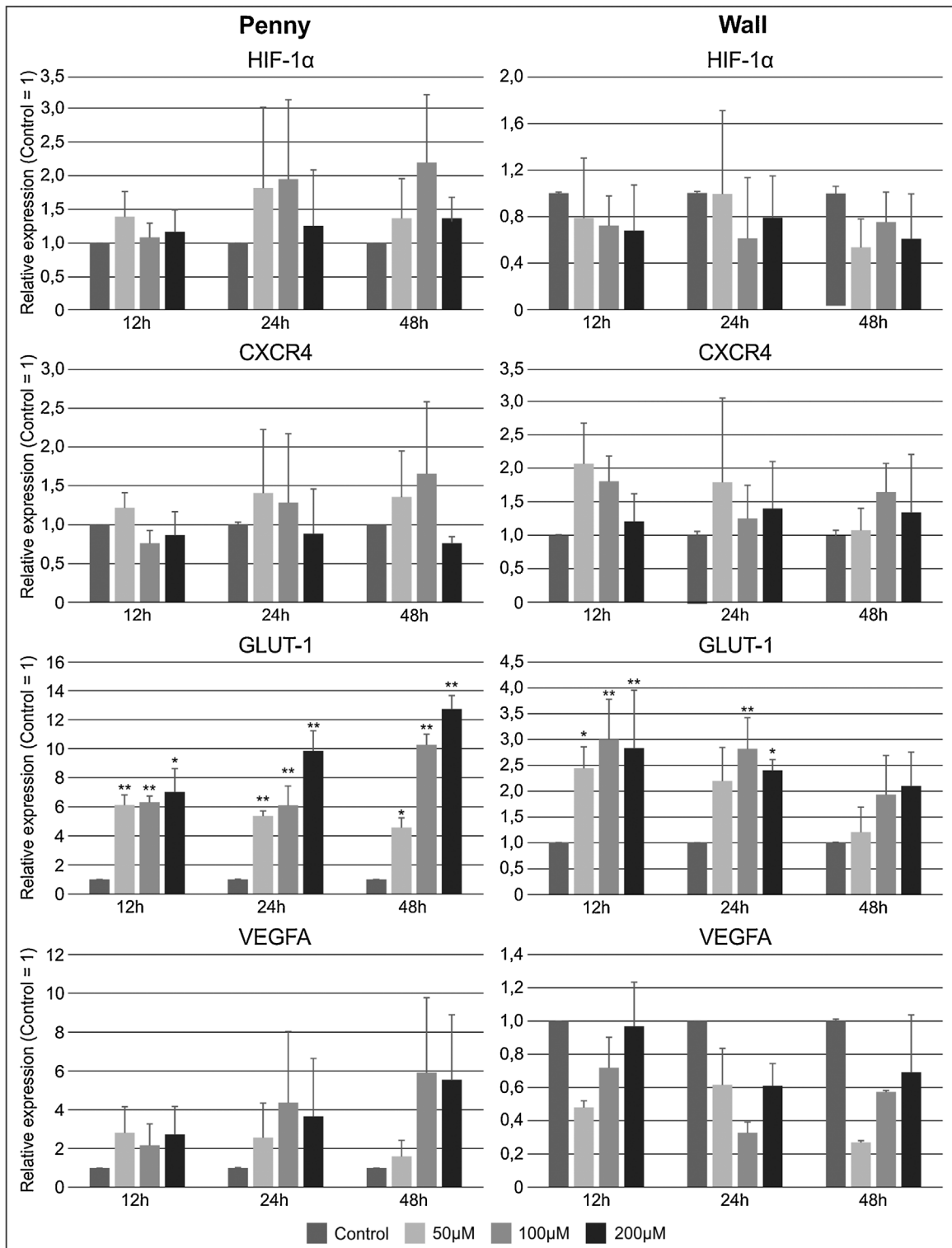
Fig. 6. Results of quantitative RT-PCR for HIF-1α, CXCR4, GLUT-1 and VEGF-A mRNAs. Expressions of these mRNAs in Penny and Wall cell lines treated with $CoCl_2$ were compared with control at different exposure times and treatment concentrations. The fold increase of each specific mRNA was calculated by normalising to the expression level in Penny or Wall untreated cell lines, and the error bars indicate the standard error of the mean of experimental triplicates. $*P < 0.05$; $**P < 0.01$.

In the present study, we first examined HIF-1α, GLUT-1, CXCR4 and VEGF-A protein expression in surgically removed cOSA samples. HIF-1α was a negative prognostic marker and was correlated with tumour grade and DFI. Additionally, dogs with a shorter OS showed a higher protein accumulation compared to dogs with a more favourable prognosis. These findings outline the potential prognostic value of HIF-1α in cOSA. A similar approach has been pursued in humans where similar data in preclinical

studies have encouraged clinical trials with drugs targeting the hypoxic microenvironment (Ajith, 2018; Semenza, 2019). GLUT-1 overexpression was associated with high-grade cOSA, and a correlation with both HIF-1α and CXCR4 was found, suggesting an interaction among these proteins, as previously reported in hOSA (Ajith, 2018). These results slightly contrast with those of Petty et al. (Petty et al., 2008), who showed that lower GLUT-1 expression was observed in cOSA but was not associated with clinical features. Although no correlation between GLUT-1 and clinical outcome was found in this study, GLUT-1 expression is an independent prognostic factor in hOSA (Fan et al., 2017). This discrepancy may be due to the small sample size, subjective measurement methods of GLUT-1 and the possible concurrence of other factors in cOSA prognosis.

No correlation between VEGF-A with clinicopathological parameters and hypoxic markers was identified. Nevertheless, our results suggest that VEGF-A is present in a meaningful percentage of samples and its serum concentration has been previously correlated with poor prognosis in cOSA (Thamm et al., 2008). VEGF-A expression is correlated with a poor clinical outcome in hOSA (Sottnik et al., 2011; Zhao et al., 2015). However, conflicting results are reported in the literature (Simpson et al., 2017), which is likely related to the low number of cases analysed or the complex network that modulates tumour angiogenesis (Mahdi et al., 2019).

To gain insight into the hypoxic microenvironment of cOSA, two primary cell lines were treated with cobalt chloride (CoCl₂), mimicking a hypoxic stimulus (Rana et al., 2019). Cell proliferation assays showed that the response to chemically-induced hypoxia differed among cell types, showing its dual role in inducing cell proliferation as well as cell death. The experiment induced an accumulation of HIF-1α, as shown by Western blot assay. In accordance with previous data, we hypothesize that this might be due to a decreased protein degradation (Jun et al., 2017; Parks et al., 2017). Although slower than the changes in HIF-1α expression levels, both CXCR4 and GLUT-1 protein expressions levels were increased by the treatment. These results suggest a direct role of HIF-1α in stimulating the upregulation of these two proteins under hypoxic conditions (Guo et al., 2014; Parks et al., 2016). Conversely, VEGF-A was never detectable in the cellular lysates, evoking rapid secretion of the protein into the medium after CoCl₂ treatment, whereas tumour cells expressed its transcript (Detwiller et al., 2005; Tsuzuki et al., 2012, 2016). To further confirm HIF-1α induction and stabilisation under hypoxic treatment, we performed an immunofluorescence assay. The results corroborated the evidence that HIF-1α is stabilised under CoCl₂-mediated hypoxia and migrates into the nucleus, avoiding proteasomal degradation in OSA cell lines (Lee et al., 2018; Rana et al., 2019). Constitutively, HIF-1α translocates into the nucleus directly to coordinate the transcription of downstream genes involved in the regulation of cell proliferation (Semenza, 2014; Jun et al., 2017). These findings reinforce the leading role of HIF-1α under hypoxic conditions in cOSA.

Finally, we performed qRT-PCR to investigate the HIF-1α-dependent transcriptional cascade under hypoxic conditions. Cell lines treated with CoCl₂ showed a significant increase in GLUT-1 mRNA levels compared to untreated cell lines. Again, this result supports a potential metabolic reprogramming process triggered by HIF-1α signalling (Parks et al., 2017). Regardless, the Warburg effect might contribute to GLUT-1 overexpression, since increased glycolytic metabolism is also reported independently of HIF-1α signalling (Ramapriyan et al., 2019). Finally, no significant variation of the HIF-1α transcript was observed (Zhao et al., 2015).

The discrepancy between HIF-1α protein and mRNA levels was not surprising and is justifiable based on the physiological proteasomal regulation of this factor (Semenza, 2014). Conversely, both CXCR4 and VEGF-A transcripts were not significantly altered by CoCl₂ treatment, and only a slight increase in VEGF-A was found. However, other genes such as EGF, TGF-β and ERRB2, could be implicated in the transcriptional regulation of CXCR4 and VEGF-A (Loureiro and D'Amore, 2005; Liao et al., 2013).

The major limitation of the current study is that in vitro experiments were performed under chemical hypoxic mimicry, so that further evaluation of real hypoxia effects in cOSA cell lines should be considered. Further studies are also needed to investigate the in vitro effects of specific inhibitors of the hypoxic pathway as potentially effective anti-cancer drugs. Notably, multiple molecular mechanisms, such as those involving tumour-derived cytokines and growth factors, may affect HIF-1α and its downstream effectors (Unwith et al., 2015; Chee et al., 2019).

Conclusions

The modifications associated with chemically induced hypoxia in cOSA were investigated. HIF-1α is a promising prognostic marker, and new therapeutic strategies targeting this factor should be considered in high-grade cOSA (Fallah and Rini, 2019; Semenza, 2019). These data also reinforce the role of the dog as a comparative animal model, since similar hypoxia signalling pathways are reported in hOSA. Further studies are also needed to investigate the in vitro effects of specific inhibitors of the hypoxic pathway as potentially effective anti-cancer drugs.

Conflict of interest

None of the authors of this paper has a financial or personal relationship with other people or organisations that could inappropriately influence or bias the content of the paper.

Acknowledgements

Appendix A. Supplementary data

Supplementary material related to this article can be found, in the online version, at doi:https://doi.org/10.1016/j.tvjl.2020.105538.

References

Agani, F., Jiang, B.H., 2013. Oxygen-independent regulation of HIF-1: novel involvement of PI3K/AKT/mTOR pathway in cancer. Current Cancer Drug Targets 13, 245–251.

Ajith, T.A., 2018. Current insights and future perspectives of hypoxia-inducible factor-targeted therapy in cancer. Journal of Basic and Clinical Physiology and Pharmacology 30, 11–18.

Boerman, I., Selvarajah, G.T., Nielen, M., Kirpensteijn, J., 2012. Prognostic factors in canine appendicular osteosarcoma — a meta-analysis. BMC Veterinary Research 8, 56.

Byrum, M.L., Pondenis, H.C., Fredrickson, R.L., Wycislo, K.L., Fan, T.M., 2016. Downregulation of CXCR4 expression and functionality after zoledronate exposure in canine osteosarcoma. Journal of Veterinary Internal Medicine 30, 1187–1196.

Chee, N.T., Lohse, I., Brothers, S.P., 2019. mRNA-to-protein translation in hypoxia. Molecular Cancer 18, 49.

D'Ignazio, L., Batie, M., Rocha, S., 2017. Hypoxia and inflammation in cancer, focus on HIF and NF-kappaB. Biomedicines 5, 21.

Detwiller, K.Y., Fernando, N.T., Segal, N.H., Ryeom, S.W., D'Amore, P.A., Yoon, S.S., 2005. Analysis of hypoxia-related gene expression in sarcomas and effect of hypoxia on RNA interference of vascular endothelial cell growth factor A. Cancer Research 65, 5881–5889.

Eales, K.L., Hollinshead, K.E., Tennant, D.A., 2016. Hypoxia and metabolic adaptation of cancer cells. Oncogenesis 5, e190.

El Naggar, A., Clarkson, P., Zhang, F., Mathers, J., Tognon, C., Sorensen, P.H., 2012. Expression and stability of hypoxia inducible factor 1alpha in osteosarcoma. Pediatric Blood and Cancer 59, 1215–1222.

Fallah, J., Rini, B.I., 2019. HIF Inhibitors: status of current clinical development. Current Oncology Reports 21, 6.

Fan, J., Mei, J., Zhang, M.Z., Yuan, F., Li, S.Z., Yu, G.R., Chen, L.H., Tang, Q., Xian, C.J., 2017. Clinicopathological significance of glucose transporter protein-1 overexpression in human osteosarcoma. Oncology Letters 14, 2439–2445.

Gardner, H.L., Sivaprakasam, K., Briones, N., Zismann, V., Perdigones, N., Drenner, K., Facista, S., Richholt, R., Liang, W., Aldrich, J., et al., 2019. Canine osteosarcoma genome sequencing identifies recurrent mutations in DMD and the histone methyltransferase gene SETD2. Communications Biology 2, 266.

Guo, M., Cai, C., Zhao, G., Qiu, X., Zhao, H., Ma, Q., Tian, L., Li, X., Hu, Y., Liao, B.M., et al., 2014. Hypoxia promotes migration and induces CXCR4 expression via HIF-1alpha activation in human osteosarcoma. PLoS One 9, e90518.

Gustafson, D.L., Duval, D.L., Regan, D.P., Thamm, D.H., 2018. Canine sarcomas as a surrogate for the human disease. Pharmacology and Therapeutics 188, 80–96.

Hansen, A.E., Kristensen, A.T., Law, I., Jorgensen, J.T., Engelholm, S.A., 2011. Hypoxia-inducible factors–regulation, role and comparative aspects in tumourigenesis. Veterinary and Comparative Oncology 9, 16–37.

Hiraga, T., 2018. Hypoxic microenvironment and metastatic bone disease. International Journal of Molecular Sciences 19, 3523.

Jun, J.C., Rathore, A., Younas, H., Gilkes, D., Polotsky, V.Y., 2017. Hypoxia-inducible factors and cancer. Current Sleep Medicine Reports 3, 1–10.

Lee, H.R., Leslie, F., Azarin, S.M., 2018. A facile in vitro platform to study cancer cell dormancy under hypoxic microenvironments using $CoCl_2$. Journal of Biological Engineering 12, 12.

Liao, Y.X., Zhou, C.H., Zeng, H., Zuo, D.Q., Wang, Z.Y., Yin, F., Hua, Y.Q., Cai, Z.D., 2013. The role of the CXCL12-CXCR4/CXCR7 axis in the progression and metastasis of bone sarcomas. International Journal of Molecular Medicine 32, 1239–1246.

Liu, Y., Zhang, F., Zhang, Z., Wang, D., Cui, B., Zeng, F., Huang, L., Zhang, Q., Sun, Q., 2017. High expression levels of Cyr61 and VEGF are associated with poor prognosis in osteosarcoma. Pathology Research and Practice 213, 895–899.

Loukopoulos, P., Robinson, W.F., 2007. Clinicopathological relevance of tumour grading in canine osteosarcoma. Journal of Comparative Pathology 136, 65–73.

Loureiro, R.M., D'Amore, P.A., 2005. Transcriptional regulation of vascular endothelial growth factor in cancer. Cytokine and Growth Factor Review 16, 77–89.

Mahdi, A., Darvishi, B., Majidzadeh, A.K., Salehi, M., Farahmand, L., 2019. Challenges facing antiangiogenesis therapy: the significant role of hypoxia-inducible factor and MET in development of resistance to anti-vascular endothelial growth factor-targeted therapies. Journal of Cellular Physiology 234, 5655–5663.

Majmundar, A.J., Wong, W.J., Simon, M.C., 2010. Hypoxia-inducible factors and the response to hypoxic stress. Molecular Cell 40, 294–309.

Maniscalco, L., Iussich, S., Morello, E., Martano, M., Biolatti, B., Riondato, F., Della Salda, L., Romanucci, M., Malatesta, D., Bongiovanni, L., et al., 2013. PDGFs and PDGFRs in canine osteosarcoma: new targets for innovative therapeutic strategies in comparative oncology. The Veterinary Journal 195, 41–47.

Misdorp, W., Van der Heul, R.O., 1976. Tumours of bones and joints. Bulletin of the World Health Organization 53, 265–282.

Morello, E., Martano, M., Buracco, P., 2011. Biology, diagnosis and treatment of canine appendicular osteosarcoma: similarities and differences with human osteosarcoma. The Veterinary Journal 189, 268–277.

Ouyang, Y., Li, H., Bu, J., Li, X., Chen, Z., Xiao, T., 2016. Hypoxia-inducible factor-1 expression predicts osteosarcoma patients' survival: a meta-analysis. The International Journal of Bioliological Markers 31, 229–234.

Parks, S.K., Cormerais, Y., Marchiq, I., Pouyssegur, J., 2016. Hypoxia optimises tumour growth by controlling nutrient import and acidic metabolite export. Molecular Aspects of Medicine 47–48, 3–14.

Parks, S.K., Cormerais, Y., Pouyssegur, J., 2017. Hypoxia and cellular metabolism in tumour pathophysiology. The Journal of Physiology 595, 2439–2450.

Petty, J.C., Lana, S.E., Thamm, D.H., Charles, J.B., Bachand, A.M., Bush, J.M., Ehrhart, E. J., 2008. Glucose transporter 1 expression in canine osteosarcoma. Veterinary and Comparative Oncology 6, 133–140.

Ramapriyan, R., Caetano, M.S., Barsoumian, H.B., Mafra, A.C.P., Zambalde, E.P., Menon, H., Tsouko, E., Welsh, J.W., Cortez, M.A., 2019. Altered cancer metabolism in mechanisms of immunotherapy resistance. Pharmacology and Therapeutics 195, 162–171.

Rana, N.K., Singh, P., Koch, B., 2019. $CoCl_2$ simulated hypoxia induce cell proliferation and alter the expression pattern of hypoxia associated genes involved in angiogenesis and apoptosis. Biological Research 52, 12.

Rankin, E.B., Giaccia, A.J., 2016. Hypoxic control of metastasis. Science 352, 175–180.

Rankin, E.B., Nam, J.M., Giaccia, A.J., 2016. Hypoxia: signaling the metastatic cascade. Trends in Cancer 2, 295–304.

Ren, Z., Liang, S., Yang, J., Han, X., Shan, L., Wang, B., Mu, T., Zhang, Y., Yang, X., Xiong, S., Wang, G., 2016. Coexpression of CXCR4 and MMP9 predicts lung metastasis and poor prognosis in resected osteosarcoma. Tumour Biology 37, 5089–5096.

Sakthikumar, S., Elvers, I., Kim, J., Arendt, M.L., Thomas, R., Turner-Maier, J., Swofford, R., Johnson, J., Schumacher, S.E., Alfoldi, J., et al., 2018. SETD2 is recurrently mutated in whole-exome sequenced canine osteosarcoma. Cancer Research 78, 3421–3431.

Schito, L., Semenza, G.L., 2016. Hypoxia-inducible factors: master regulators of cancer progression. Trends in Cancer 2, 758–770.

Schott, C.R., Tatiersky, L.J., Foster, R.A., Wood, G.A., 2018. Histologic grade does not predict outcome in dogs with appendicular osteosarcoma receiving the standard of care. Veterinary Pathology 55, 202–211.

Semenza, G.L., 2014. Oxygen sensing, hypoxia-inducible factors, and disease pathophysiology. Annual Review of Pathology 9, 47–71.

Semenza, G.L., 2019. Pharmacologic targeting of hypoxia-inducible factors. Annual Review of Pharmacology and Toxicology 59, 379–403.

Shibuya, M., 2013. Vascular endothelial growth factor and its receptor system: physiological functions in angiogenesis and pathological roles in various diseases. The Journal of Biochemistry 153, 13–19.

Simpson, S., Dunning, M.D., de Brot, S., Grau-Roma, L., Mongan, N.P., Rutland, C.S., 2017. Comparative review of human and canine osteosarcoma: morphology, epidemiology, prognosis, treatment and genetics. Acta Veterinaria Scandinavica 59, 71.

Sottnik, J.L., Hansen, R.J., Gustafson, D.L., Dow, S.W., Thamm, D.H., 2011. Induction of VEGF by tepoxalin does not lead to increased tumour growth in a canine osteosarcoma xenograft. Veterinary and Comparative Oncology 9, 118–130.

Thamm, D.H., O'Brien, M.G., Vail, D.M., 2008. Serum vascular endothelial growth factor concentrations and postsurgical outcome in dogs with osteosarcoma. Veterinary and Comparative Oncology 6, 126–132.

Tsuzuki, T., Okada, H., Cho, H., Tsuji, S., Nishigaki, A., Yasuda, K., Kanzaki, H., 2012. Hypoxic stress simultaneously stimulates vascular endothelial growth factor via hypoxia-inducible factor-1alpha and inhibits stromal cell-derived factor-1 in human endometrial stromal cells. Human Reproduction 27, 523–530.

Tsuzuki, T., Okada, H., Shindoh, H., Shimoi, K., Nishigaki, A., Kanzaki, H., 2016. Effects of the hypoxia-inducible factor-1 inhibitor echinomycin on vascular endothelial growth factor production and apoptosis in human ectopic endometriotic stromal cells. Gynecological Endocrinology 32, 323–328.

Unwith, S., Zhao, H., Hennah, L., Ma, D., 2015. The potential role of HIF on tumour progression and dissemination. Interantional Journal of Cancer 136, 2491–2503.

Yeldag, G., Rice, A., Del Rio Hernandez, A., 2018. Chemoresistance and the self-maintaining tumor microenvironment. Cancers 10, 471.

Zhang, B., Li, Y.L., Zhao, J.L., Zhen, O., Yu, C., Yang, B.H., Yu, X.R., 2018. Hypoxia-inducible factor-1 promotes cancer progression through activating AKT/Cyclin D1 signaling pathway in osteosarcoma. Biomedicine and Pharmacotherapy 105, 1–9.

Zhao, H., Wu, Y., Chen, Y., Liu, H., 2015. Clinical significance of hypoxia-inducible factor 1 and VEGF-A in osteosarcoma. Internal Journal of Clinical Oncology 20, 1233–1243.

Veterinary and Comparative Oncology WILEY

In vitro and in vivo effects of toceranib phosphate on canine osteosarcoma cell lines and xenograft orthotopic models

Raquel Sánchez-Céspedes[1] | Paolo Accornero[2] | Silvia Miretti[2] |
Eugenio Martignani[2] | Francesca Gattino[2] | Lorella Maniscalco[2] | Cecilia Gola[2] |
Selina Iussich[2] | Marina Martano[2] | Emanuela Morello[2] | Paolo Buracco[2] |
Luca Aresu[2] | Raffaella De Maria[2]

[1]Department of Comparative Pathology, Veterinary Faculty, University of Córdoba, Córdoba, Spain

[2]Department of Veterinary Science, University of Turin, Grugliasco, Italy

Correspondence
Paolo Accornero, Department of Veterinary Science, University of Turin, Largo Braccini 2, Grugliasco 10095, Italy.
Email: paolo.accornero@unito.it

Abstract

Canine osteosarcoma (OSA) is the most common primary malignant bone tumour in dogs, and it has a high metastatic rate and poor prognosis. Toceranib phosphate (TOC; Palladia, Zoetis) is a veterinary tyrosine kinase inhibitor that selectively inhibits VEGFR-2, PDGFRs and c-Kit, but its efficacy is not yet fully understood in the treatment of canine OSA. Here, we evaluated the functional effects of TOC on six OSA cell lines by transwell, wound healing and colony formation assays. Subsequently, two cell lines (Wall and Penny) were selected and were inoculated in mice by intra-femoral injection to develop an orthotopic xenograft model of canine OSA. For each cell line, 30 mice were xenografted; half of them were used as controls, and the other half were treated with TOC at 40 mg/kg body weight for 20 days. TOC inhibited cell growth of all cell lines, but reduced invasion and migration was only observed in Penny and Wall cell lines. In mice engrafted with Penny cells and subjected to TOC treatment, decreased tumour growth was observed, and PDGFRs and c-Kit mRNA were downregulated. Immunohistochemical analyses demonstrated a significant reduction of Ki67 staining in treated mice when compared to controls. The results obtained here demonstrate that TOC is able to slightly inhibit cell growth in vitro, while its effect is evident only in a Penny cell xenograft model, in which TOC significantly reduced tumour size and the Ki67 index without modifying apoptosis markers.

KEYWORDS

comparative oncology, in vitro models, mouse models, toceranib phosphate, tyrosine kinase

1 | INTRODUCTION

Considering the high similarity at the clinical, histopathological and molecular levels, spontaneous tumours in dogs are considered excellent models for human diseases, representing an alternative to rodents for studying cancer biology and therapy.[1,2] Canine osteosarcoma (OSA) represents the most common primary malignant bone tumour in dogs, accounting for more than 80% of all bone tumours; it is locally aggressive and is characterized by a high metastatic potential and poor prognosis.[1,3,4] Furthermore, the role of several tyrosine kinase receptors (TKRs) in the pathogenesis of canine OSA was recently demonstrated,[5-7] which reveals the utility of tyrosine kinase inhibitors (TKIs) against specific targets.[8,9]

TKIs have radically changed the treatment approach and prognosis of several human tumours[10,11]; further, in veterinary medicine, this class of molecules has been shown to be promising in the treatment of a few cancer histotypes.[12-15] Toceranib phosphate (TOC; Palladia, Zoetis) is a specific veterinary TKI that selectively inhibits VEGFR-2,

PDGFRs and c-Kit and is currently approved for the treatment of mast cell tumours.[16,17] However, there is increasing evidence that other solid tumours, such as anal sac, head-neck and thyroid carcinomas, and OSA can be successfully treated with TOC.[18,19] Clinical trials performed on canine OSA patients showed controversial results when using Palladia as a single agent in canine metastatic OSA or in combination with other drugs, suggesting that more data are needed to clarify its benefit.[20-24] Xenograft mouse models represent important tools for investigating the in vivo response to cancer therapeutic interventions. Previously reported canine OSA mouse models, which are heterotopic, were obtained by implanting OSA cells intramuscularly or subcutaneously in mice[25-27]; however, intrinsic limitations existed, such as OSA cells not being exposed to the constitutive microenvironment. Consequently, the biological behaviour of the xenograft tumour and its response to therapy may have not completely reflected the disease progress. Orthotopic mouse models represent a more reliable approach for evaluating tumour progression and pharmacological treatment efficacy. As mentioned previously, the clinical use of TOC in canine OSA is still scientifically debated, and further investigations are needed. Considering the relevance of canine OSA both in veterinary medicine and comparative oncology, the aims of this study were to evaluate the functional effects of TOC in primary OSA cell lines and to develop orthotopic mouse models of canine OSA. In addition, mRNA and protein changes to the preferred targets of TOC, as well as the clinical response, were also evaluated in vivo.

2 | MATERIALS AND METHODS

2.1 | Cell-line validation statement and culture conditions

Seven primary canine OSA cell lines ("Penny," "Wall," "Desmond," "Sky," "Dark," "Lord," and "Pedro") that were previously established and validated by Maniscalco et al.[6] were used in this study. All cell lines were maintained in Iscove's standard medium supplemented with 10% foetal bovine serum (FBS), 1% glutamine, 100 μg/mL penicillin and 100 μg/mL streptomycin. Cells were cultured at 37°C in a humidified atmosphere of 5% CO_2, and they were passaged upon reaching confluence. A normal osteoblastic cell line (OSB) was isolated from a healthy dog using a previously described procedure.[5]

2.2 | Migration and invasion assays

The migration capability of all OSA cell lines was evaluated as follows. Cells were trypsinized, resuspended in Iscove's standard medium and counted in Bürker chambers. Subsequently, 1.5×10^4 cells (for invasion 2.5×10^4 cells) were resuspended in 200 μL of supplemented Iscove's standard medium and added to the noncoated upper chamber of a transwell with an 8 μm pore size filter (Corning, Cambridge, Massachusetts). To test the effects of TOC on the migratory capability of

canine OSA cell lines, 800 μL of supplemented Iscove's standard medium with 1 μM TOC was added to the lower chamber (treated groups) of the wells. For controls, 800 μL of supplemented Iscove's standard medium without TOC was added. After 48 hours of incubation, cells on the upper side of the filter were mechanically removed with a cotton swab, and both the cells migrated to the lower side of the transwell and those that reached the bottom of the wells were incubated with 5 μg/mL Hoechst 33342 (Sigma Diagnostic, St. Louis, Missouri) in 1 mL of culture medium at 37°C under 5% CO_2 for 20 minutes; then, the cells were rinsed with PBS (phosphate buffer solution) for 10 minutes three times. An invasion assay was performed on Wall and Penny cell lines as follows. The upper chamber was coated with 10 μg of Growth Factor Reduced Basement Membrane Matrix (Matrigel; Corning) that was diluted in 60 μL of ddH₂O, and the chamber was left to dry in a biological hood for approximately 4 hours. Both the filter and the bottom of the wells were photographed with a fluorescent equipped microscope at 100×, and cells were counted using the ImageJ software. Analyses were performed in triplicate.

2.3 | Cell proliferation assay

Considering the results obtained by transwell assay, Penny and Wall cell lines were selected for time-course proliferation assays. OSA cell lines were plated in six-well plates at a density of 1.5×10^5 cells/well. After 8 hours, the cells were either left untreated (control) or were treated with 1 μM TOC. After 12, 24, 48, and 72 hours, the cells were incubated with 5 μg/mL Hoechst 33342 (Sigma Diagnostic) for 20 minutes. Nuclei were then photographed at 100× (10 random fields for every experiment analysed) and were counted using the public available software Cell Profiler (https://cellprofiler.org/) version 3.1.8. Analyses were performed in triplicate.

2.4 | Wound healing assay

Considering the results obtained from the transwell assays, Penny and Wall cell lines were selected for mobility assays. After trypsinization, 2×10^5 cells/well were plated in six-well plates to grow. When confluence was reached, the monolayer was wounded by applying a manual scratch with a sterile 20 μL pipette tip. The cellular debris was removed with a gentle wash with complete medium, and then supplemented Iscove's medium with 1 μM of TOC (treated groups) or without TOC (control groups) was added to the cells. The ability of the cells to repair the wound was evaluated by real-time microscopy for 48 hours. Cell migration was monitored using a Leica AF6000 LX (Leica Microsystems, Wetzlar, Germany) inverted microscope equipped with a Leica DFC350FX digital camera, and photographs were taken every 30 minutes for 48 hours. The distance between two parallel lines was measured in five different areas along the length of the wound, and the analysis was performed in duplicate.

2.5 | Colony formation assay

Penny and Wall cells were resuspended in 0.4% type VII low melting agarose in DMEM (10% FBS) at 2×10^4 cells/well, and then they were plated on a layer of 0.8% agarose in Iscove's medium (10% FBS) in six-well culture plates and were cultured at 37°C with 5% CO_2. After 24 hours, the medium was removed and was replenished with fresh medium with 1 μM TOC (treated groups) or without TOC (control groups). The medium was changed every 3 days, and after 3 weeks, colonies >100 and <100 μm in diameter were counted under an inverted phase-contrast microscope. Colony formation assays were repeated in triplicate.

2.6 | Orthotopic xenograft mouse model

A total of 60 female *nu/nu* mice, 4 to 5 weeks old, were purchased from Charles River Laboratories (Calco, Milan) and were housed under
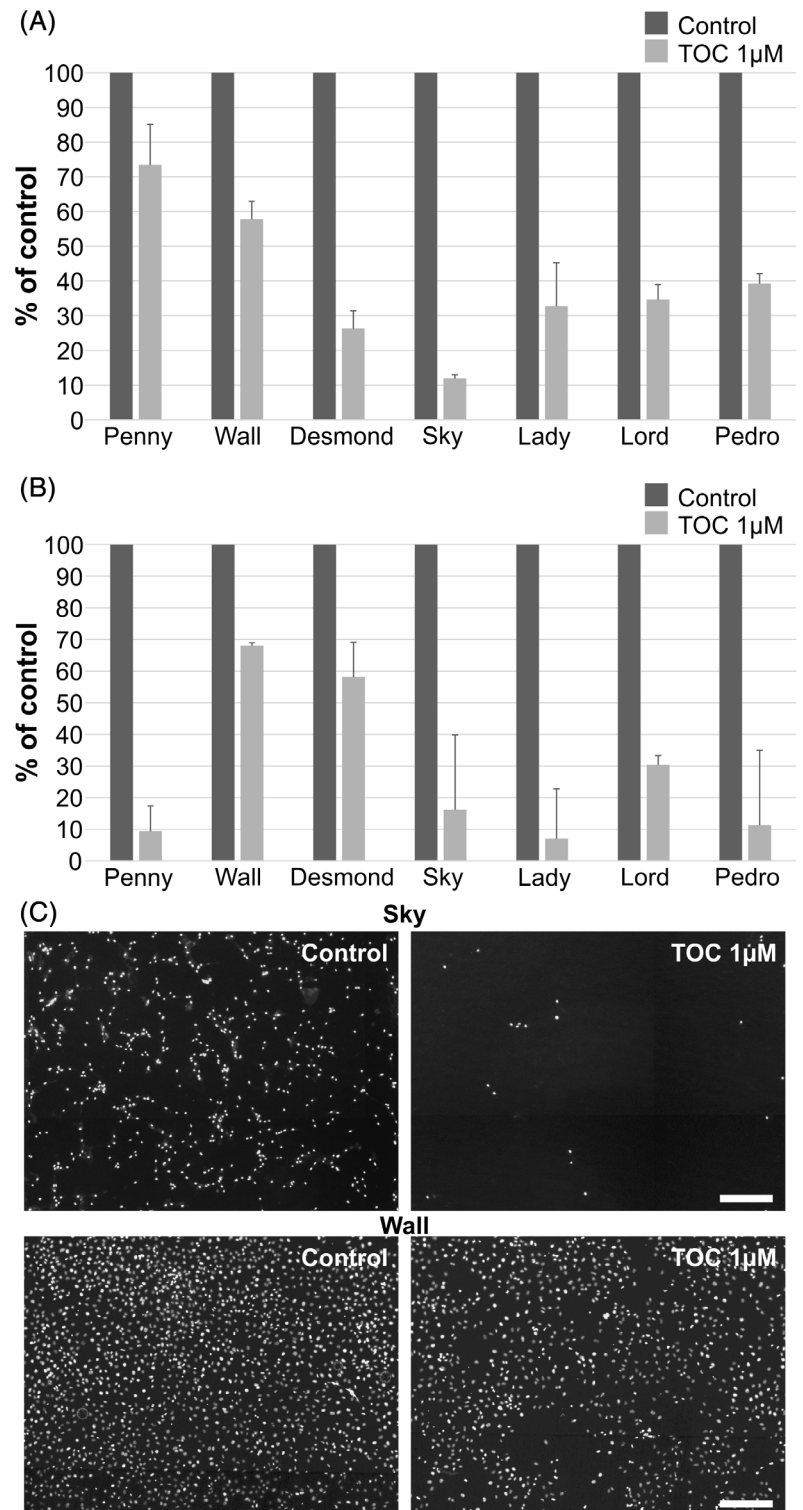
FIGURE 1 Cellular migration by transwell assay. A, Percentage of cells attached to the lower side of the membrane and, B, the bottom of the lower chamber in all canine OSA cell lines treated with Toceranib (1 μM) compared to the control (untreated). Error bars represent standard deviation of experimental triplicates. C, Immunofluorescence assay showing cells migrated to the bottom of the lower chamber in Sky and Wall cell lines treated with TOC compared to the untreated cell lines (Hoechst, ×100, Scale bar = 250 μm). OSA, osteosarcoma; TOC, Toceranib phosphate

pathogen-free conditions with a 12 hours light/12 hours dark schedule; they were fed autoclaved standard chow and water ad libitum. Mice were manipulated and housed according to protocols approved by the Turin University Bioethical Committee and the Italian Ministry of Health (Authorization note no. 149401894128). For intrafemoral injections, exponentially growing cells (Penny and Wall) were harvested, counted and resuspended in PBS to a final concentration of 1×10^7 cells/mL. The animals were anaesthetized with zolazepam/tiletamine (45 mg/kg) and xylazine (7.5 mg/kg). The knee of the mouse was fixed beyond 90°, and 1×10^6 cells resuspended in 100 μL of PBS were injected into the distal femur using a 25-gauge needle. On day 0, 30 mice were injected with Penny and Wall cells. Twice a week, mice were monitored to determine the appearance and/or clinical signs of the engrafted tumour. When an average tumour size of 0.5 cm at the largest diameter was obtained, daily treatment with TOC or a vehicle was initiated. Mice were randomly assigned to each group. According to the literature, mice were treated once daily with TOC at 40 mg/kg body weight in citrate buffered (pH 3.5) solution[28,29] for 20 days by oral gavage using rigid dosing cannula. Control mice were treated with only citrate buffered saline that was administered by the same procedure. Tumour growth was evaluated twice a week by measuring the tumour size with a calliper. Tumour length (L) and width (W) were measured to calculate tumour volume (V) as follows: $(L \times W^2)/2$. Additionally, body weight was measured. Five mice were not inoculated and were used as body weight controls.

Mice were monitored for up to 20 days posttreatment or until the animal endpoint criteria were reached (ill thrift, visible lameness, pain or severe weight loss), then they were humanely euthanized by an intravenous overdose injection of sodium pentobarbital. At postmortem examination, the tumours were excised and cut into two pieces: one piece was to be frozen in liquid nitrogen for RNA extraction, and the other was fixed in 10% neutral buffered formalin for routine histological examination and immunohistochemistry.

2.7 | RNA extraction and quantitative reverse transcription PCR expression analysis

Total RNA from all the OSA cell lines and the OSB cells, as well as from engrafted tumours, was extracted using 1 mL of TRI Reagent (Sigma-Aldrich), and any residual genomic DNA was removed using a DNAse I recombinant RNase free kit (Roche, Mannheim, Germany). RNA concentration was determined by spectrophotometry (BioPhotometer, Eppendorf, Hamburg, Germany). The ratio of the optical densities measured at 260 and 280 nm was >1.9 for all RNA samples. cDNA was synthesized from 1 μg of total RNA by a RT high-capacity cDNA reverse transcription kit (Applied Biosystems, Foster City, California) according to the manufacturer's protocol. To determine the relative amounts of specific PDGFR-α, PDGFR-β, VEGFR2 and c-Kit transcripts, quantitative reverse transcription PCR (RT-qPCR) was performed using a CFX Connect Real-Time PCR System (Bio-Rad, Hercules, California). Primers for target and reference genes were designed based on *Canis familiaris* GenBank messenger RNA (mRNA) sequences using the Primer 3 Software (version 4.0). Oligonucleotides were designed to cross exon/exon boundaries to minimize the amplification of contaminating genomic DNA, and using an IDT tool (available at http://www.idtdna.com/scitools/scitools.aspx) they were analysed for hairpin structures and dimer formation. Primer specificity was verified with BLAST analysis against the genomic NCBI database. Multiple housekeeping genes were selected among five potential internal control mRNAs in the dog
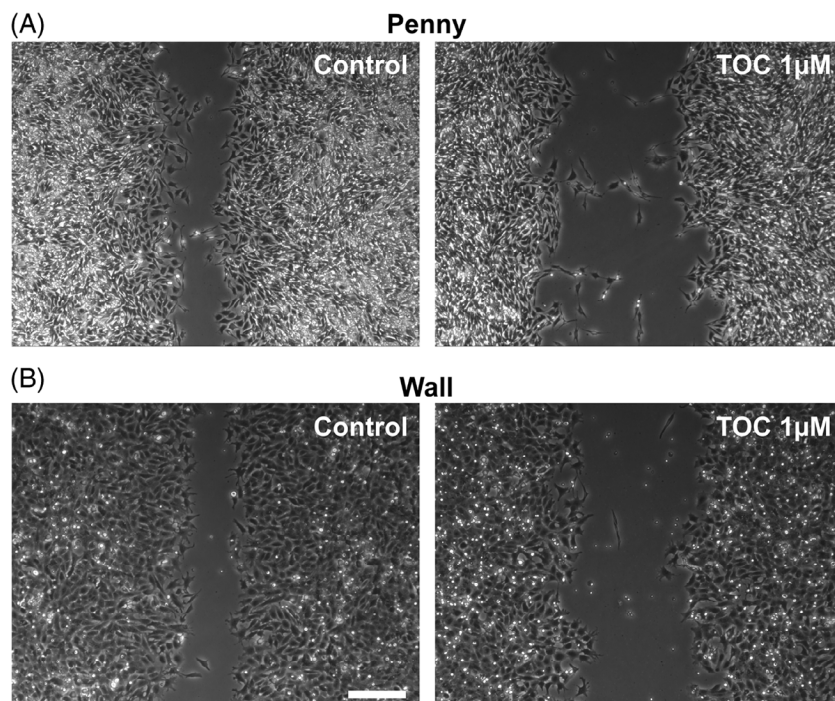

FIGURE 2 Wound healing migration assay. Penny cell line, A, and Wall cell line, B, after 48 hours of treatment with TOC (1 μM) with, respectively, not treated cell lines (×400, Scale bar = 100 μm). TOC, Toceranib phosphate

(HPRT, GAPDH, RP13a, RP18s and RP32), and based on the efficiency value, GAPDH was selected as the most suitable for this purpose.

Table S1 summarizes the primer information, sequences, gene accession number and amplicon sizes. Real-time PCR parameters were as follows: cycle 1, 95°C for 30 seconds; and cycle 2, 95°C for 10 seconds, 60°C for 30 seconds for 40 cycles. Gene expression was calculated using the formula of $2^{-\Delta\Delta Cq}$ (fold increase), where $\Delta\Delta Cq = \Delta Cq$ (target) $- \Delta Cq$ (control), and ΔCq is the Cq of the target gene subtracted from the Cq of the housekeeping gene.

2.8 | Histopathological and immunohistochemical analysis

Systemic organs and tumours obtained from mice were fixed in 10% buffered formalin for 24 hours. When needed, tumours were decalcified in 10% formic acid, and procedures for histological examination were applied. Additionally, several histological parameters were selected and scored (see Table S2).

Immunohistochemistry (IHC) was performed on 4 μm thick paraffin sections derived from OSA originated in mice using an automated immunostainer (DAKO). After blocking peroxidase activity and performing heat-induced antigen retrieval, sections were incubated with Ki67, c-Kit, PDGFR-α, PDGFR-β, VEGFR-2 and caspase 3 antibodies (see Table S3). Positive immunostaining for Ki67 was determined by counting 1000 cells in 10 high power randomly selected neighbouring, nonoverlapping fields. The number of Ki67-positive and Ki67-negative cells was assessed by image analysis using ImageJ freeware, and the number of positive cells was expressed as the percentage of positively stained cells out of the total number of cells.[30] Immunohistochemical evaluation of caspase 3 was carried out by taking images with a 40× microscope objective from 10 random fields per tumour to provide an average index of caspase 3-positive cells.[31] For the IHC evaluation of c-Kit, PDGFR-α, PDGFR-β and VEGFR-2 expression, the percentage of positively stained tumour cells and the relative intensity were scored according to the literature.[6,32,33]

2.9 | Statistical analysis

Immunohistochemistry results were grouped into contingency tables and were analysed using Fisher's exact tests or X^2 tests, while qPCR and in vitro data assays were analysed using Student's t tests and two-way ANOVA. Data were analysed using the MedCalc Statistical Software version 13.3 (MedCalc Software bvba). A P value lower than .05 was considered statistically significant.
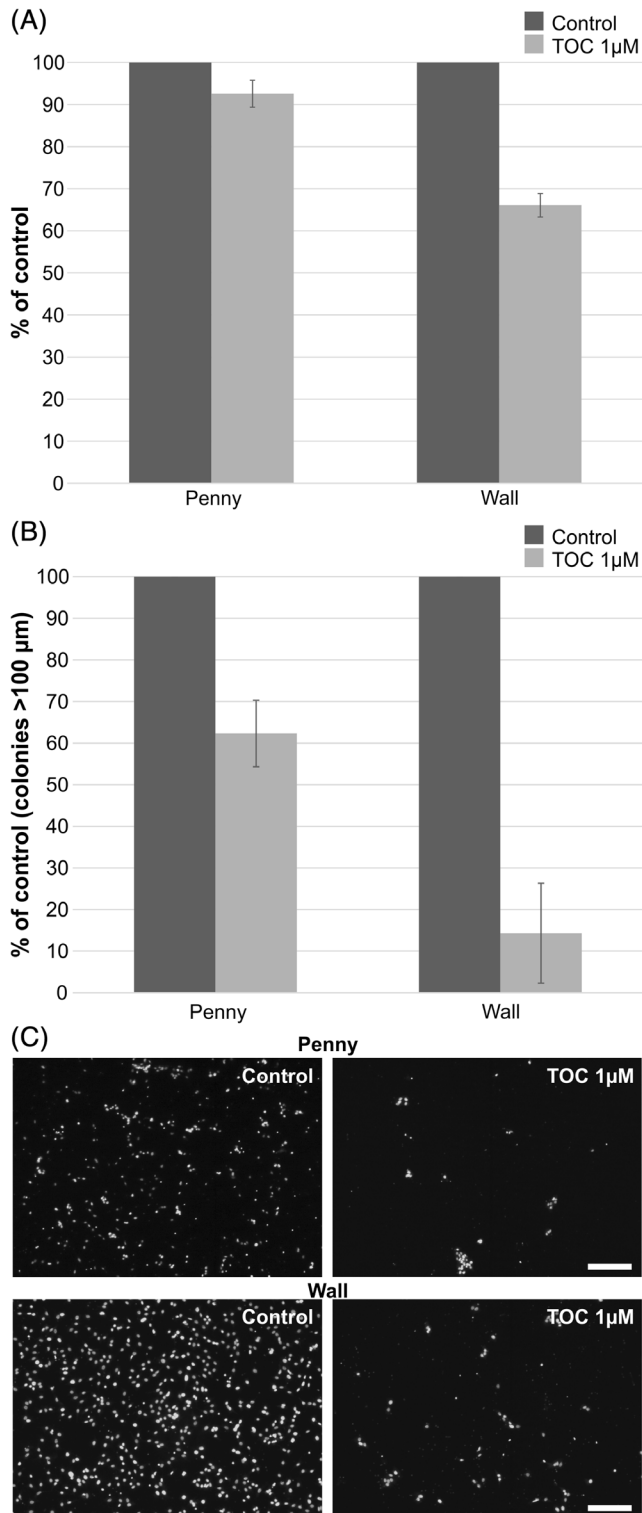

FIGURE 3 Legend on next page.

FIGURE 3 Colony formation assay. A, Percentage of colonies formed in agarose in Penny and Wall cell lines treated with TOC 1 μM compared to the untreated cells. B, Percentage of colonies (>100 μm diameter) formed in agarose in Penny and Wall cell lines treated with TOC 1 μM. Error bars represent standard deviation of experimental triplicates. Transwell migration assay. C, Penny cells attached to the lower side of the membrane after 48 hours incubation with (left) or without (right) TOC treatment. D, Wall cells attached to the lower side of the membrane after 48 hours incubation with (left) or without (right) TOC treatment (Hoechst, ×100; Scale bar = 200 μm). TOC, Toceranib phosphate
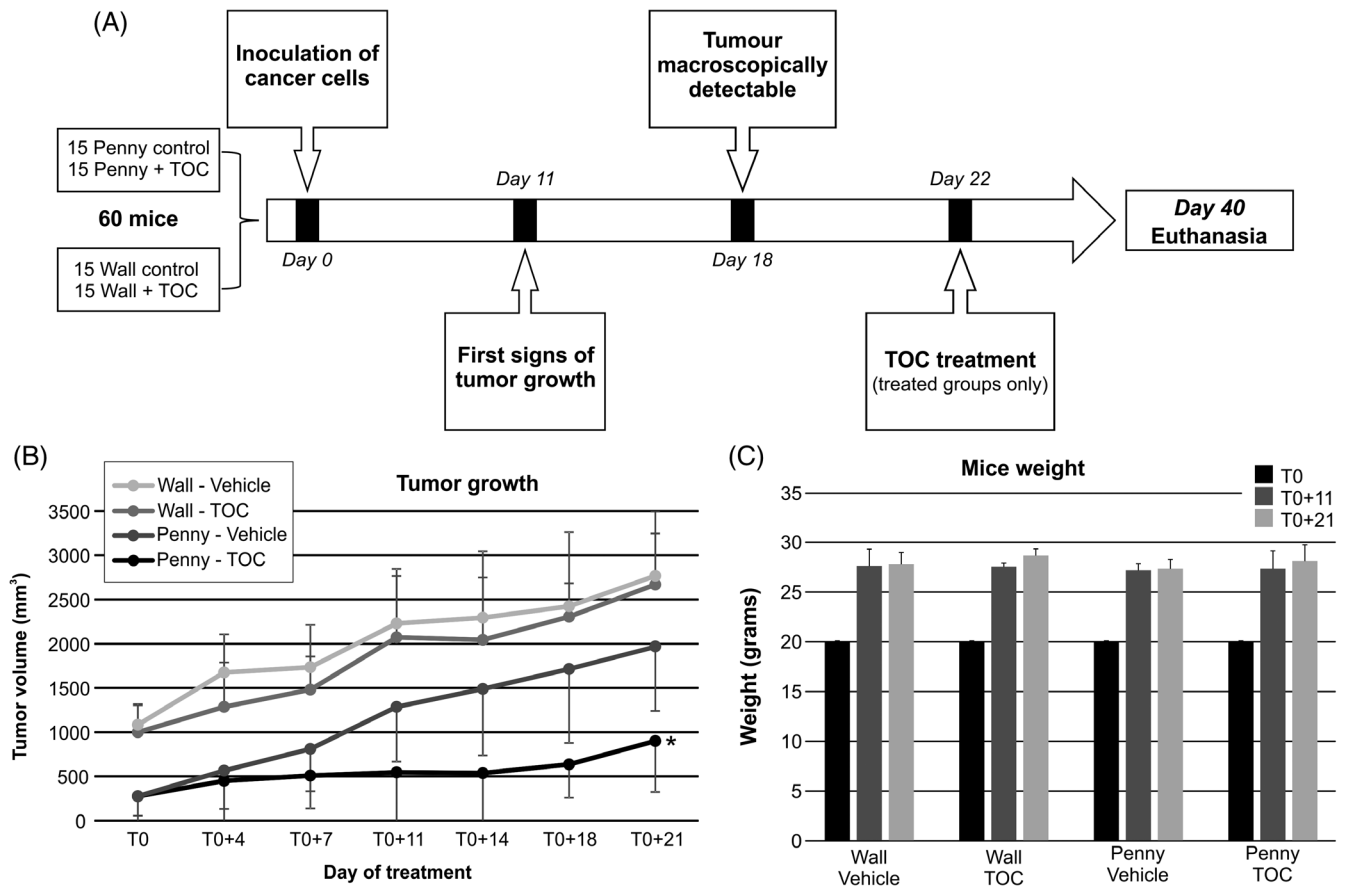
FIGURE 4 Experimental xenograft design. A, Experimental timeline of OSA xenograft on mice and TOC treatment. B, Measurements of tumour volume of xenografts of Wall or Penny cell lines in mice, along the treatment with TOC and with a vehicle (from T0 to T0 + 21 days). As shown in the figure mice inoculated with Penny cells and treated with TOC showed a significant smaller tumour volume compared to those treated with a vehicle (*$P < .05$). Error bars indicate standard deviation of tumour volume. C, Mean weight of mice with Wall or Penny xenografts, treated with TOC or with vehicle at T0, T0 + 11 and T0 + 21. Error bars represent standard deviation of mice weight. OSA, osteosarcoma; TOC, Toceranib phosphate

3 | RESULTS

3.1 | TOC inhibits OSA cell migration in vitro

The effect of TOC on OSA cell migration was assessed by transwell migration and wound healing assays. All the canine OSA cell lines showed the ability to migrate through the membrane and to attach to the lower side. Few cells detached and reached the bottom of the wells. Conversely, TOC treatment reduced the number of OSA cells migrating to the bottom of the membrane, ranging from 26.5 ± 11.6% (Penny) to 88.1 ± 1.1% (Sky; Figure 1A) of what was seen in the control. Attachment was inhibited by TOC, such that the number of attached cells ranged from 32 ± 0.9% (Wall) to 93 ± 15.7% (Lady; Figure 1B) compared to the control. Representative images of Hoechst-stained nuclei in untreated controls and TOC-treated cells are shown in Figure 1C. The wound healing assay showed a similar inhibitory effect in TOC-treated OS cell lines (Video S1 shows time-lapse cell migration from administration to 48 hours after treatment). The migration rate decreased to 43.9 ± 24.8% in Penny (Figure 2A) and 71.0 ± 14.3% in Wall (Figure 2B) of what was seen in the controls. Considering these preliminary results, Penny and Wall cells were selected for the following in vitro and in vivo experiments.

3.2 | TOC does not impair cell growth but inhibits anchorage-independent growth and invasion

To assess the time-dependent effect of TOC on growth, Penny and Wall cells were exposed to 1 μM TOC for 24, 48 and 72 hours. TOC treatment slightly reduced cell growth in both the Penny and Wall cell lines, but a significant difference was found only in the Penny cell lines after 72 hours of treatment ($P < .005$; Figure S1). To investigate OSA cell growth under anchorage-independent conditions, a colony formation assay was performed. Both cell lines formed colonies when grown resuspended in agarose, but TOC treatment in Penny and Wall cells slightly decreased the colony numbers compared to that of untreated cells (Figure 3A). When exclusively considering the colonies that were >100 μm in diameter, TOC treatment showed a higher inhibition of colony formation, with a reduction of 37.7% ± 8.0% for Penny cells and 85.7% ± 12.0% for Wall cells (Figure 3B). Invasion assays mimicking the ability of cancer cells to invade the surrounding stroma showed that both cell lines had a significant decrease in the ability to degrade the extracellular matrix after treatment. TOC treatment in both cell lines also reduced OSA cell invasion by over 85% compared to the control cells (Figure 3C and Table S4).
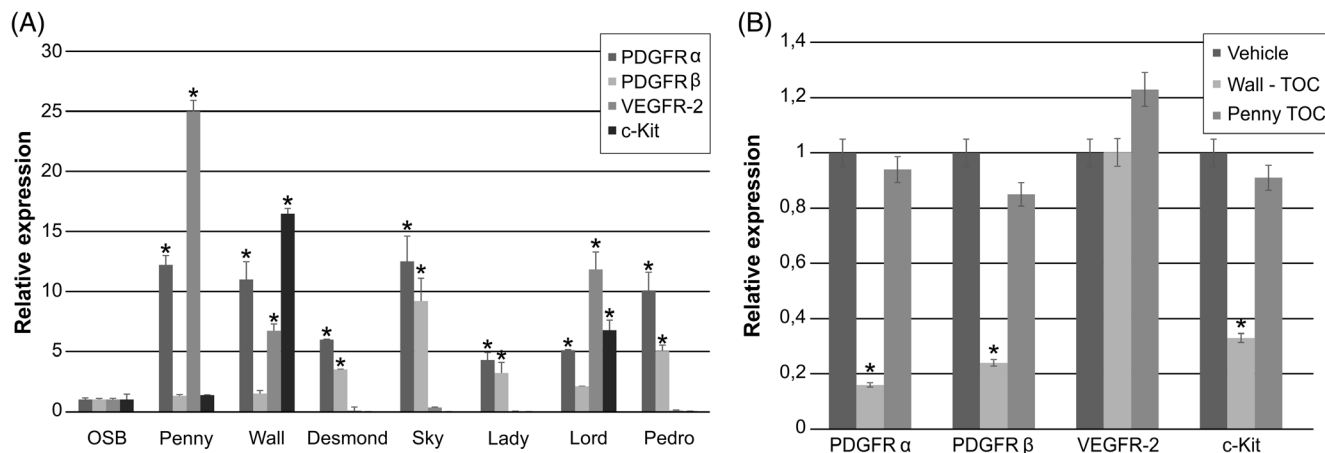
FIGURE 5 Quantitative PCR. A, Expression of PDGFR-α, PDGFR-β, VEGFR-2 and c-Kit transcripts in primary osteosarcoma (OSA) cell lines. PDGFR-α mRNA were expressed at higher levels in 7/7 OSA cell lines, PDGFR-β in 4/7, VEGFR-A transcript had a higher expression in 4/7 OSA cell lines and c-Kit in 2/7, compared to the normal cell line (OSB; *P < .05). The fold increase of each specific mRNA was normalized with normal OSB cell line and the error bars indicate the standard deviation of experimental triplicates. B, Expression by quantitative PCR of PDGFR-α, PDGFR-β, VEGFR-2 and c-Kit in primary Wall and Penny OS cell lines treated with TOC, compared to the control (untreated). Wall cell line showed a lower expression of PDGFR-α, PDGFR-β and c-Kit when treated (*P < .05). Penny cell did not show any significant variation. The fold increase of each specific mRNA was normalized with the control cell line and the error bars indicate the standard deviation of experimental triplicates. OSA, osteosarcoma; OSB, osteoblastic cell line

3.3 | TOC only reduces in vivo tumour growth in the Penny xenograft model

To evaluate the activity of TOC in vivo, we generated two orthotopic xenograft mouse models using Penny and Wall cells. Both cell lines were tumourigenic, and 18 days after injection, primary tumours were macroscopically visible in 85% of mice (*n* = 51) with a volume of approximately 3 to 4 mm^3. TOC treatment was started at 22 days postinoculation and was completed at day 42. The experimental design and the timelines of the treatment are shown in Figure 4A. Six mice engrafted with Penny cells (20%) and three mice engrafted with Wall cells (10%) did not develop tumours at any time, which was also confirmed at necropsy. Drug-related side effects were observed after 3 to 4 days of treatment, including dermatitis in five (33.3%) and four (26.7%) mice inoculated with Penny and Wall cells, respectively. However, TOC significantly decreased tumour growth in mice inoculated with Penny cells but not with Wall cells (Figure 4B). Additionally, no differences in body weight between the four different groups were evident (Figure 4C).

3.4 | TOC treatment reduces PDGFR-α, PDGFR-β, VEGFR2 and c-Kit mRNA expression in both in vivo and in vitro models

Quantitative RT-PCR results (Figure 5A) revealed that all the OSA cell lines had higher mRNA expression of both PDGFR-α and PDGFR-β compared to the OSB control cell line (*P* < .05). The only exception was PDGFR-α expression in the Dark cell line. VEGFR-2 and c-Kit mRNAs were increased in three out of seven OS cell lines (Penny, Wall and Lord) when compared to the OSB cell lines (*P* < .05). Finally, we examined PDGFR-α, PDGFR-β, VEGFR-2 and c-Kit mRNA

expression in tumours obtained from TOC-treated and control mice. A significant downregulation of PDGFR-α, PDGFR-β and c-Kit in mice inoculated with Penny cells and treated with TOC was found when compared to controls (Figure 5B), whereas no differences were observed in mice inoculated with Wall cells (Figure 5B).

3.5 | TOC treatment influences tumour cell density and KI-67 score

Histological examination of xenograft tumours confirmed a chondroblastic OSA from Penny cells (Figure 6A) and an osteoblastic OSA (Figure 6B) from Wall cells.[7] No differences in anisocytosis, anisokaryosis, presence of haemorrhages, vascular invasion, bone marrow invasion or muscular invasion were found after treatment. Notably, the grade of anisocytosis and anisokaryosis was always elevated (Figure 6C) in association with necrosis and haemorrhages (Figure 6D). Conversely, bone marrow invasion occurred in 12/51 tumours (23%; Figure 6E), and muscular invasion occurred in 48/51 samples (93%; Figure 6F); however, no differences were found between the two groups. Of note, in the only mouse in the study (belonging to the Wall control group) in which vascular invasion was diagnosed, the presence of lung metastasis was also observed (Figure 6G).

Histologically, TOC-treated Penny and Wall xenograft models had a decrease in tumour cell density when compared to vehicle-treated animals (*P* = .015 and *P* = .03, respectively). Although the differences were not significant, a trend towards a decrease in the amount of matrix and in necrosis was observed after TOC treatment in tumours originating from Penny and Wall cells. Immunohistochemistry revealed that tumours from TOC-treated mice showed a lower Ki-67 score (Figure 6H) than the tumours grown in vehicle-treated mice
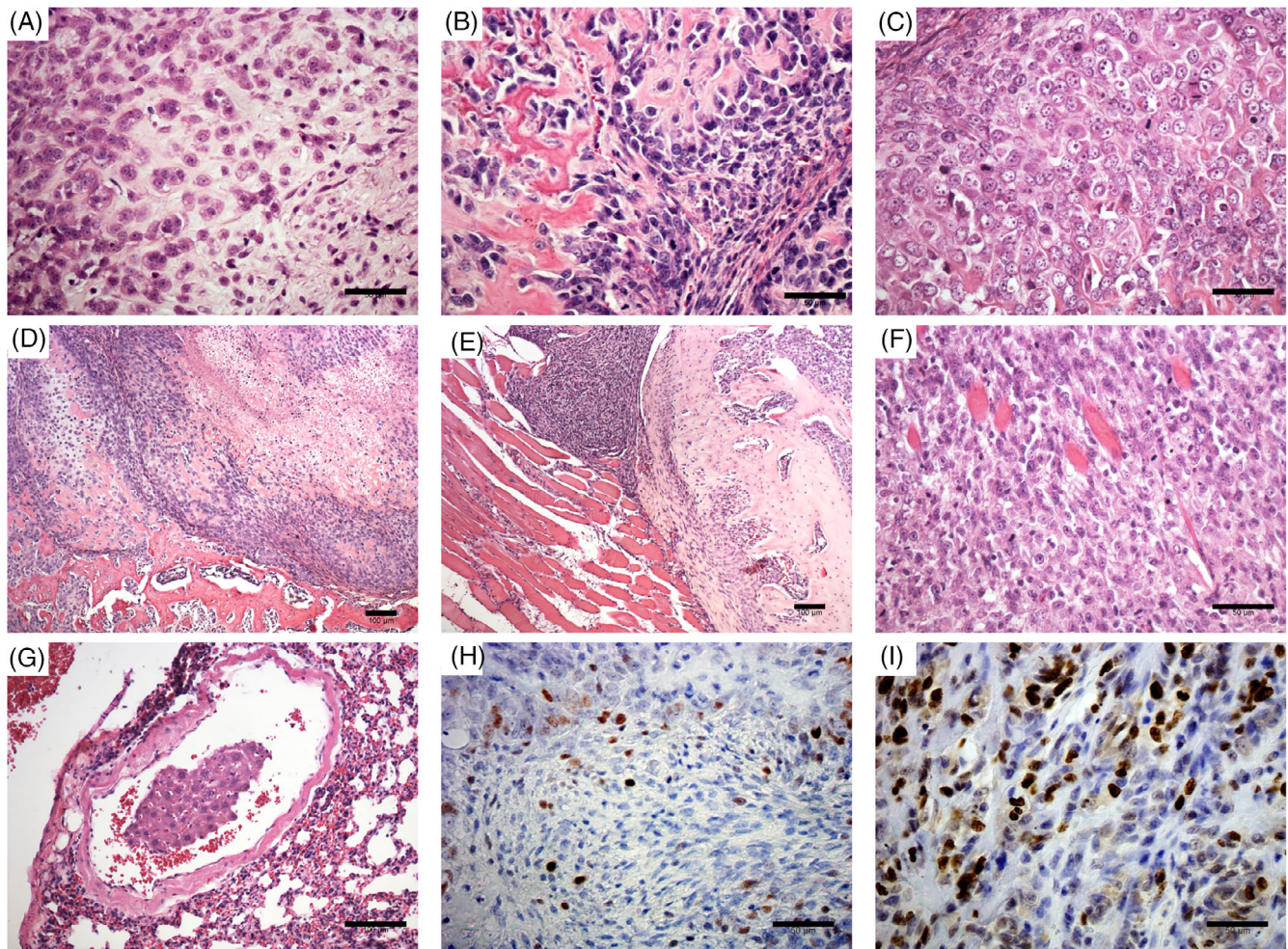
FIGURE 6 Histological features of osteosarcoma xenografts. A, Penny cell line xenograft showing chondroblastic. Neoplastic cells have a chondrocyte-like morphology and are located within lacunae. H&E (×400; Scale bar = 50 μm). B, Wall cell line xenograft showing, osteoblastic histotype: neoplastic cells surrounded by irregular trabeculae of osteoid matrix. H&E and, C, Marked anisocytosis and anisokaryosis (×400; Scale bar = 50 μm). D, Necrosis involving the 30% of the neoplastic tissue (×200; Scale bar = 100 μm). E, Bone marrow invasion (×200; Scale bar = 100 μm). F, Muscular invasion (×200; Scale bar = 100 μm). G, Pulmonary metastasis (×200; Scale bar = 100 μm). Nuclear Ki-67 immunolabelling, respectively, in Penny xenograft, H, treated with TOC and not treated mice, I. Streptavidin-biotin-peroxidase method. Mayer's haematoxylin counterstain (400x, Scale bar = 50 μm). TOC, Toceranib phosphate

(Figure 6I). Additionally, a significant reduction in cellular density was obtained in both Penny and Wall cell-engrafted tumours ($P < .005$). Conversely, caspase 3 expression was not influenced by TOC treatment. Finally, PDGFR-α, PDGFR-β, c-Kit and VEGFR-2 expression did not show any significant difference between the treated and control groups in Wall and Penny xenografts (Table S5). Figure 7 shows representative images of positive immunohistochemical results.

4 | DISCUSSION

Osteosarcoma represents the most common primary malignant bone tumour in dogs, and it has a high metastatic potential and poor prognosis.[1] In humans, this disease is still scarcely curable and has a high rate of metastasis.[34,35] Comparative oncology studies have shown many similarities between OSA occurring in human and canine

patients; in veterinary oncology, the development of xenograft models[36] in mice currently represents an important alternative for investigating the microenvironment and the molecular mechanisms driving cancer growth, as well as for evaluating the biological effects of novel therapeutic agents such as TKIs.

In our study, we developed an orthotopic model of canine OSA and further tested the biological and pharmacological effects of specific treatments. To identify the most appropriate cell line, TKR targets of TOC were first evaluated by RT-qPCR in seven canine OSA cell lines. All of them showed a heterogeneous amount of mRNA, indicating cell-line specific gene expression. Interestingly, similar variations were previously described when considering protein levels.[6,7,33]

Cell lines were further investigated with several biological assays to determine whether cell migration was affected by treatment with TOC. Transwell assays demonstrated that all OSA cell lines were able to migrate in the absence of chemo-attractive factors; conversely,

FIGURE 7 Immunohistochemical stainings in OSA xenografts. A, Low (left) and high (right) IHC staining of PDGFR-α; B, Low (left) and high (right) IHC staining of PDGFR-β; C, low (left) and high (right) IHC staining of VEGFR-A; D, Negative (left) and positive (right) IHC staining of c-Kit (×400; Scale bar = 50 μm). IHC, immunohistochemistry; OSA, osteosarcoma
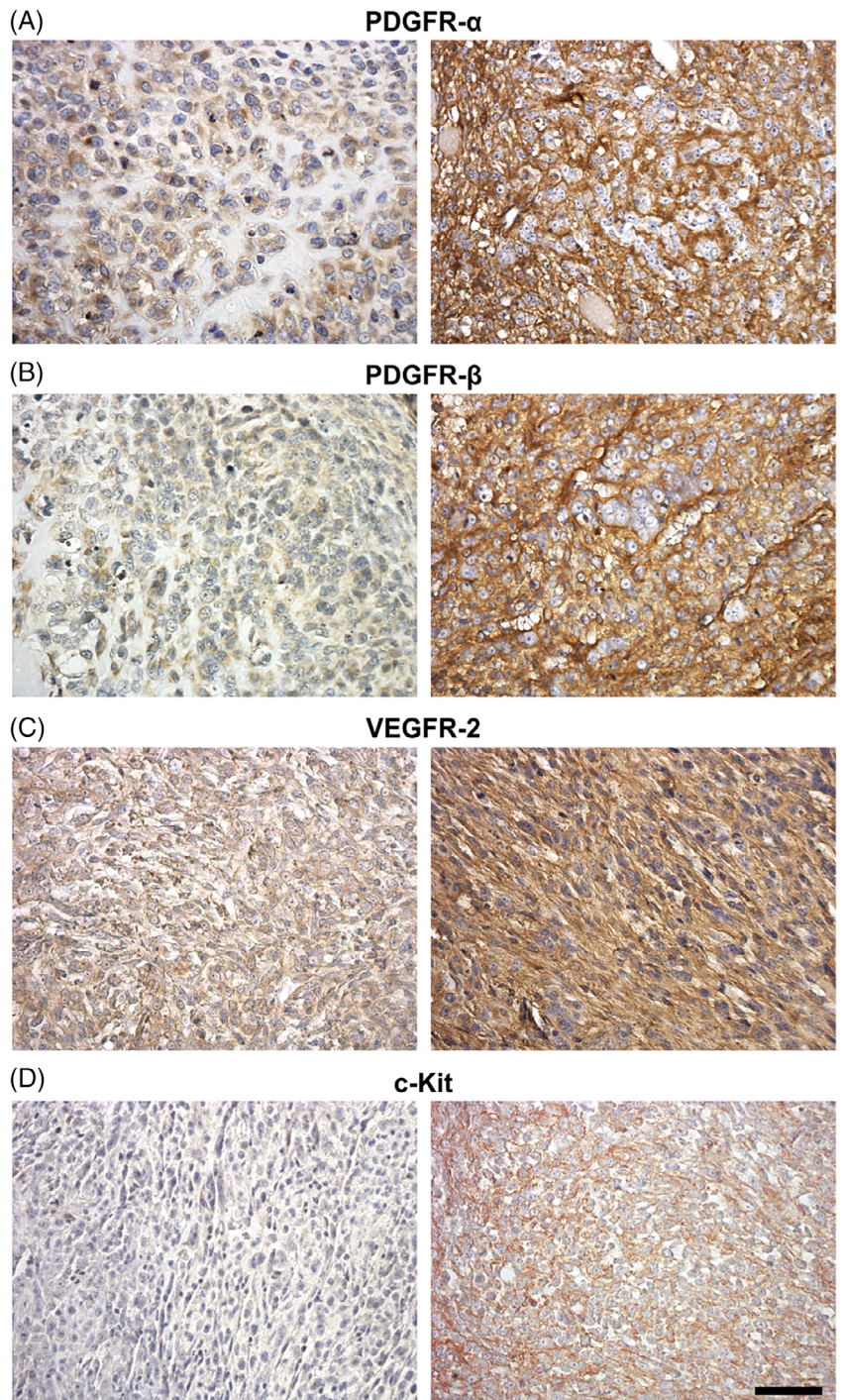
migration was negatively affected by TOC, although to a different extent among cell lines, while the migration score was the highest in Penny cells and the lowest in Wall cells. Wound healing migration rate, colony formation and cell growth rate in soft agar assays revealed that both Penny and Wall cells were negatively affected by TOC treatment. Moreover, if we consider the invasion assay, TOC significantly reduced the invasiveness proprieties of Wall and Penny cell lines, mirroring and confirming the results obtained by wound healing assay. These results suggest that TOC mainly reduces the ability of cells to degrade the extracellular matrix, while its anti-proliferating

effect on the Penny cell line is evident only after 72 hours of treatment.

Overall, these in vitro results suggested that Wall and Penny cells responded to TOC treatment mainly by reducing invasion rather than proliferation. This behaviour might be due to the ability of TOC to inhibit the kinase activity of the target receptors expressed in both cell lines and consequently the downstream activated pathways involved in invasion and migration processes, as demonstrated previously.[6,37-39]

To validate the in vitro results, both Penny and Wall cell lines were inoculated in an orthotopic model, and the cellular growth of

OSA was monitored. The results demonstrated that both Penny and Wall cells were highly tumourigenic, showing engraftment after 18 days. Additionally, tumour histology confirmed that both cell lines conserved their original morphological features. Interestingly, TOC treatment decreased tumour growth in mice inoculated with Penny cells but not those inoculated with Wall cells. Regarding the selected histological parameters, tumour cell density was reduced in treated mice compared to control mice regardless of the cell line, suggesting that TOC can also act at stromal level to modulate angiogenesis and the microenvironment, which is similar to mechanism of sunitinib.[40,41]

It is worth noting that vascular invasion as well as lung metastasis was reported only in one mouse from the Wall control group. No mRNA expression modification of PDGFRs, VEGFR2 or c-Kit was found in tumours removed from control vs TOC-treated Wall xenografts while a slight down regulation of PDGFRs in Penny TOC-treated xenografts vs control was found. However, these data were not confirmed by immunohistochemistry. This incongruence may need different experimental approaches other than the one considered in our study.

Ki67 results demonstrated a lower proliferation index in TOC-treated tumours than in the ones of control mice (in both Penny and Wall groups). This data indicates a TOC effect in decreasing tumour proliferation, but not on cell apoptosis, as shown by caspase-3 results.

To our knowledge this is the first study investigating the effect of TOC on mice xenografts and the dosage administered was selected on the basis of similar experiment conducted in xenografts of human osteosarcoma with Sunitinib (SU11248), molecule structurally similar to TOC.[42] Although the high similarity between the two molecules, we are aware that this approach has limitations such as directly transfer our results in dogs.

Today, clear indications for using TOC in canine OS treatment are not available, and recent clinical trials did not support the use of TOC as a single agent or in combination with other commonly used therapies.[21-24] In conclusion, our results demonstrate that TOC is able to mildly inhibit cell growth in vitro, while its effect is more relevant in xenograft models. Considering the high expression of PDGFRs, c-Kit and VEGFR-2 in Penny, these data suggest that TOC treatment might be more effective in OSA expressing these targets, however further studies are needed to test and validate the efficacy of this molecule in canine OSA.

ACKNOWLEDGEMENTS

CONFLICT OF INTEREST

None of the authors of this article has a financial or personal relationship with other people or organizations that could inappropriately influence or bias the content of the article.

DATA AVAILABILITY STATEMENT

The data that support the findings of this study are available from the corresponding author upon reasonable request.

ORCID

Raquel Sánchez-Céspedes https://orcid.org/0000-0003-3282-7187
Luca Aresu https://orcid.org/0000-0002-7893-1740
Raffaella De Maria https://orcid.org/0000-0002-7028-2280

REFERENCES

1. Morello E, Martano M, Buracco P. Biology, diagnosis and treatment of canine appendicular osteosarcoma: similarities and differences with human osteosarcoma. *Vet J*. 2011;189(3):268-277.
2. Withrow SJ, Powers BE, Straw RC, Wilkins RM. Comparative aspects of osteosarcoma - dog versus man. *Clin Orthop Relat Res*. 1991;1(270): 159-168.
3. Farese JP, Kirpensteijn J, Kik M, et al. Biologic behavior and clinical outcome of 25 dogs with canine appendicular chondrosarcoma treated by amputation: a veterinary society of surgical oncology retrospective study. *Vet Surg*. 2009;38(8):914-919.
4. Casteleyn C, Sleeckx N, De Spiegelaere W, Heindryckx F, Coulon S, Van Steenkiste C. New therapeutic targets in veterinary oncology: man and dog definitely are best friends. *Vet J*. 2013;195(1):6-7.
5. De Maria R, Miretti S, Iussich S, et al. Met oncogene activation qualifies spontaneous canine osteosarcoma as a suitable pre-clinical model of human osteosarcoma. *J Pathol*. 2009;218(3):399-408.
6. Maniscalco L, Iussich S, Morello E, et al. PDGFs and PDGFRs in canine osteosarcoma: new targets for innovative therapeutic strategies in comparative oncology. *Vet J*. 2013;195(1):41-47.
7. Maniscalco L, Iussich S, Morello E, et al. Increased expression of insulin-like growth factor-1 receptor is correlated with worse survival in canine appendicular osteosarcoma. *Vet J*. 2015;205(2):272-280.
8. Mantovani FB, Morrison JA, Mutsaers AJ. Effects of epidermal growth factor receptor kinase inhibition on radiation response in canine osteosarcoma cells. *BMC Vet Res*. 2016;12:82.
9. Fahey CE, Milner RJ, Kow K, Bacon NJ, Salute ME. Apoptotic effects of the tyrosine kinase inhibitor, masitinib mesylate, on canine osteosarcoma cells. *Anticancer Drugs*. 2013;24(5):519-526.
10. Hojjat-Farsangi M. Small-molecule inhibitors of the receptor tyrosine kinases: promising tools for targeted cancer therapies. *Int J Mol Sci*. 2014;15(8):13768-13801.
11. Wu P, Nielsen TE, Clausen MH. FDA-approved small-molecule kinase inhibitors. *Trends Pharmacol Sci*. 2015;36(7):422-439.
12. Downing S, Chien MB, Kass PH, Moore PE, London CA. Prevalence and importance of internal tandem duplications in exons 11 and 12 of c-kit in mast cell tumors of dogs. *Am J Vet Res*. 2002;63(12):1718-1723.
13. Amagai Y, Tanaka A, Matsuda A, et al. Heterogeneity of internal tandem duplications in the c-kit of dogs with multiple mast cell tumours. *J Small Anim Pract*. 2013;54(7):377-380.
14. London CA. Small molecule inhibitors in veterinary oncology practice. *Vet Clin North Am Small Anim Pract*. 2014;44(5):893-908.
15. London CA. Tyrosine kinase inhibitors in veterinary medicine. *Top Companion Anim Med*. 2009;24(3):106-112.
16. Robat C, London C, Bunting L, et al. Safety evaluation of combination vinblastine and toceranib phosphate (Palladia(R)) in dogs: a phase I dose-finding study. *Vet Comp Oncol*. 2012;10(3):174-183.
17. London CA, Malpas PB, Wood-Follis SL, et al. Multi-center, placebo-controlled, double-blind, randomized study of oral toceranib phosphate (SU11654), a receptor tyrosine kinase inhibitor, for the treatment of dogs with recurrent (either local or distant) mast cell tumor following surgical excision. *Clin Cancer Res*. 2009;15(11):3856-3865.

18. London C, Mathie T, Stingle N, et al. Preliminary evidence for biologic activity of toceranib phosphate (Palladia((R))) in solid tumours. *Vet Comp Oncol*. 2012;10(3):194-205.

19. Gardner HL, London CA, Portela RA, et al. Maintenance therapy with toceranib following doxorubicin-based chemotherapy for canine splenic hemangiosarcoma. *BMC Vet Res*. 2015;11:131.

20. Laver T, London CA, Vail DM, Biller BJ, Coy J, Thamm DH. Prospective evaluation of toceranib phosphate in metastatic canine osteosarcoma. *Vet Comp Oncol*. 2018;16(1):E23-E29.

21. Kim C, Matsuyama A, Mutsaers AJ, Woods JP. Retrospective evaluation of toceranib (Palladia) treatment for canine metastatic appendicular osteosarcoma. *Can Vet J*. 2017;58(10):1059-1064.

22. Gieger TL, Nettifee-Osborne J, Hallman B, et al. The impact of carboplatin and toceranib phosphate on serum vascular endothelial growth factor (VEGF) and metalloproteinase-9 (MMP-9) levels and survival in canine osteosarcoma. *Can J Vet Res*. 2017;81(3):199-205.

23. Wouda RM, Hocker SE, Higginbotham ML. Safety evaluation of combination carboplatin and toceranib phosphate (Palladia) in tumour-bearing dogs: a phase I dose finding study. *Vet Comp Oncol*. 2018;16 (1):E52-e60.

24. London CA, Gardner HL, Mathie T, et al. Impact of Toceranib/Piroxicam/Cyclophosphamide maintenance therapy on outcome of dogs with appendicular osteosarcoma following amputation and carboplatin chemotherapy: a multi-institutional study. *PLoS One*. 2015; 10(4):e0124889.

25. Coomer AR, Farese JP, Milner R, et al. Development of an intramuscular xenograft model of canine osteosarcoma in mice for evaluation of the effects of radiation therapy. *Am J Vet Res*. 2009;70(1):127-133.

26. Farese JP, Fox LE, Detrisac CJ, Van Gilder JM, Roberts SL, Baldwin JM. Effect of thalidomide on growth and metastasis of canine osteosarcoma cells after xenotransplantation in athymic mice. *Am J Vet Res*. 2004;65(5):659-664.

27. Hong SH, Kadosawa T, Mochizuki M, Matsunaga S, Nishimura R, Sasaki N. Effect of all-trans and 9-cis retinoic acid on growth and metastasis of xenotransplanted canine osteosarcoma cells in athymic mice. *Am J Vet Res*. 2000;61(10):1241-1244.

28. London CA, Hannah AL, Zadovoskaya R, et al. Phase I dose-escalating study of SU11654, a small molecule receptor tyrosine kinase inhibitor, in dogs with spontaneous malignancies. *Clin Cancer Res*. 2003;9 (7):2755-2768.

29. Mendel DB, Laird AD, Xin X, et al. In vivo antitumor activity of SU11248, a novel tyrosine kinase inhibitor targeting vascular endothelial growth factor and platelet-derived growth factor receptors: determination of a pharmacokinetic/pharmacodynamic relationship. *Clin Cancer Res*. 2003;9(1):327-337.

30. Dolka I, Sapierzynski R, Krol M. Retrospective study and immunohistochemical analysis of canine mammary sarcomas. *BMC Vet Res*. 2013;9:248.

31. McCleese JK, Bear MD, Fossey SL, et al. The novel HSP90 inhibitor STA-1474 exhibits biologic activity against osteosarcoma cell lines. *Int J Cancer*. 2009;125(12):2792-2801.

32. Miiji LN, Petrilli AS, Di Cesare S, et al. C-kit expression in human osteosarcoma and in vitro assays. *Int J Clin Exp Pathol*. 2011;4(8): 775-781.

33. Gattino F, Maniscalco L, Iussich S, et al. PDGFR-alpha, PDGFR-beta, VEGFR-2 and CD117 expression in canine mammary tumours and evaluation of the in vitro effects of toceranib phosphate in neoplastic mammary cell lines. *Vet Rec*. 2018;183(7):221.

34. Ferguson WS, Goorin AM. Current treatment of osteosarcoma. *Cancer Invest*. 2001;19(3):292-315.

35. Vormoor B, Knizia HK, Batey MA, et al. Development of a preclinical orthotopic xenograft model of Ewing sarcoma and other human malignant bone disease using advanced in vivo imaging. *PLoS One*. 2014;9(1):e85128.

36. Guan G, Lu Y, Zhu X, et al. CXCR4-targeted near-infrared imaging allows detection of orthotopic and metastatic human osteosarcoma in a mouse model. *Sci Rep*. 2015;5:15244.

37. Yancey MF, Merritt DA, Lesman SP, Boucher JF, Michels GM. Pharmacokinetic properties of toceranib phosphate (Palladia, SU11654), a novel tyrosine kinase inhibitor, in laboratory dogs and dogs with mast cell tumors. *J Vet Pharmacol Ther*. 2010;33(2):162-171.

38. Halsey CH, Gustafson DL, Rose BJ, et al. Development of an in vitro model of acquired resistance to toceranib phosphate (Palladia(R)) in canine mast cell tumor. *BMC Vet Res*. 2014;10:105.

39. Cao Y. Multifarious functions of PDGFs and PDGFRs in tumor growth and metastasis. *Trends Mol Med*. 2013;19(8):460-473.

40. Voce P, D'Agostino M, Moretti S, et al. Sunitinib inhibits tumor vascularity and growth but does not affect Akt and ERK phosphorylation in xenograft tumors. *Oncol Rep*. 2011;26(5):1075-1080.

41. Kitano H, Kitadai Y, Teishima J, et al. Combination therapy using molecular-targeted drugs modulates tumor microenvironment and impairs tumor growth in renal cell carcinoma. *Cancer Med*. 2017;6 (10):2308-2320.

42. Kumar RM, Arlt MJ, Kuzmanov A, Born W, Fuchs B. Sunitinib malate (SU-11248) reduces tumour burden and lung metastasis in an intratibial human xenograft osteosarcoma mouse model. *Am J Cancer Res*. 2015;5(7):2156-2168.

SUPPORTING INFORMATION

Additional supporting information may be found online in the Supporting Information section at the end of this article.

ACKNOWLEDGEMENTS